UC San Diego

UC San Diego Electronic Theses and Dissertations

Title

Energy-resolved annihilation studies : vibrational Feshbach resonances and positron-molecule bound states

Permalink

https://escholarship.org/uc/item/30t2f1mp

Author

Young, Jason Asher

Publication Date

2007

Peer reviewed|Thesis/dissertation

eScholarship.org Powered by the California Digital Library
University of California

UNIVERSITY OF CALIFORNIA, SAN DIEGO

Energy-resolved annihilation studies: Vibrational Feshbach resonances and positron-molecule bound states

A dissertation submitted in partial satisfaction of the requirements for the degree of Doctor of Philosophy

in

Physics

by

Jason Asher Young

Committee in charge:

Clifford M. Surko, Chairman
Leonid Butov
Robert Continetti
Charles Perrin
Lu Sham

2007

Copyright
Jason Asher Young, 2007
All rights reserved.

The dissertation of Jason Asher Young is approved and it is acceptable in quality and form for publication on microfilm.

_____

_____

_____

_____

_____

_____

Chairman

University of California, San Diego

2007

Table of Contents

Signature Page . . . iii
Table of Contents . . . iv
List of Figures . . . viii
List of Tables . . . xi
List of Symbols . . . xii
Acknowledgments . . . xiii
Vita, Publications and Fields of Study . . . xv
Abstract . . . xvii

Chapter 1 Introduction . . . 1
1.1 The discovery of positrons . . . 2
1.2 Research and applications of antimatter . . . 2
1.3 Positron interactions with free molecules . . . 4
1.4 Outline of the dissertation . . . 6

Chapter 2 Background . . . 8
2.1 Annihilation rates . . . 9
2.2 Trends in thermal Z_{eff} . . . 10
2.3 Energy-resolved Z_{eff} . . . 13
2.4 Annihilation theory . . . 17
2.4.1 Direct annihilation . . . 18
2.4.2 The Vibrational Feshbach Resonance . . . 19
2.4.3 Enhanced Z_{eff} . . . 21
2.4.4 Suppressed Z_{eff} . . . 22
2.4.5 Binding . . . 22

Chapter 3 Experimental Methods . . . 23
3.1 Positron source and moderator . . . 23
3.2 The Buffer Gas Trap . . . 26
3.3 Characterizing the positron beam . . . 30

3.3.1 Beam energy . . . 30
3.3.2 Positron pulse strength . . . 33
3.4 The annihilation cell . . . 35
3.5 Delivery of gases and vapors . . . 37
3.6 Cold gas cell apparatus . . . 38
3.6.1 Temperature measurement and constraints . . . 40
3.6.2 Pressure measurement and constraints . . . 40
3.7 A typical experiment . . . 41
3.8 Calculating the annihilation rate . . . 42
3.9 Sources of error . . . 43
3.9.1 Pressure . . . 43
3.9.2 Pulse strength . . . 44
3.9.3 Number of passes through the cell . . . 45
3.9.4 Counting errors . . . 45
3.9.5 Three body effects . . . 46
3.9.6 Errors in energy . . . 47

Chapter 4 VFR in small molecules . . . 48
4.1 The halomethanes . . . 49
4.2 Small molecule model . . . 51
4.3 The deuterated halomethanes . . . 57
4.3.1 Higher-order shifts in peak position . . . 58
4.4 Propane, a "large" molecule . . . 61
4.5 Methanol . . . 62
4.5.1 Z_{eff} spectrum of methanol . . . 62
4.5.2 An adapted Gribakin-Lee model . . . 64
4.5.3 Overtone & combination mode VFRs . . . 67
4.6 Two-carbon molecules . . . 69
4.6.1 Acetylene, ethylene, and ethane . . . 69
4.6.2 Ethanol . . . 74
4.7 Propane and cyclopropane . . . 75
4.8 Comparison of "small," "large," and "suppressed" molecules . . . 77
4.9 VFR-weak or inactive molecules . . . 79
4.9.1 CO_2 and H_2O . . . 79
4.9.2 Spectra for CO_2 and H_2O with increased signal-to-noise . . . 82
4.10 Bound and virtual states . . . 85
4.11 VFR precursors . . . 88
4.12 Concluding remarks . . . 90

Chapter 5 VFR in Large Molecules **92**
5.1 Hexane and cyclohexane 94
5.2 Benzene and d-benzene 95
5.3 1-Chlorohexane 98
5.4 The atom trend 100
5.5 The temperature dependence of Z_{eff} 104
5.5.1 Z_{eff} of cold alkane molecules 105
5.5.2 Analysis of the cold cell data 107
5.6 Fluoroalkanes 108
5.6.1 1-Fluoropropane 110
5.6.2 1-Fluorobutane 111
5.7 The origin of "suppressed" Z_{eff} 112
5.7.1 Inelastic escape channels 114
5.7.2 Suppression in other substituted alkanes 116
5.8 Other perturbations to the magnitude of Z_{eff} 116
5.8.1 Dark states 117
5.8.2 Partially Deuterated Benzenes 117
5.8.3 A tiered IVR model 118
5.9 Multi-mode VFR 119
5.10 Naphthalene and d-naphthalene 121
5.11 12, 14, and 16-carbon alkanes 124
5.12 A zero-range potential model 127
5.13 Trends in binding energy 129
5.14 Concluding remarks 132

Chapter 6 Conclusions **134**
6.1 Open questions 135
6.1.1 The IVR process 136
6.1.2 The capture rate 136
6.1.3 Positron binding energy 137
6.1.4 Other phenomena 137
6.2 Future experiments 138
6.2.1 Changes in molecular structure 138
6.2.2 Particularly interesting molecules 139
6.2.3 A hot cell 139
6.2.4 Gamma-ray spectra 140
6.2.5 Scattering processes 140
6.2.6 A cold positron beam 142

6.2.7 Fragmentation analysis 142

Appendices **144**

Appendix A Table of positron-molecule annihilation data **144**

References **148**

List of Figures

Figure 2.1: Thermal Z_{eff}/Z vs. Z 12

Figure 2.2: Energy-resolved Z_{eff} for butane 14

Figure 2.3: The VFR model 15

Figure 2.4: Alkane trends 16

Figure 3.1: Schematic of the positron source assembly 25

Figure 3.2: Moderator growth cycle 27

Figure 3.3: Schematic diagram and potential phases of the positron accumulator 28

Figure 3.4: A typical cutoff measurement 31

Figure 3.5: The positron pulse total energy distribution 34

Figure 3.6: Schematic of the annihilation cell region 36

Figure 3.7: Cold cell apparatus 39

Figure 4.1: Z_{eff} for methyl halides 50

Figure 4.2: Gribakin-Lee model for methyl halides 56

Figure 4.3: Gribakin-Lee model for deuterated methyl halides 59

Figure 4.4: Propane with fit 61

Figure 4.5: Z_{eff} for methanol 63

Figure 4.6: Adapted Gribakin-Lee model for methanol 65

Figure 4.7: Z_{eff} for acetylene, ethylene, and ethane 70

Figure 4.8: Z_{eff} spectrum for ammonia 72

Figure 4.9: Z_{eff} for ethanol, with Gribakin-Lee model 74

Figure 4.10: Structures for propane and cyclopropane 76

Figure 4.11: Z_{eff} for propane and cyclopropane 78

Figure 4.12: Z_{eff} for CH_4 and CH_3F 80

Figure 4.13: Z_{eff} for CO_2 and H_2O 81

Figure 4.14: Z_{eff} for CO_2, and H_2O, 40μs bounce window 83

Figure 5.1: Molecular structures of hexane and cyclohexane. 94

Figure 5.2: Z_{eff} spectra for hexane and cyclohexane. 95

Figure 5.3: Z_{eff} for benzene and benzene-d6 97

Figure 5.4: Z_{eff} for 1-chlorohexane and hexane 99

Figure 5.5: Normalized Z_{eff} *vs* number of atoms 101

Figure 5.6: Energy-resolved Z_{eff} for cold pentane and heptane 106

Figure 5.7: Z_{eff} for 1-fluorononane and 1-fluorohexane 109

Figure 5.8: Z_{eff} for propane, 1-fluoropropane, and 2,2-difluoropropane . . . 110

Figure 5.9: Z_{eff} for butane and 1-fluorobutane 112

Figure 5.10: Normalized Z_{eff} *vs* the number of atoms, including suppressed-Z_{eff} species 113

Figure 5.11: Z_{eff} and IR for benzene 120

Figure 5.12: Molecular structure of naphthalene 121

Figure 5.13: Z_{eff} for naphthalene 123

Figure 5.14: Z_{eff} for 12, 14, and 16-carbon alkanes 125

Figure 5.15: ZRP model binding in alkanes 128

Figure 5.16: Binding energy *vs* polarizability 130

Figure 5.17: Binding energy *vs* α^2/N 131

List of Tables

Table 4.1: Physical properties of CH_3Cl vibrational modes 55

Table 4.2: Physical properties of methanol vibrational modes 66

Table 4.3: Binding energy for small & medium-sized molecules 87

Table 5.1: Z_{eff}/g for various species 102

Table 5.2: Thermal Z_{eff} for partially deuterated benzenes 117

Table 5.3: Binding energy & Z_{eff} for molecules with 2^{nd} bound states 126

Table A.1: Table of positron-molecule annihilation data. 145

List of Symbols

For more in depth explanations of these symbols, consult Sections 2.4 and 4.2.

ϵ	incident positron kinetic energy
ϵ_b	positron-molecule binding energy
$f(\epsilon)$	positron beam energy distribution function
F	empirical proportionality constant, $F = 2\pi\rho_{ep}/\kappa$
g	explicit energy scaling, $g = \sqrt{\epsilon_b/\epsilon}$, of a vibrational Feshbach resonance (VFR)
Γ_ν	natural width for a positron-molecule VFR due to vibration ν
Γ^a_ν	annihilation rate for a VFR due to vibration ν; usually just Γ^a
Γ^e_ν	resonant elastic capture (and re-emission) rate for a VFR due to vibration ν
$h(\xi)$	in Gribakin-Lee theory, a function describing the energy dependence of Γ^e_ν
κ	inverse scattering length associated with bound s-wave positron wave function
N	number of atoms in a molecule
ω_ν	energy of vibration ν
r_0	classical electron radius
ρ_{ep}	electron-positron overlap density
Z	number of molecular electrons
Z_{eff}	normalized annihilation rate (see Eqn. 2.1)
$Z^{(dir)}_{eff}$	non-resonant normalized annihilation rate
$Z^{(th)}_{eff}$	normalized annihilation rate for room temperature positrons
$Z^{(res)}_{eff}$	resonant normalized annihilation rate (i.e. the contributions from VFR)
$Z^{(CH)}_{eff}$	normalized annihilation rate at the energy of the C-H stretch mode VFR

Acknowledgments

One important lesson I learned in graduate school is that both scientific and personal progress do not occur in a vacuum. There are many people who inspired, educated, guided, and supported me throughout my graduate career. For this I am deeply grateful.

I would like to start by thanking Cliff Surko, who is, in my opinion, an advisor and scientist of rare quality. I thank him for his sage guidance in the art of experiment and practice of science, his thoughtful and thorough critiquing of papers and theses (c.f. page xiii of Ref. [1]), and his love of Latin abbreviations.

I am also indebted to various current and former members of our lab. If I ever meet him, I will have to thank Koji Iwata for that table of annihilation data in this thesis. Steve Gilbert, Rod Greaves, James Sullivan, Levi Barnes and Joan Marler also deserve kudos for developing and refining that wonderful apparatus I used to perform my experiments. In particular, I'd like to thank Levi, who helped me do my first annihilation experiments and was a joy to work with. He inspired a lot of my later research and deserves a share of the credit for my earliest research. I'd also like to thank James Danielson, whose simple but intelligent questions sometimes had really interesting answers. In general, I am thankful for the friendly and stimulating work environment provided by Cliff, Gene Jerzewski, Judy Winstead, Pitt Schmitt, Levi, Joan, James, and more recently Toby Weber.

A special thanks goes to Gene, our technical wizard. He taught me (and countless others) nearly everything I know about troubleshooting, assembling and repairing equipment in the lab. I doubt I could have made it without him. Also, I should thank Gleb

Gribakin and Chris Lee, for countless enlightening conversations and their invaluable theoretical insight into the process of positron-molecule annihilation. Much of Chapter 4 is devoted to tests of their theory. Many thanks also go to my committee and to the folks who helped proofread my thesis.

Finally, I'd like to thank my wife Amber and my family for supporting me throughout my research. Their positive attitude always got me through the low times.

Vita

1979	Born, Philadelphia, Pennsylvania, U. S. A.
2001	Sc.B., Physics, Brown University.
2002-2004	Laboratory Instructor, University of California, San Diego.
2003	Teaching Assistant, University of California, San Diego.
2007	Ph.D., Physics, University of California, San Diego.

Publications

ARTICLES

1. J. A. Young and C. M. Surko "Dependence of resonant positron-molecule annihilation on molecular temperature," *Nucl. Instrum. Meth. B*, submitted for publication (2007).

2. J. A. Young and C. M. Surko. "Role of binding energy in feshbach-resonant positron-molecule annihilation," *Phys. Rev. Lett.*, **99**, 133201 (2007).

3. L. D. Barnes, J. A. Young, and C. M. Surko. "Energy-resolved positron annihilation rates for molecules." *Phys. Rev. A*, **74**, 012706 (2006).

4. J. A. Young and C. M. Surko "Charged particle motion in spatially varying electric and magnetic fields," *Nucl. Instrum. Meth. B*, **247**, 147 (2006).

5. J. P. Marler, L. D. Barnes, S. J. Gilbert, J. P. Sullivan, J. A. Young, and C. M. Surko "Experimental Studies of the interaction of low-energy positrons with atoms and molecules," *Nucl. Instrum. Meth. B*, **221**, 84 (2004).

INVITED TALKS

- J. A. Young, "Resonant Positron-molecule annihilation - Distinguishing Binding and Mode Effects." XXV International Conference on Photonic, Electronic and Atomic Collisions. Freiburg, Germany, July 2007.
- J. A. Young, "New results on positron-molecule annihilation, vibrational Feshbach resonances and bound states." XIIIth International Workshop on Positron and Positronium Physics. Campinas, Brasil, July 2005.

Fields of Study

Major Field: Physics

Studies in Atomic and Molecular Physics
Professor Clifford M. Surko

Studies in Positron Physics
Professor Clifford M. Surko

ABSTRACT OF THE DISSERTATION

Energy-resolved annihilation studies: Vibrational Feshbach resonances and positron-molecule bound states

by

Jason Asher Young

Doctor of Philosophy in Physics

University of California, San Diego, 2007

Professor Clifford M. Surko, Chairman

The focus of this thesis research is the vibrational Feshbach resonance (VFR) mechanism for positron annihilation on molecules below the threshold for positronium formation. This process results in resonances in the positron-molecule annihilation rate when the incident positron has energy $\epsilon = \omega_\nu - \epsilon_b$, where ω_ν is the energy of a molecular vibration and ϵ_b is the positron-molecule binding energy. To understand this process, annihilation rates are measured as a function of positron energy for a variety of molecular species. These experiments provide new insight into the VFR process. In small molecules, the annihilation spectrum can be described well by a recent theory, which was brought to fruition with the assistance of data presented here. It is shown that the magnitudes of the VFR resonances in these molecules depend only on a simple scaling factor $g = \sqrt{\epsilon_b/\epsilon}$. This theory fails in larger molecules, where the magnitudes of annihilation resonances rise rapidly with molecular size. However in hydrocarbons, when the scaling factor g is normalized out, the resonance due to the C-H stretch mode follows a

universal scaling with the number of vibrational degrees of freedom. This is interpreted as evidence that the VFR are being enhanced by intramolecular vibrational relaxation (IVR). To date, only fluoroalkane molecules deviate from this trend, exhibiting a suppression of annihilation above a certain energy threshold. It is demonstrated that a resonant inelastic process involving the C-F stretch mode is responsible for this behavior. Data are presented for a number of deeply bound species and compared to molecules of similar size. The relationship between binding energy and various physical parameters is explored. A number of other phenomena are discussed, including the observation of combination-mode VFR, providing added insight into the annihilation process.

Chapter 1

Introduction

The positron is a unique little particle which continues to confound and delight experimentalists and theorists even three quarters of a century after its discovery. Since it is the antiparticle of the electron, the positron has identical mass and spin to the electron, but opposite charge. For whatever reason, countless physicists and chemists, when they first consider the implications of positron-matter interactions, have underestimated the impact of this seemingly benign sign change.

The positron is not simply an electron which happens to be positive or a proton which happens to be light. Discrepancies in the behavior of low energy electron and positron projectiles cannot be 'fixed' by a small perturbation to the scattering equations. Positron interactions with matter are decidedly different from electron interactions. Since positrons are attracted to and distinguishable from electrons, highly correlated electron-positron states are possible. Add to this the fact that positrons can form bound states with electrons and even annihilate with them completely, leaving only gamma rays, and it is easy to see why this research continues to captivate many scientists.

Today, antimatter is being used in studies of condensed matter, material processing, astrophysics, tests of CPT invariance, and even medicine. Technologies such as the neon moderator and the Penning-Malmberg buffer gas trap have made cold antimatter more accessible than ever before. This has opened up new possibilities for research even outside

the realm of atomic and molecular physics. In many cases, basic research performed in the positron community, including our lab, has played a crucial role in improving and understanding antimatter (and even matter) technology (e.g. the Penning-Malmberg trap).

1.1 The discovery of positrons

The existence of an antimatter particle was first proposed by P. A. M. Dirac in 1930 [2]. His relativistic formulation of quantum mechanics seemed to require an infinite number of negative mass-energy states for the electron. To resolve this issue, he declared that nearly all these states were filled and identified (mistakenly) the positively-charged "holes" in this sea of states as protons. Furthermore, he proposed that an electron falling into such a "hole" would be converted into pure energy, in the form of gamma-ray photons [3]. It later became clear that the proton was not the antiparticle of the electron – it was too massive. Three years later C. D. Anderson discovered a light, positively charged particle in the tracks of his cloud chamber [4, 5]. These electron-like particles, found among cosmic rays, were correctly identified as Dirac's hole states. Anderson gave them the name which they still have today: positrons.

1.2 Research and applications of antimatter

The most widely recognized application of antimatter is Positron Emission Tomography (PET) [6]. In this medical procedure, a biological chemical, such as sugar, is tagged with a positron-emitting radioisotope. This tagged chemical is then introduced into the body of a patient. By detecting the direction and energy of the pair of gamma rays emitted when a positron annihilates with electrons in the body, it is possible to pinpoint the location of the tagged chemical. Thus, one can create an image showing the rate a tagged chemical is absorbed and metabolized in various parts of the body. Antimatter may also have therapeutic applications. For instance, high energy anti-protons may be

able to selectively destroy cancer cells by creating large amounts of ionizing radiation at specific penetration distances within the body [7].

Moving into the realm of the physical sciences, positrons have been used to probe various properties of ordinary matter. Positrons tend to migrate towards defects and voids in solids, where they can survive longer before annihilating with nearby electrons [8]. One technique, called positron annihilation lifetime spectroscopy (PALS), detects these defects and voids, as well as various surface properties, by measuring how long it takes for a positron to annihilate in a solid [9]. A scanning positron microscope takes this to the next step by moving a focused positron beam across the surface of the material to provide a 2D image of the lifetimes [10]. These techniques have the advantage that they are relatively non-destructive.

In the center-of-mass frame, when the electron and positron annihilate, they can leave two anti-parallel 511 keV gamma rays. In the laboratory frame, these photons will be Doppler shifted and have an angle less than 180° due to the momentum of the electron. In both condensed and gas phases, one can look at the energy and direction of the emitted gamma-rays to determine which orbitals the annihilated electrons were in. One can either measure the Doppler Broadening (DB), Angular Correlation of Annihilation Radiation (ACAR), or some combination of both. The DB technique was used in our lab to determine that positrons tend to annihilate with only valence electrons in free molecules [1, 11, 12].

Evidence of positrons can be found in cosmic rays, and they are believed to exist deep in space. This is confirmed by the presence of strong 511 keV radiation emitted from the center of the galaxy. The origin of these positrons and the nature of the material they are annihilating with are active areas of research [13, 14].

One exciting scientific pursuit is the production, trapping, and eventual spectroscopy of cold anti-hydrogen [15–18]. These atoms, composed of a positron and an anti-proton, should act just like hydrogen. If anti-hydrogen is any different from hydrogen, as determined by spectroscopy, for example, it would be a violation of *CPT*, a fundamental symmetry of nature required by most particle field theories. One group is trying to test

if anti-hydrogen has a different gravitational coupling than hydrogen [19]. The present experiments would not be possible without the positron accumulation and cooling technology developed in our lab.

Ultimately, as antimatter storage and manipulation technology improves, even more challenging applications will be possible. A sufficiently high density gas of positronium (Ps) atoms (i.e., each composed of a bound positron and electron) could form Ps molecules and even a Bose-Einstein condensate (BEC) [20]. Annihilation within this BEC could be exploited to produce a gamma-ray laser [21]. It has also been suggested for many years that antimatter would be the ideal rocket fuel. A review of the various antimatter propulsion schemes (which require *many* orders of magnitude more antimatter than has ever been stored before and generally appear to be far-fetched) can be found in Ref. [22].[1]

1.3 Positron interactions with free molecules

One particularly interesting area of research deals with the interaction of positrons with free atoms and molecules. In this limit, one can examine the nature of positron-matter dynamics at its most fundamental level. Using a Penning-Malmberg buffer gas trap, it is now possible to investigate these interactions with unprecedented positron energy resolution (~ 25 meV). This has helped elucidate a rich collection of phenomena which can occur during the brief encounter of a positron with an atom or molecule.

One process which makes positron interactions so unique is that of annihilation. A positron is figuratively speaking, a "ticking time bomb" when in the presence of electrons. During even the briefest interaction with a molecule, there is a chance that the positron will annihilate with an electron and produce two 511 keV gamma rays. This chance increases significantly if the positron becomes attached to the molecule. By looking at the annihilation rate as a function of positron impact energy, one can probe indirectly the state of the positron-molecule system immediately preceding annihilation.

[1] Note that at the moment, antimatter starships are still safely within the realm of science fiction.

The main focus of my thesis research is *vibrational Feshbach resonances* (VFR) and the positron-molecule bound states which support them. *A VFR occurs when an incident positron becomes temporarily bound to a molecule after resonantly transferring its excess energy into a vibrational mode of the molecule.* This leads to enhanced annihilation rates at specific energies, shifted below the energies of the vibrational modes by an offset, namely the positronic binding energy [23, 24]. In other words, the presence of a VFR indicates the existence of a positronic bound state and the energy of the VFR provides a measure of the binding energy. By examining binding energy and VFR magnitudes in a variety of molecules, one can better understand the internal dynamics of the positron-molecule complex.

Studies of positron-molecule interactions have been linked synergistically to advances in positron technology. For instance, recent cross section measurements have clarified why nitrogen and CF_4 make such good buffer gasses in positron accumulators [25, 26]. The very strong inelastic channels in these molecules help to slow down and thermalize positrons in the trap. On a related note, contamination with large hydrocarbons can result in measurable background annihilation. Because of this sensitivity, some have suggested that positron annihilation could even be used to measure very low pressures [27]. As theory improves and technology becomes cheaper and better, positron annihilation spectra could provide a complementary "fingerprint" which could be used to identify small quantities of a substance. For instance, adding nitrogen-containing functional groups to benzene increases its annihilation rate with thermal positrons by over an order of magnitude [1].

On a different note, positron-based processes present an important challenge to theorists. Quantifying positron-molecule interactions often requires re-examining all the approximations used to calculate electron-molecule interactions. Hence, this research may lead to a better understanding of both positron *and* electron behavior.

1.4 Outline of the dissertation

Chapter 2 provides some background information about positron-molecule interactions. It includes an abridged history of positron-molecule annihilation research, including several key experiments with thermal and energy-resolved positron beams. It shows how the annihilation rate measurements of Gilbert and Barnes, using energy-resolved positron beams, provide the best evidence to date that positrons bind to molecules via vibrational Feshbach resonances (VFR). Most of this thesis focuses on trying to better understand these resonances and their underlying bound states.

Also presented in chapter 2 is a theoretical framework for describing energy-resolved positron annihilation, due mostly to Gleb Gribakin (Queens University, Belfast). In particular, the VFR mechanism will be described as well as other important processes.

Chapter 3 discusses the experimental apparatus used in the current research. This includes a description of the positron source, moderator and the Penning-Malmberg trap used to accumulate and cool the positrons for energy-resolved annihilation experiments. The procedure for a typical annihilation measurement will also be described, along with a discussion of the various systematic and random errors.

Chapter 4 focuses on positron annihilation experiments with small and intermediate-sized molecules (e.g. those with one or two carbon atoms). These experiments led to the first successful, quantitative theory of annihilation in small molecules by Gribakin and Lee. In this chapter, this theory is extended in various ways to improve its applicability. However, it will become clear that certain molecules fall outside this theoretical framework. These molecules either have exceedingly large annihilation resonances or no resonances at all. The former will be referred to as "large" or enhanced-Z_{eff} molecules, while the latter will be termed VFR-weak or -inactive molecules. At the end of this chapter, there is a brief discussion of other features, besides VFR, that can be found in the annihilation spectra of small molecules, as well as speculation regarding the physical requirements for positron binding.

Chapter 5 focuses on understanding annihilation and binding trends in larger mole-

cules. For these molecules, there is, as yet, no quantitative model for the VFR-mediated annihilation that is observed. One goal of the present measurements is to tease apart the roles of positronic binding energy, molecular structure and size, and other physical parameters. It is shown that the magnitude of the annihilation resonances depends only weakly on positron binding energy and much more strongly on the number of vibrational degrees of freedom. Some unusual behavior in fluoroalkanes, first noticed several years ago, is explained and other phenomena, such as multi-mode VFR, are also discussed. Finally, the possible origins of positron binding energy are examined.

Chapter 6 recapitulates our current understanding of positron annihilation in molecules. The present results are summarized, and some important open questions are posed. A number of future avenues of research are also discussed.

Chapter 2

Background

Positrons and electrons have many similar interactions with atoms and molecules. Like the electron, a positron can undergo elastic collisions, electronic and vibrational excitation collisions, direct ionization, and fragmentation collisions. These ordinary interactions with a molecule AB in vibrational state ν can be depicted as,

$$e^+ + AB(\nu) \rightarrow e^+ + AB(\nu) \quad \text{(elastic)} \tag{2.1}$$

$$e^+ + AB(\nu) \rightarrow e^+ + AB(\nu') \quad \text{(vibrational excitation)} \tag{2.2}$$

$$e^+ + AB(\nu) \rightarrow e^+ + AB^*(\nu') \quad \text{(electronic excitation)} \tag{2.3}$$

$$e^+ + AB(\nu) \rightarrow e^+ + e^- + AB^+(\nu') \quad \text{(direct ionization)} \tag{2.4}$$

$$e^+ + AB(\nu) \rightarrow e^+ + A^- + B^+ \quad \text{(fragmentation)} \tag{2.5}$$

Each of these reactions has the same impact energy thresholds as for electrons. For instance, vibrational excitation occurs only if the positron energy is greater than that of a vibrational quantum. Ionization occurs only if the positron energy exceeds the ionization energy E_i. However, because the positron is the antiparticle to the electron, there are additional interactions. In particular, a positron can pick off an electron and form a bound state, known as a positronium atom (Ps):

$$e^+ + AB(\nu) \rightarrow \mathrm{Ps} + AB^+(\nu') \quad \text{(positronium formation)} \tag{2.6}$$

This process can occur if the incident positron energy is greater than $E_i - 6.8$ eV, where 6.8 eV is the binding energy of Ps. For most of the molecules studied here, this is the first channel to open after vibrational excitation. If $E_i < 6.8$ eV, the positronium channel is always open, as is the case for alkali atoms. A good review of these interactions can be found in Refs. [25, 28–30].

There is one last type of interaction: annihilation. In this situation, the positron annihilates with an electron still on the molecule, usually producing two antiparallel 511 keV gamma rays:

$$e^+ + AB(\nu) \rightarrow 2\gamma + AB^+(\nu') \quad \text{(annihilation)}. \tag{2.7}$$

This process is far more rare but particularly intriguing. An important subcategory of this process is resonant annihilation, in which the positron forms a temporary bound state with the molecule. The nature of this particular interaction, including its magnitude and energy dependence, is the subject of this thesis.

2.1 Annihilation rates

The positronium atom is a nice starting point for understanding annihilation. It can occur in the spin-aligned triplet state called orthopositronium (o-Ps) or the anti-aligned singlet state called parapositronium (p-Ps). The former has a lifetime of 142.0 ns and decays into three gamma rays with a total energy of 1022 keV.[1] The latter has a much shorter lifetime of 125.1 ps and decays into two anti-parallel 511 keV gammas.

In positron-molecule collisions at energies less than the positronium threshold, $E_i - 6.8$ eV, it is not possible to remove an electron and form free positronium. Nonetheless, the annihilation channel may still occur during the brief time of positron-molecule interaction. In this case, the short-lifetime 2γ process dominates. The spin averaged 2γ annihilation cross section for positron-electron scattering has a simple form, due to

[1] Note the triplet lifetime is reduced considerably in a magnetic field, due to spin mixing [31]

Dirac [2]:

$$\sigma_{2\gamma} = \pi r_0^2 c/v \tag{2.8}$$

where r_0 is the classical electron radius (derived by finding the distance at which the energy associated with the electron rest mass equals the electric potential energy between two electrons), c is the speed of light, and v is the impact velocity.

As a matter of convention, the annihilation cross section for molecules or atoms, σ_a, is described in terms of a dimensionless parameter Z_{eff},

$$Z_{\mathit{eff}} = \sigma_a/\sigma_{2\gamma} = \frac{\sigma_a v}{\pi r_0^2 c}. \tag{2.9}$$

The original thinking was that, in some limit, the electrons in the molecule would act as a free electron gas, so that Z_{eff} would be close to Z, the total number of electrons in the atom or molecule [32]. As it turns out, Z_{eff} can be orders of magnitude larger than Z. As discussed in a later section, a more accurate description is that Z_{eff} is proportional to the positron-electron overlap density.

2.2 Trends in thermal Z_{eff}

Early investigations were limited to measuring Z_{eff} in a thermalized distribution of positrons and atoms or molecules (e.g. at 300 K). In the earliest experiments, the test species itself was used as a moderator, slowing down fast positrons from a radioactive source. In such an experiment, a sodium-22 atom would decay, producing a positron and a "prompt" 1.28 MeV gamma; the positrons (with a broad spectrum of energies up to 500 keV) would rapidly thermalize with the test gas and then annihilate. The annihilation rate could be derived from the distribution of delay times between the "prompt" gamma and a 511 keV gamma. In a seminal experiment, Paul and Saint-Pierre showed that thermal Z_{eff} were orders of magnitude larger than Z in the alkanes [33]. Furthermore, they found that Z_{eff} grew with molecular size. This led to speculation that the positron and molecule could form attached states [33–35].

Later experiments used trapped, room-temperature positrons in a Penning-Malmberg buffer-gas trap. In this arrangement, there is no need to thermalize with the test gas. Instead, the test gas is introduced into an already thermalized collection of positrons (about 10^6) in the final stage of the trap. Thermal Z_{eff} could then be derived from the decay in the measured annihilation signal as a function of time. Since much lower gas pressures could be used, it was possible to eliminate three-body effects. These experiments were performed over a much broader range of molecules, revealing many interesting behaviors [36–38]. A good review of these results can be found in Koji Iwata's thesis [1].

Fig. 2.1 shows a plot of thermal Z_{eff}/Z vs. Z from Ref. [1]. As one can see, Z_{eff} can be up to four orders of magnitude larger than the number of electrons, Z, on the target. The growth of Z_{eff} with molecular size, first observed by Paul and St. Pierre [33] in alkanes (simple hydrocarbon chains of the form C_nH_{2n+2}), occurs in many other species. However, there is also a strong chemical sensitivity. For instance, the perfluorinated alkanes and noble gases have smaller values of Z_{eff}, much closer to Z [1].

Long before the buffer gas trap, Smith and Paul had speculated that the large annihilation rates seen in polyatomics could be due to vibrational resonances [39]. The first major publication on the buffer-gas trap gave further credence to this idea, providing a simple model for resonant positron-molecule annihilation in alkanes [35]. Drawing from more recent experimental results, Gribakin developed a robust theoretical framework for this process [23,38,40]. However, with room temperature positrons one could only study implicitly the energy-dependent structure predicted by theory. To solve this problem, an adapted Penning-Malmberg trap was constructed that could be used to produce tuneable monoenergetic positron beams [41,42]. This apparatus made it possible to measure positron-molecule interactions as a function of incident positron energy.

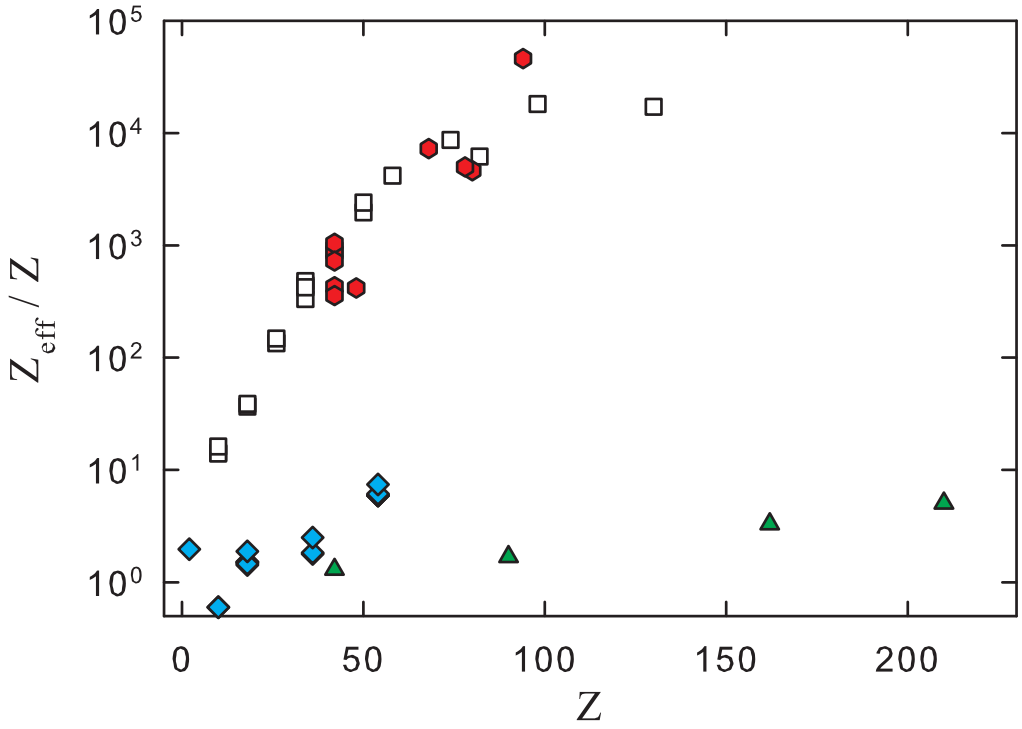

Figure 2.1: Thermal Z_{eff}/Z vs. Z measured using a thermal distribution of positrons in the final stage of a buffer-gas trap (from Ref. [1]). Results are shown for alkanes (□); aromatic molecules (red hexagons); noble gases (cyan ⋄); and perfluorinated alkanes (dark green △).

2.3 Energy-resolved Z_{eff}

Among the first experiments performed with the cold positron beam were energy-resolved measurements of Z_{eff} for various alkanes [24,43]. These measurements revealed a startling amount of structure. Shown in Fig. 2.2 is the energy-resolved Z_{eff} spectrum for butane (C_4H_{10}). This spectrum has clear structures which are strongly correlated with the energies of the vibrational modes. In particular, there is a peak at ~ 320 meV which is about 35 meV below the C-H stretch vibrational mode at 355 meV (or 2850 cm^{-1}). For this reason we refer to it here as the C-H stretch peak. A similar peak can be found in deuterated butane (C_4D_{10}), 35 meV below the C-D stretch mode. It should be noted that neither of these molecules have features above 400 meV. In other words, high-energy overtone and combination mode resonances are largely absent.

This is exactly the behavior predicted by the resonant annihilation model of Gribakin [23]. However, his treatment did not recognize that there would be distinct peaks due to fundamental vibrations and observable downshifts in the peak energies due to the positron-molecule binding energy. Each Z_{eff} peak is the result of a *vibrational Feshbach resonance* (VFR) mediated by a positron-molecule bound state. When the positron has just the right energy, it can excite a vibrational quantum in a molecule and drop into a bound state of depth ϵ_b. Once bound to the molecule, the positron has a greatly enhanced probability of annihilation with the molecular electrons due to strong positron-electron overlap. Naturally, *this requires that such a bound state exists.* This process is illustrated by the cartoon shown in Fig. 2.3. The result is a large Z_{eff} peak shifted below the energy of the vibrational quantum by the binding energy ϵ_b. In this context, the low energy Z_{eff} plateau in butane corresponds to C-H bend and C-C modes. The breadth of the peaks is entirely due to the energy distribution of the positron beam [44].

As shown in Fig. 2.4, a number of interesting trends were observed when comparing alkane spectra [24]. Similar to the thermal Z_{eff}, the C-H stretch peak grows exponentially with the size of the molecule. Furthermore, the shift due to binding energy grows by ~ 20 meV with each additional carbon atom, while the overall spectrum maintains the

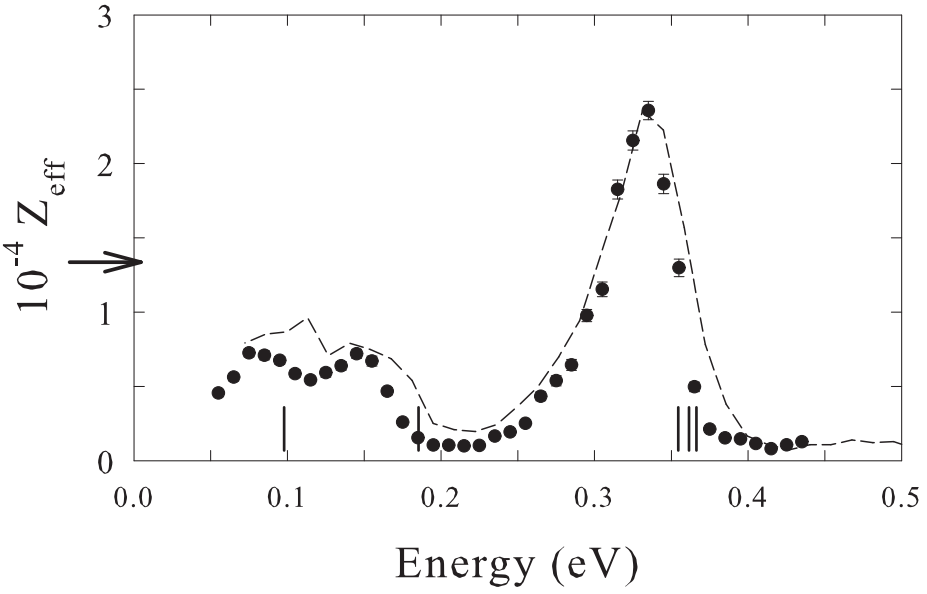

Figure 2.2: Energy-resolved Z_{eff} for (•) butane and (- -) scaled d-butane from [24]. The d-butane energy is scaled empirically by a factor nearly equal to the ratio of C-H and C-D stretch mode energies (after correcting for binding). The magnitude of this curve is normalized arbitrarily. The arrow on the ordinate indicates the thermal Z_{eff} for butane. The vertical bars at the bottom indicate the energies of fundamental vibrational modes. See Ref. [24] for details.

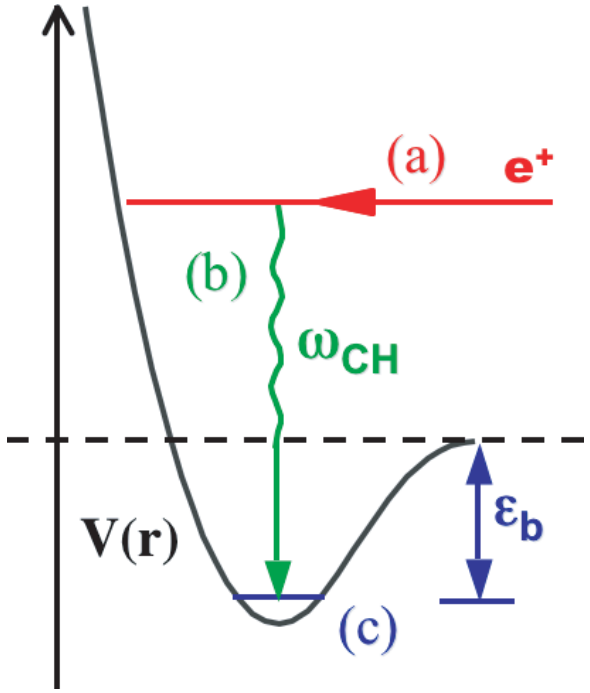

Figure 2.3: A cartoon of the VFR model consisting of three steps: (a) the positron approaches the molecule along coordinate r with energy $\omega_\nu - \epsilon_b$; (b) the positron excites a molecular vibration of energy ω_ν; and simultaneously, (c) the positron drops into a positron-molecule bound state of depth ϵ_b where it may annihilate with molecular electrons. Note that this is merely a qualitative representation of the interaction which ignores all other degrees of freedom outside of the positron approach coordinate r.

same shape. In all cases, the C-H stretch peak appears to dominate over the low energy peaks, and only the fundamental modes appear to participate. As a result, there are no features above 400 meV or in the gap between the highest energy C-H bend mode VFR and the C-H stretch mode VFR (e.g. 200-250 meV in butane).

In small molecules these resonant behaviors are frequently less clear-cut [24, 43]. Molecules like partially fluorinated methanes, acetylene, and ethylene have much smaller VFR peaks. The relative magnitudes of the high and low energy peaks are no longer fixed, and low energy peaks tend to dominate. Some molecules, like methane and CF_4,

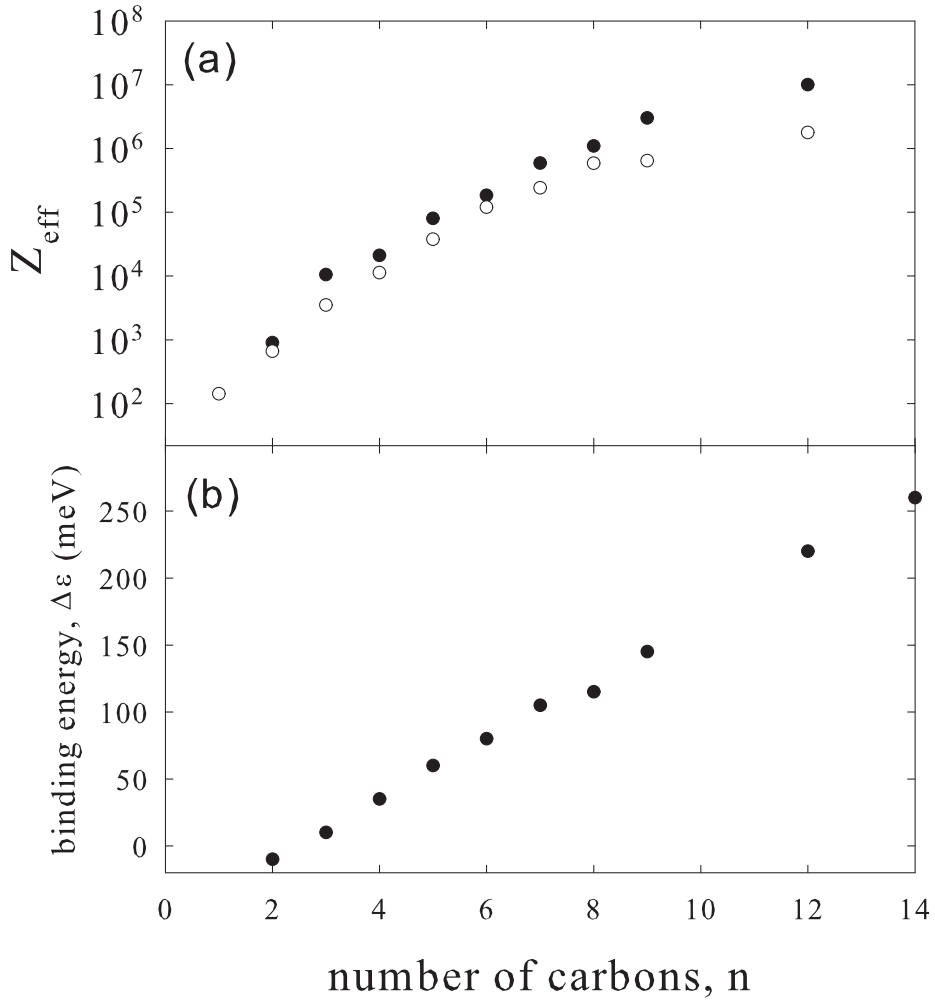

Figure 2.4: Trends in alkane molecules (C_nH_{2n}). (a) The (○) thermal and (●) C-H stretch peak Z_{eff} vs. the number of carbon atoms, n; and (b) the binding energy (as determined by C-H stretch peak energy shift) vs. the number of carbons. Note that ethane ($n = 2$) has an apparent negative binding energy because its C-H stretch peak occurs slightly above the C-H stretch mode energy.

appear to have no resonant peaks at all. Even more puzzling is the dramatic suppression in Z_{eff} observed in large molecules like 1-fluorohexane and 1-fluorononane [43, 45]. The C-H stretch peaks in these molecules are two or more times smaller than those in the analogous non-fluorinated alkanes.

This research, undertaken primarily by Gilbert and Barnes, led to a number of new questions. For instance, what determines the relative peak heights and binding energies? Why do small molecules act differently than large molecules? How can Z_{eff} grow so rapidly with size? While Gribakin's theoretical framework described the general annihilation phenomenon quite well, there were few quantitative predictions. Also, with few studies of large molecules other than the alkanes, it was difficult to construct robust empirical laws. The research presented in this dissertation addresses these issues.

2.4 Annihilation theory

As mentioned before, the annihilation rate is typically expressed in terms of the parameter Z_{eff} [32]. This represents the probability that an electron and positron can be found in the same location, within an atomic or molecular target. It can be written (c.f. Ref. [46]),

$$Z_{eff} = \int \sum_{i=1}^{Z} \delta(\mathbf{r} - \mathbf{r}_i) |\Psi(\mathbf{r}_1, ..., \mathbf{r}_Z, \mathbf{r})|^2 d\mathbf{r}_1 ... d\mathbf{r}_Z d\mathbf{r}, \tag{2.10}$$

where Ψ is the overall positron-electron wave function, $\mathbf{r}$ is the positron coordinate, and $\mathbf{r}_i$ is the coordinate of one of the target electrons. Note that, if the interaction with the positron and target is ignored (i.e., the positron is described by a plane wave), this integral approaches Z, the total number of electrons. This is the result expected for a free electron gas. The proper determination of Z_{eff} requires knowledge of Ψ. The following sections summarize a derivation of this quantity by Gribakin [23, 40].

2.4.1 Direct annihilation

To lowest order, outside the molecule, Ψ separates into the positron wave function and the electronic wave function of a neutral molecule, Φ_0. The positron wave function can be written as a sum of incident and scattered waves, so that the combined wave function is,

$$\Psi_0(\mathbf{r}_1, ..., \mathbf{r}_Z, \mathbf{r}) = \Phi_0(\mathbf{r}_1, ..., \mathbf{r}_Z) \left[e^{i\mathbf{k}\cdot\mathbf{r}} + f(\Omega)\frac{e^{ikr}}{r} \right], \tag{2.11}$$

where $f(\Omega)$ is the positron scattering amplitude as a function of the outgoing angular coordinates Ω. The "direct" annihilation rate can be found by inserting this expression into the equation for Z_{eff},

$$Z_{eff}^{(dir)} = \langle \Psi_0 | \sum_{i=1}^{Z} \delta(\mathbf{r} - \mathbf{r}_i) | \Psi_0 \rangle. \tag{2.12}$$

This describes a so-called "pick-off" annihilation, which occurs during the course of an ordinary scattering event as a result of the temporary overlap of the positron and electron wave functions. In order to complete this calculation, one must first know what happens to the positron wave function close to the molecule. Because of the strong nuclear repulsion, the positron cannot penetrate deeply into the electronic core of the target. As a result, the positron-electron overlap occurs primarily within a shell on the "surface" of the molecule. If the shell has radius R, thickness δR, and electron density ρ_e, and the positron momentum is small [23],

$$Z_{eff}^{(dir)} \approx 4\pi\rho_e\delta R(R^2 + \sigma_{el}/4\pi + 2R\mathrm{Re}f_0), \tag{2.13}$$

where

$$\sigma_{el} = \frac{4\pi}{k^2 + \kappa^2}. \tag{2.14}$$

In these expressions, σ_{el} is the elastic cross section, f_0 is the s-wave scattering amplitude, and κ is the inverse scattering length, which must be small for this expression to be valid. Note that if $\kappa > 0$, the positron forms a weakly bound state with binding $\epsilon_b = \kappa^2/2$, whereas if $\kappa > 0$, the positron produces a virtual state [47]. The first term in $Z_{eff}^{(dir)}$ is due to "pick-off" annihilation with the incident positron, the second is due to the scattered

wave, and the last is due to the interference between these processes. At low energies, the elastic scattering term is expected to dominate.

Note that higher order scattering terms have been omitted in the above expression. These terms may be nontrivial in some molecules, especially if one includes polarization of the target. The $\rho_e \delta R$ factor can be estimated by comparison with more rigorous calculations of this process in atoms [40, 48]. All told, however, it is not possible to achieve a Z_{eff} larger than about a thousand with only direct annihilation (assuming room temperature positrons) [23]. Experiments in our lab are consistent with this estimate [24].

2.4.2 The Vibrational Feshbach Resonance

As discussed earlier, one way to achieve large Z_{eff} is via a vibrational Feshbach resonance. This is introduced in the theory by allowing a coupling, V, to the nuclear degrees of freedom, resulting in an additional perturbation to the positron-electron wave function [23]:

$$|\Psi\rangle = |\Psi_0\rangle + \sum_{\nu} \frac{|\Psi_\nu\rangle\langle\Psi_\nu|V|\Psi_0\rangle}{\epsilon - \epsilon_\nu + (i/2)\Gamma_\nu}. \tag{2.15}$$

Each Ψ_ν describes a bound positron and molecule in the ν^{th} vibrational state. The perturbation term is strongest when the energy of the positron ϵ is close to a resonance energy, ϵ_ν. The factor Γ_ν describes the total width of the resonance due to the lifetime of the bound state. It includes the annihilation width, Γ^a_ν, and the elastic scattering width, Γ^e_ν (i.e. the resonant capture or re-emission width). Note that the total wave function, Ψ_ν, must now include the nuclear degrees of freedom.

Inserting this wave function into the expression for Z_{eff} results in some important extra terms:

$$\begin{aligned} Z_{\mathit{eff}} &= \langle\Psi_0|\sum_{i=1}^{Z}\delta(\mathbf{r}-\mathbf{r}_i)|\Psi_0\rangle + (\text{interference terms}) \\ &\quad + \sum_{\nu\mu} \frac{\langle\Psi_0|V|\Psi_\nu\rangle\langle\Psi_\nu|\sum_{i=1}^{Z}\delta(\mathbf{r}-\mathbf{r}_i)|\Psi_\mu\rangle\langle\Psi_\mu|V|\Psi_0\rangle}{[\epsilon-\epsilon_\nu-(i/2)\Gamma_\nu][\epsilon-\epsilon_\mu+(i/2)\Gamma_\mu]}. \end{aligned} \tag{2.16}$$

As expected, the first term is the direct Z_{eff}. The remainder of the expression can be further simplified by recognizing that the off-diagonal terms ($\mu \neq \nu$) are negligible.

Also, the interference terms are expected to average to zero when a broad experimental energy distribution is assumed (which is appropriate for the experiments conducted to date). The last term can then be defined as $Z_{eff}^{(res)}$, the resonant annihilation due to a vibrational Feshbach resonance.

At this point, it is useful to define the annihilation width, Γ_ν^a, and elastic width, Γ_ν^e. As one might expect, the resonant annihilation rate has a similar form to the non-resonant rate:

$$\Gamma_\nu^a = \sigma_{2\gamma} v \rho_{ep}^\nu = \pi r_0^2 c \rho_{ep}^\nu, \tag{2.17}$$

where

$$\rho_{ep}^\nu \equiv \langle \Psi_\nu | \sum_{i=1}^{Z} \delta(\mathbf{r} - \mathbf{r}_i) | \Psi_\nu \rangle. \tag{2.18}$$

Actually calculating this rate is difficult without knowing the bound state wave function of the positron. One can estimate crudely that Γ_ν^a is on the order of 1 μeV based on the overlap density of positronium [23]. A better estimate will be provided in a later chapter. For s-wave scattering, that elastic rate also has a simple form [23]:

$$\Gamma_\nu^e = \frac{k}{\pi} |\langle \Psi_0 | V | \Psi_\nu \rangle|^2. \tag{2.19}$$

Calculations of this factor will be motivated by the research in this thesis. The final form for the resonant part of Z_{eff} is a series of Breit-Wigner resonances. Assuming the experimental energy distribution $f(\epsilon)$ is much broader than the natural line widths Γ_ν,

$$Z_{eff}^{(res)} = \frac{2\pi^2}{k} \sum_\nu \left(\frac{\rho_{ep}^\nu \Gamma_\nu^e}{\Gamma_\nu^e + \Gamma_\nu^a} \right) f(\epsilon - \epsilon_\nu) = \frac{2\pi^2}{k} \left\langle \frac{\rho_{ep}^\nu \Gamma_\nu^e}{D(\Gamma_\nu^e + \Gamma_\nu^a)} \right\rangle. \tag{2.20}$$

The brackets denote averaging due to the experimental resolution. When there are many resonances within the experimental width, the resonance is enhanced by $1/D$ where D is the spacing of the resonant states ν. In this form, the process leading to enhanced annihilation is apparent. The positron is captured into resonance ν at the rate Γ_ν^e. It can then either annihilate or escape. The probability of annihilation is $\Gamma_\nu^a/(\Gamma_\nu^e + \Gamma_\nu^a)$. It turns out that if $\Gamma_\nu^e \gg \Gamma_\nu^a$, and D^{-1} is large, it is possible to get resonant annihilation rates which are much larger than the direct rate [23].

2.4.3 Enhanced Z_{eff}

In energy-resolved spectra of large alkane molecules, only fundamental modes appear to produce resonances. According to the above model, that would mean that Z_{eff} should rise only linearly with molecular size, not exponentially as in Fig. 2.4. This apparent discrepancy can be addressed if the large number of multi-mode states, which increases rapidly with molecular size, can somehow be made accessible.

One way to do this is to employ a model in which positron capture occurs primarily through so-called "doorway" states (e.g. due to the fundamental vibrations) [49]. These states are then coupled to a much larger bath of multi-mode states, ν, within some spreading width Γ_{spr}. These "bath" states are not accessible by direct VFR, and are termed "dark" states. To lowest order, the initial vibrational energy irreversibly "spreads" into these additional states in a characteristic time $1/\Gamma_{spr}$. This process is called *intramolecular vibrational redistribution* (IVR).

One result of this process is that an isolated single-mode VFR can be enhanced by the number of multi-mode bath states within a spreading width of the resonance. In other words, if ρ_b is the density of bath states, $\rho_b\Gamma_{spr}$ is the enhancement. In fact, it has been shown that if all vibrational states are included, and $\Gamma^e_\nu \sim \Gamma_\nu$, Z_{eff} grows far too rapidly with molecular size in the alkanes [49]. One solution to this problem is to reduce the number of bath states. Another is to require $\Gamma^e_\nu < \Gamma_\nu$ for a significant fraction of states. Presently, there is no way to tell which, if either of these possibilities, is correct.

There may be other ways to achieve large Z_{eff}. Enhanced annihilation could be attributed to the electronic rather than the vibrational properties of the molecule. The thermal Z_{eff} values for a number of species seem to follow empirical scaling law based on the ionization energy of the molecule E_i [1, 38]:

$$\log Z^{(th)}_{eff} \sim \frac{A}{E_i - 6.8\text{eV}} + B. \tag{2.21}$$

Laricchia and Wilkin suggested that this effect was due to virtual positronium formation [50, 51]. However, it was later shown that their mechanism does not produce the right scaling [52]. Furthermore, this model does not take into account the rich vibrational

energy dependences later discovered in energy-resolved annihilation experiments. Still, the influence of electronic degrees of freedom cannot be entirely dismissed without better evidence for IVR. One goal of this dissertation is to provide this evidence.

2.4.4 Suppressed Z_{eff}

Some molecules have surprisingly small values of Z_{eff}. A single fluorine substitution in an alkane appears to have a dramatic effect. The C-H stretch peaks of 1-fluorohexane and 1-fluorononane are much smaller than those of hexane and nonane respectively [43]. This is in spite of their similar vibrational structure and infrared absorption spectra [45]. A proper investigation of Z_{eff} enhancement would be incomplete without an investigation of Z_{eff} suppression. As it turns out, the latter provides clues to the former.

2.4.5 Binding

While there are many models for determining positron binding to atoms, determining binding to polyatomic molecules has so far proven much more difficult [53]. A big problem is that, unlike an electron, the positron does not experience an exchange interaction. As a result, it does not fall into a predictable orbital, orthogonal to the other filled electronic orbitals. Instead, it is strongly correlated with the outer electrons of the target and would be correlated with the inner electrons too were it not for the repulsion of the nuclei. Furthermore, it can form virtual positronium. As a result, many of the assumptions made to simplify typical electron-molecule interactions must be tossed aside. At best, one can assume a fixed core, as is done in many atom calculations [53]. That still leaves the computationally challenging problem of determining the interaction of a positron with (typically several) valence electrons in a fixed external field. The end result is that there are few exact results to compare with experiment. In the current research, experimentally measured binding energies in various molecules are examined in attempt to understand general behaviors. Some qualitative models will also be discussed.

Chapter 3

Experimental Methods

In this chapter, the techniques used for measuring energy resolved positron-on-molecule annihilation are discussed. Crucial to these measurements is the ability to produce cold, energy-tuneable pulses of positrons. This is done by taking positrons from a radioactive decay process, slowing them to electron-Volt energies using solid neon, then trapping and cooling them in a Penning-Malmberg buffer-gas trap. Since the apparatus which performs this essential process was, for the most part, completed prior to the research described in this dissertation, the discussion of its operation and important design elements will be abridged. More detailed information on positron trapping and manipulation techniques can be found in Refs. [24, 41, 42, 54].

3.1 Positron source and moderator

Positrons can be produced in a number of ways. They can be produced by pair production during collisions of accelerated electrons with a high-Z material [55]. They can also be produced during interactions with intense laser fields [56]. However, the simplest and cheapest way to get positrons is from radioactive isotopes. Such isotopes can either be created *in situ* or be provided by an outside vendor. In our lab, a pre-packaged 50 mCi sodium-22 (^{22}Na) source is used. The dominant decay process (90.5

%) for this isotope is,

$$^{22}\mathrm{Na} \rightarrow ^{22}\mathrm{Ne} + e^{+} + \nu_e + \gamma(1.28\mathrm{MeV}), \tag{3.1}$$

where the ν_e is an electron neutrino and the γ is a photon, usually called the "prompt" gamma. This photon is frequently used in time-resolved experiments to signal that a positron has been produced. Sodium-22 has a number of advantages over other isotopes. Its half-life is 2.6 years, which means that it can be used continuously for several years. For the earlier experiments in this dissertation, a 150 mCi ^{22}Na from 1997 was used. In 2005, this was replaced by 50 mCi from iThemba Labs [57]. To avoid this constant replacement, some groups have been working on *in situ* production of positron-emitting isotopes (c.f. Refs. [55, 58, 59]).

Another advantage of ^{22}Na is its favorable branching ratio. Over 90% of all decays produce positrons. The rest are mostly electron-capture processes which result in X-rays or Auger electrons. Furthermore, in ^{22}Na there is less absorption of the positrons within the material than in many other isotopes.

There is an art to the construction of a "good" positron source. If the isotopic material is too thick or the cover window is too thick, most of the positrons will be converted to 511 keV gamma rays before leaving the source. For this reason, the window and the layer of isotope must be as thin as possible, which makes the manufacturing process especially difficult. One must also contend with the fact that the positrons are emitted isotropically. To reflect a decent fraction of the backwards flux, our source is mounted on an elkonite rod.

The next issue to tackle is the energy spread of the positrons, which typically have hundreds of keV in energy. The solution to this problem is to use a "moderating" material. These materials work by thermalizing the positrons first via ionization and hole creation, and then by phonon creation [1]. Reflection or transmission through thin metal films such as tungsten can achieve sub-eV energy spreads. However, around 99.9% of the original positron flux is lost. Moderators made of solid noble gases have a far superior efficiency of about 2.6%, while producing beams with modest eV (electron

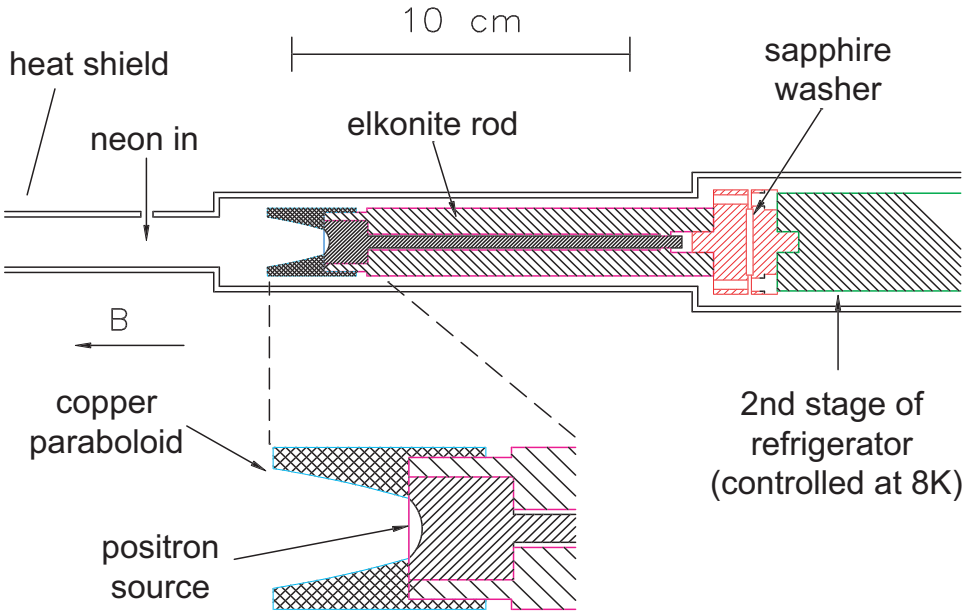

Figure 3.1: A schematic of the positron source assembly from Ref. [1].

Volt) widths [60]. In our lab, a solid neon moderator is used.

In order to grow a layer of solid neon, the source is cooled to low temperatures. To achieve this, the source is mounted on the cold finger of a closed-cycle He refrigerator. The experimental setup is shown in Fig 3.1. For good efficiency, the neon is deposited on a parabolic copper substrate with the source at the apex [1,61]. The source, elkonite rod, and cold finger are enclosed in a heat shield and kept at an ambient pressure of $\sim 1 \times 10^{-7}$ torr.

The process for growing and maintaining the neon crystal has evolved over time. Originally, neon gas was introduced into the source chamber at a low, constant pressure, and the crystal was allowed to grow over the course of a few hours at 7 K. Sometimes two consecutive "layers" were grown in this way. These moderators would be "cured" overnight to reach full efficiency. At the suggestion of Rod Greaves, we switched to a faster growth cycle. The current process begins by first heating the cold finger to between

50 and 80 K to remove the previous moderator and some contaminants. After pumping down and cooling to 8 K, about 3×10^{-3} torr of neon is introduced into the chamber for 1-3 minutes. Then the neon valve is shut off, and the cold head is allowed to adsorb the remaining neon. Sometimes a second layer is grown like this, depending on the outcome of the first growth. A typical plot of temperature, pressure, and moderated positron flux vs. time is shown in Fig. 3.2. With the present source, it is possible to get 4-6 million moderated positrons per second using this procedure.

There is still much to be learned about this moderator growth process. Presumably there is some ideal layer depth and crystal quality that needs to be achieved. Annealing and levels of contamination are likely important factors. The efficiency and lifetime of moderators grown under apparently similar conditions can vary greatly. The typical moderator can last anywhere from a few days to a couple weeks. Usually they decay gradually in efficiency, but occasionally they "die" completely.

3.2 The Buffer Gas Trap

The moderator is forward-biased to 28 V to give the positrons a sizeable transport energy. Positrons escaping from the moderator are confined radially by a magnetic field of ~ 150 G and guided into a Penning-Malmberg buffer-gas trap (BGT). This apparatus is used to trap and cool the positrons to room temperature, then eject them at regular intervals. A thorough discussion of this device can be found in Refs. [24, 41, 42, 54]. As illustrated in Fig. 3.3, it consists of a series of cylindrical electrodes that can produce various confining potentials in the axial direction, aligned with the axis of a uniform magnetic field. Spatially varying pressures of nitrogen and CF_4 buffer gasses slow the positrons down, resulting in trapping and cooling.

Since the BGT is a pulsed device, it is run in several electrostatic "phases," also shown in Fig. 3.3. During the initial "fill" phase, there are three, ~ 10 V downward steps forming a potential well. Inelastic collisions with the buffer gas slow the moderated positrons down until they are trapped at the bottom of this well. The step heights and

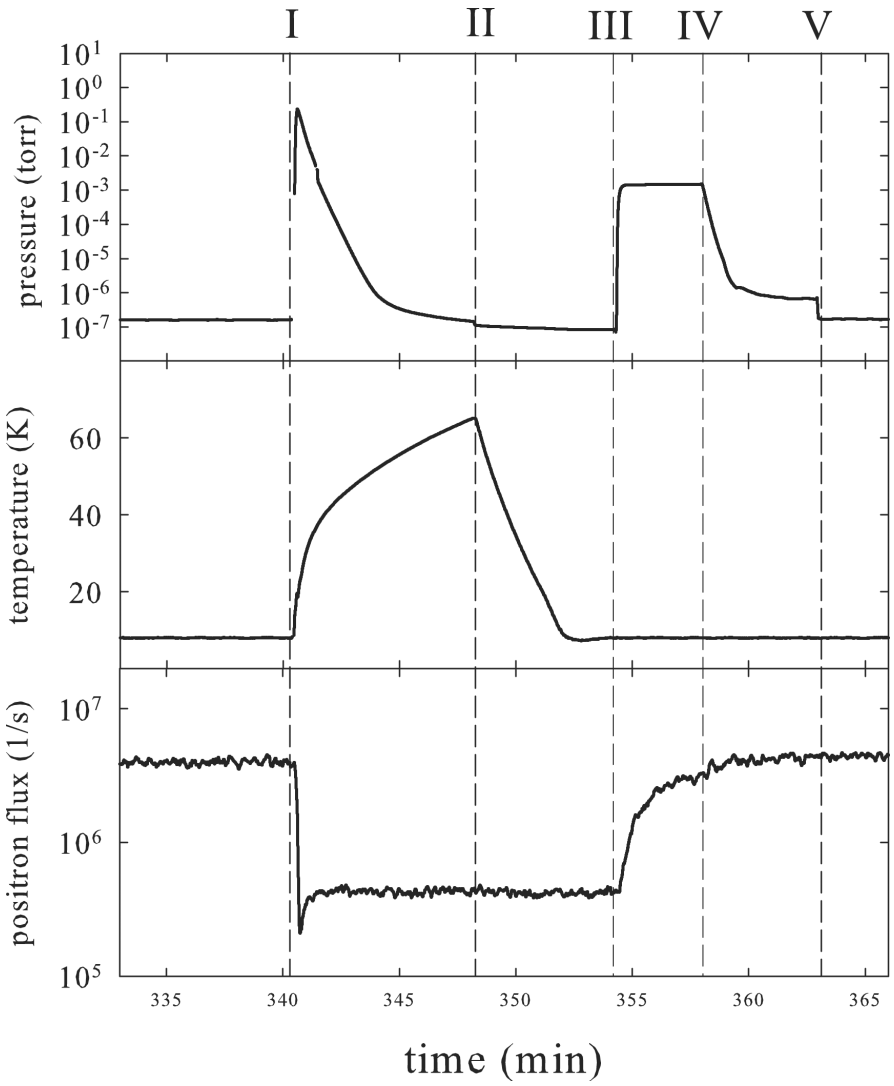

Figure 3.2: A typical moderator growth cycle. The vertical dashed lines, labeled by roman numerals, indicate important events in the cycle: (I) First the old moderator must be blown off by heating the cold finger to 65 K while evacuating the chamber using a diaphragm pump. (II) Then the ion pump is switched on, and the cold finger is cooled down to 8 K. (III) Now the moderator growth begins. The ion pump is switched off and $\sim$ 3 μtorr neon is introduced through an inlet close to the source cone. Note the rapid increase in positron current from the moderator. (IV) After a few minutes, the neon is shut off, and the remaining gas is allowed to adsorb on the source cone. (V) Finally, the solid neon moderator is ready, and the ion pump can be switched on again.

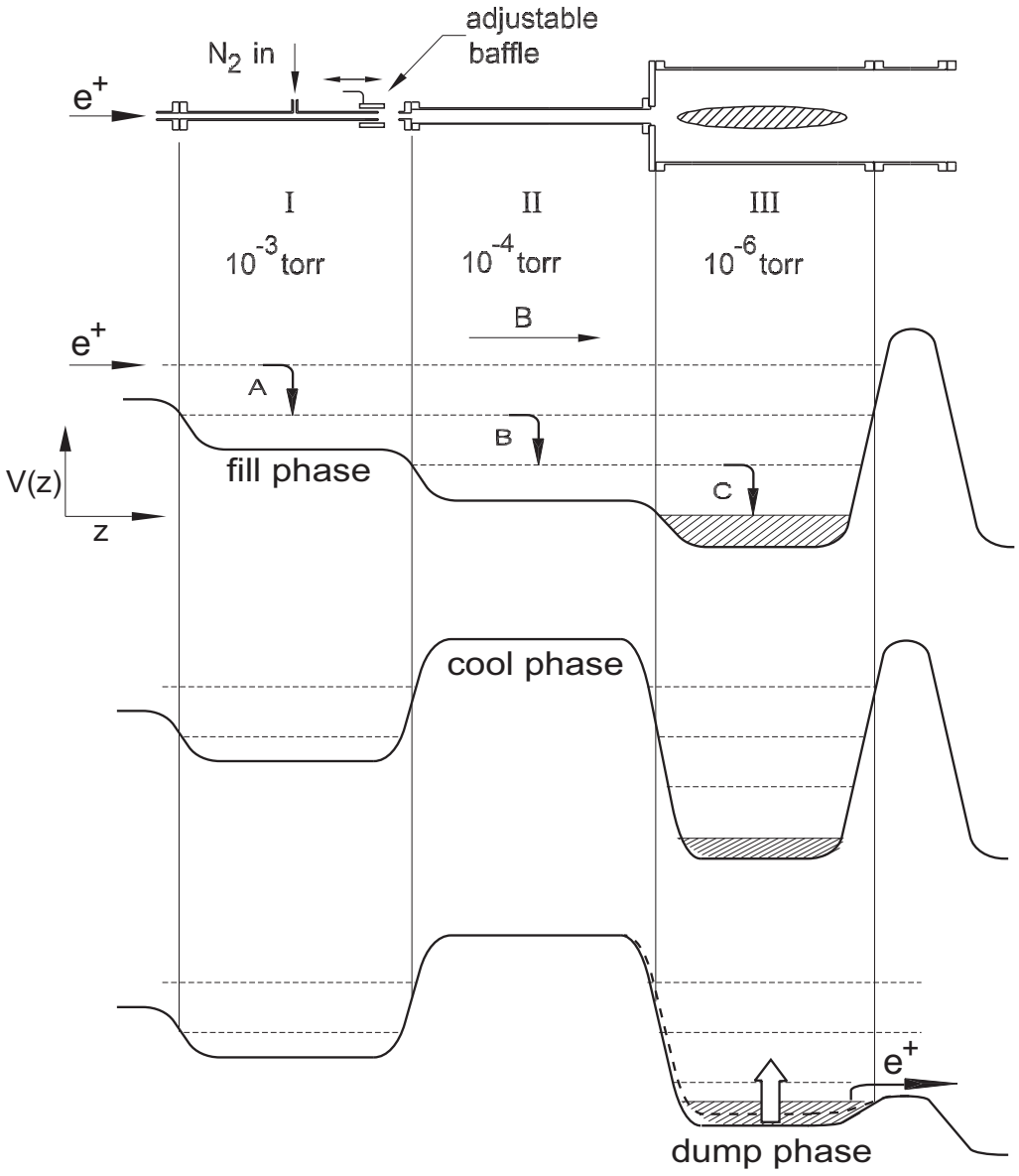

Figure 3.3: On top is a schematic diagram of the Penning-Malmberg buffer gas trap from Ref. [62]. Below is a representation of the electrostatic potential for each of the phases described in the text. In the filling phase, A, B, and C represent consecutive inelastic collisions of positrons with the buffer gas. In the cooling phase, the positrons are isolated in the stage III electrodes. In the dump phase, the electrostatic barrier on the right is reduced to the desired transport voltage V_a, then the well voltage is raised to eject the positrons.

the pressure profile were chosen empirically to maximize the inelastic interactions with the buffer gas while minimizing loss processes such as positronium (Ps) formation. It was later discovered that 10 eV is very close to the energy where the electronic excitation cross section exceeds the positronium formation cross section in N_2 [25, 26, 30]. The duration of this "fill" phase determines the number of positrons accumulated in the well.

Cryopumps on either side of the BGT provide differential pumping of the buffer gasses. The trap electrodes have increasing diameters, so that the nitrogen pressure is highest nearest to the moderator and lowest near the bottom of the electrostatic well. As a result, the opportunities for annihilation and other collision-induced losses are reduced as the positrons become trapped.

In the next phase, "cooling," one of the electrostatic "steps" is replaced by an electrostatic barrier, which further confines positrons accumulated in the well and blocks further positron flux from the moderator. The positrons are now allowed to thermalize to the electrode temperature. This is aided by collisions with CF_4 gas, introduced from just outside the well. As later discovered [29], this molecule has a huge inelastic vibrational cross section compared to other small molecules. It also has tiny thermal [1] and energy-resolved annihilation cross sections [43] due to the apparent lack of a positron bound state. The "cooling" phase typically lasts 100 ms.

In the final "dump" phase, the cool positrons are ejected from the well in the form of a mono-energetic pulse. This is done by lowering the exit electrostatic barrier to the desired transport voltage V_a, then raising the well until it is about 0.25 eV or more above this barrier. If done correctly, this results in a positron pulse with energy $\sim eV_a$ parallel to the magnetic field and a narrow spread in total energy ($\sim$ 50 meV). Furthermore, the shot-to-shot pulse strength is fairly consistent. Methods for characterizing the energy distribution and the pulse strength will be discussed in the next section.

The efficiency of the trapping, cooling, and beam formation processes is typically around 10% but up to 30% has been achieved in the past. For the current experiments, the repetition rate is typically 4 Hz which results in $< 10^5$ positrons per pulse. Better efficiency can be achieved with longer fill times. Note that sometimes, as the moderator

decays, the trapping efficiency is also reduced. This may be related to the fact that the optimal portion of the inelastic electronic excitation cross section in N_2 is only a few eV wide [26], and poor moderators have larger energy spreads.

3.3 Characterizing the positron beam

In order to conduct absolute energy-resolved annihilation cross section experiments, it is necessary to know the precise energy and number of particles in a given positron pulse. It is also useful to know the energy distribution of the beam. There are two primary ways to measure beam energy: cutoff and time-of-flight.

3.3.1 Beam energy

Cutoff energy can be measured using a biased cylindrical electrode, called a retarding potential analyser (RPA). In a constant magnetic field, one can assume that energy parallel and perpendicular to the field is conserved. If the RPA potential exceeds the parallel transport energy, the positron beam is reflected. The cutoff energy is defined as the RPA potential V_c at which exactly half of the positron beam is reflected. The energy eV_c then corresponds approximately to the mean *parallel* energy. If the magnetic field at the RPA is identical to that in the trap, one can further assume that the perpendicular energy does not change. At room temperature, the distribution of positron momenta perpendicular to the B-field causes the peak of the positron energy distribution to shift upward by 12 meV. Thus, the *total* energy at the peak is $E_{tot} = eV_c + 12$ meV.

As shown in Fig. 3.4, a typical cutoff measurement involves determining the transmitted positron flux for a series of RPA voltages. In addition to providing V_c, this gives the integrated parallel energy distribution of a positron pulse. Assuming a Gaussian profile, the FWHM of this pulse can be approximated by finding the energy difference between 88% and 12% transmission. For most experiments in this dissertation, the FWHM was about 27 meV.

Time-of-flight analysis provides another measure of positron transport energy [30,63].

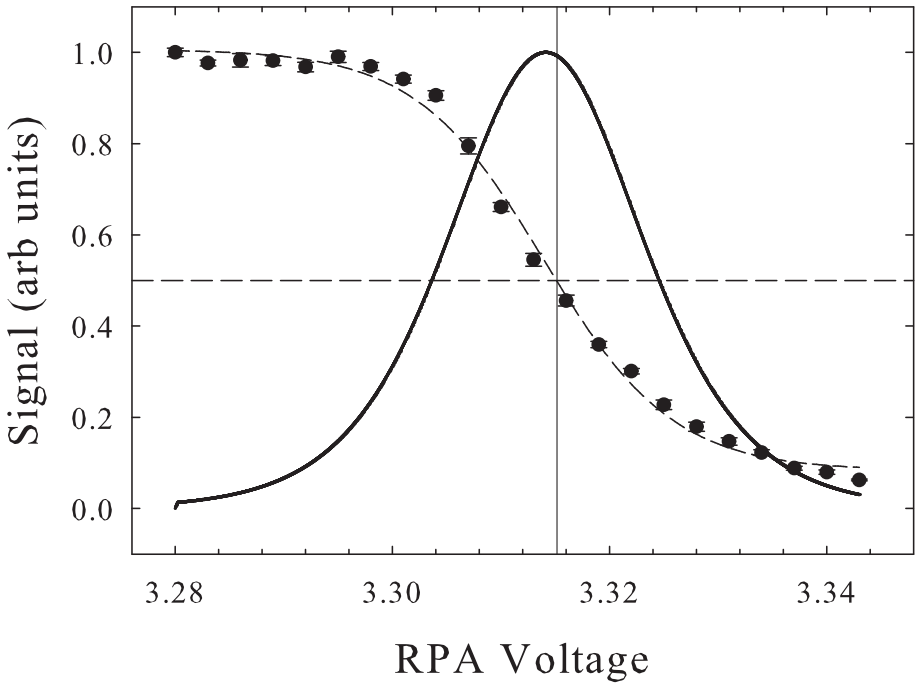

Figure 3.4: A typical cutoff measurement: normalized positron flux (•) vs. RPA voltage. The dashed curve (- -) shows a sigmoidal fit, and the solid curve (—) shows the normalized derivative of this fit (i.e. the positron parallel energy distribution). The cutoff occurs at 3.315 V, as indicated by the vertical line. The FWHM of the derived beam distribution is 21 meV. At the same time, 68% of the flux occurs within 13 meV of the cutoff, indicating a 30 meV FWHM if the distribution were Gaussian. In other words, the fitted distribution has slightly more flux in the tails.

Instead of measuring flux as a function of RPA voltage, one measures pulse delay. The parallel kinetic energy of a positron with transport energy eV_c in a cylindrical electrode with potential V is $(eV_c - eV)$. Thus, the time to traverse a cell of length l is equal to $l/\sqrt{2(eV_c - eV)/m} + t_0$ where t_0 is an arbitrary constant. The values eV_c and t_0 can be found by fitting to the experimental data. This method is less convenient than the cutoff method, and so is used more as an occasional verification.

Time-of-flight measurements are more useful for determining the actual potential experienced by positrons inside a cylindrical electrode. That is, the voltage applied to a cylindrical electrode is not necessarily identical to the potential felt by the positron inside the electrode. The potential varies along the length of the electrode, only approaching the applied voltage at the middle and for large radii. The cutoff only measures the point at which the highest point of this potential equals the parallel transport energy. Ignoring dispersion, time-of-flight measures a weighted average of the potential. In some cases, the difference between them has been as large as 100 meV. This difference, which is not fully understood, is usually fixed unless there is a change in the experimental procedure or apparatus. Note that the spurious potentials that contribute to this effect are larger when there is metal close to the positron beam, as is typical in our positron scattering cells [30]. The annihilation gas cells used here have larger diameters which result in much better uniformity, such that the mismatch between the cutoff and time-of-flight measurements is usually less than 10 meV.

As it turns out, the best measurement of the true total energy distribution can be seen in energy-resolved annihilation data [44]. Ignoring the details of this measurement for now, the shape of an isolated VFR peak is a mirror image of the energy distribution of the beam. This is because the natural width of the resonance is found theoretically and experimentally to be much smaller than the beam width. The distribution can be described as a convolution of a room temperature (25 meV) Boltzmann distribution in the perpendicular direction with a 25 meV FWHM Gaussian distribution in the parallel

direction. The resulting line shape function, $f(\epsilon)$, is [44]:

$$f(\epsilon) = \frac{1}{2k_B T_\perp} \exp\left[\frac{\sigma^2}{2(k_B T_\perp)^2} + \frac{\epsilon}{k_B T_\perp}\right]\left[1 + \mathrm{erf}\left(-\frac{1}{\sqrt{2}}\left(\frac{\epsilon}{\sigma} + \frac{\sigma}{k_B T_\perp}\right)\right)\right]. \qquad (3.2)$$

In this expression, $\mathrm{erf}(x)$ is the standard error function, $T_\perp$ is the perpendicular temperature, and $\sigma = \delta_z\sqrt{8\ln 2}$ where δ_z is the FWHM of the Gaussian. As shown in Fig. 3.5, this function fits remarkably well to the line shape of the C-H stretch peak in propane.[1]

While the origin of the thermal perpendicular energy distribution is clear, the origin of the Gaussian-like parallel energy distribution is less clear. It has been pointed out that the parallel distribution *before* leaving the BGT should be thermal.[2] However, the "dumping" process somehow results in a more symmetric energy distribution, which is evident from cutoff measurements (e.g. Fig. 3.4).

It should be noted that previous annihilation measurements assumed that the shift in resonance peak positions due to the perpendicular energy contribution was 16 meV instead of the present assessment of 12 meV [24, 43, 45]. Thus, these older results should be shifted downward by 4 meV.

3.3.2 Positron pulse strength

We use two methods to measure positron pulse strength: charge and annihilation rate. Measuring positron charge is similar to measuring electron charge. In our lab, the positrons are allowed to impinge on a reverse-biased collector plate and, by annihilating with electrons, create holes. The hole charge can then be determined by measuring the change in voltage on a capacitor, using a suitable amplifier. For a known capacitance, this gives an absolute measurement of the number of positrons per pulse. However, because of the small signal, many averages are needed, especially for beams of a few thousand positrons.

The two 511 keV gamma rays produced when a positron annihilates with an electron on the collector plate provide a much stronger signal. These gamma rays are detected

[1] Thus, the asymmetric line shape, first noted by L. Barnes, is now fully explained [62].

[2] J. R. Danielson, private communication.

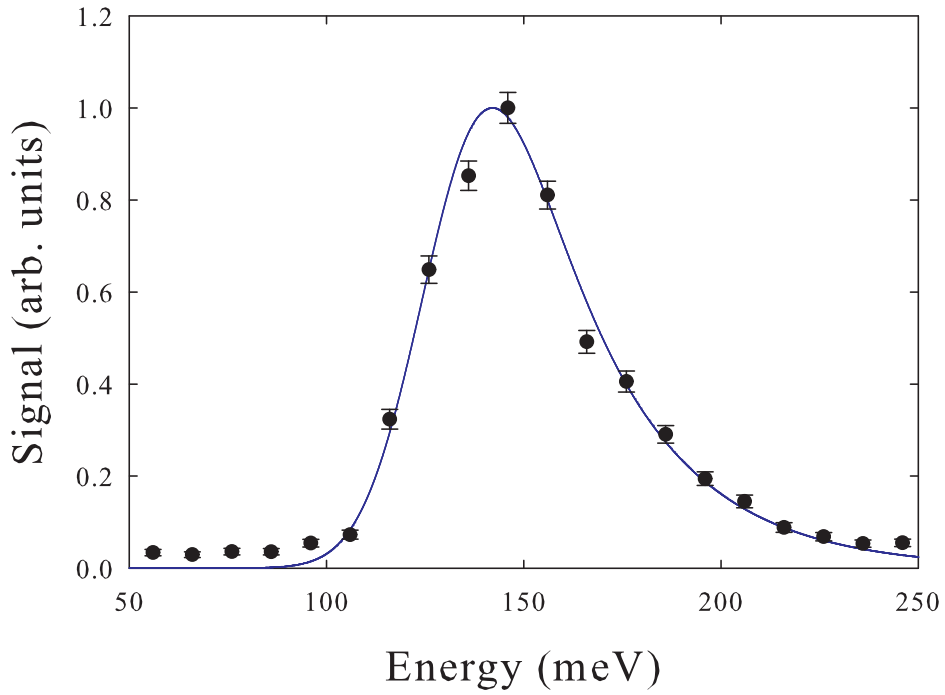

Figure 3.5: The positron pulse energy distribution function (—), as described in the text. The distribution is arbitrarily normalized, shifted in energy, and fitted to the energy-reversed, normalized C-H stretch peak Z_{eff} of propane (•). In this case, the perpendicular temperature is ~ 26 meV and the parallel energy FWHM is ~ 27 meV.

using a NaI crystal and a photomultiplier. The integrated voltage output of this device provides a measure of the relative pulse strength. The downside of this technique is that it is not absolute and is susceptible to background radiation. Still, it is quite useful for cutoff and time-of-flight measurements.

3.4 The annihilation cell

The energy-resolved annihilation experiment uses the annihilation cell depicted in Fig. 3.6. The design has changed little over the years [24, 43, 45]. The annihilation takes place in a 27 cm long cylindrical electrode which we call the gas cell. The diameter of this cell is 4.4 cm. By adjusting the bias on this electrode, one can control the kinetic energy of the positrons as they interact with a test gas within the cell. The annihilation rate is determined by the number of 511 keV gammas, which is monitored by a detector adjacent to the cell.

The test gas is allowed to enter from the "back" (i.e., the collector-electrode side). Copper baffles with narrow apertures are placed on either side of the gas cell. They ensure a nearly constant pressure along the length of the gas cell (less than 10% variation) and a rapid drop in pressure on the trap side of the cell. As a result, a significant fraction of all positron-gas interactions occur within the gas cell and at a constant pressure.

Absolute pressure in the cell is measured with a capacitance manometer via a tube that goes through the back baffle. This can measure pressure accurately down to a few μtorr. For lower pressures, an ion gauge is used, which is located closer to the gas source. Since the ion gauge can only measure relative pressures, it must be calibrated using the manometer for each test-gas species. Also, it must be shut off during the experiment to prevent the introduction of electrons and molecular fragments into the gas cell.

Annihilations are detected via a CsI crystal and a photodiode. Each gamma produces a pulse whose height is proportional to the energy of the gamma. These pulses are then sent to a single-channel analyzer (SCA), which outputs a 0.5 μs square wave pulse whenever the input pulse height is that expected for a 511 keV gamma.

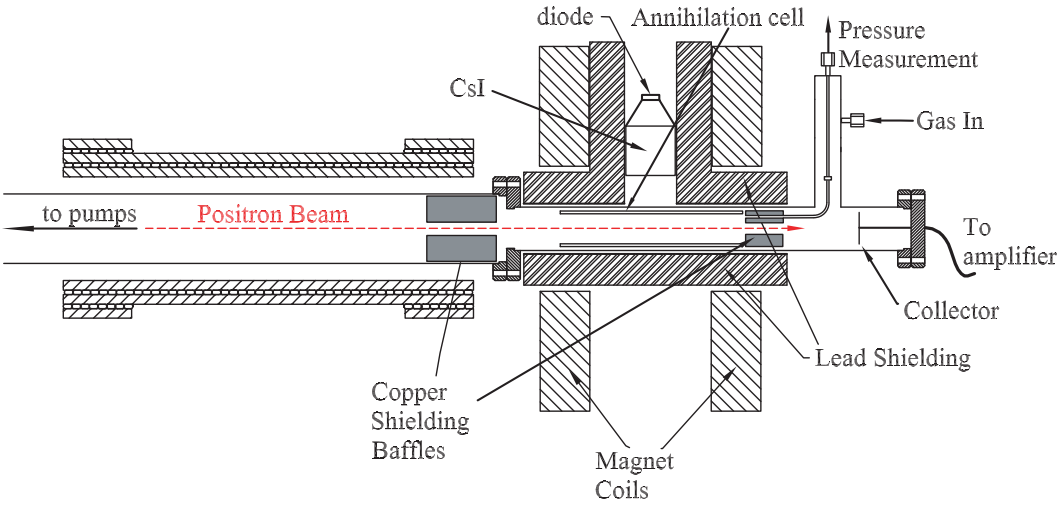

Figure 3.6: A schematic diagram of the annihilation cell region (not to scale). The arrangement is similar to that described in Ref. [62]. However, the original "mushroom" shaped front baffle was replaced by a grounded cylindrical baffle in the adjacent chamber. Also note the electrically-isolated gas cell inlet tube, which was used for most of the later experiments. This permits a more accurate measurement of the test-gas pressure (i.e., otherwise one must correct for pressure drops due to gas conduction through the chamber).

To reduce counts from spurious annihilation outside the gas cell, the annihilation chamber and detector are encased in lead. The thick copper baffles inside the vacuum chamber (described above) provide additional shielding. To further reduce the background, the detector is displaced several centimeters from the cell, aperturing the field of view such that a smaller fraction of the measured annihilation originates from outside the cell. As discussed in Ref. [62], the gamma-ray detection efficiency $D(z)$ was determined empirically as a function of displacement along the axis of the gas cell z. This measurement indicated that the efficiency was highest within a $\sim$ 10 cm region inside the cell. The *integrated* detector efficiency for annihilations in a gas cell of length ℓ is,

$$\eta_D = \frac{2}{\ell} \int_0^{\ell/2} D(z) \mathrm{d}z. \tag{3.3}$$

If ℓ = 22.5 cm and the detector is 8.0 cm from the center of the cell, the integrated efficiency is $\sim 1.3 \times 10^{-2}$ [62]. Since the contributions outside this region are negligible, the integrated efficiency for larger ℓ is proportionally smaller.

3.5 Delivery of gases and vapors

There are separate systems for delivering gas and vapor to the annihilation cell. In the former case, a lecture bottle with the test gas is attached via the appropriate pressure regulator to the gas line. This line is evacuated with a properly vented diaphragm pump. To remove air and contaminants, the line is flushed with the test gas and evacuated a few times. After changing gases, this line is baked a few days under vacuum to further eliminate adsorbed impurities.

The test species is then introduced into the gas line at about 15 psi. Flow into the annihilation cell is controlled by a piezoelectric valve. The voltage on this piezo valve is regulated via a proportional-integral-derivative (PID) controller using the capacitance manometer pressure as the input. This results in a reliable and steady gas cell pressure during the course of the experiment, limited only by the accuracy of the manometer and the response of the piezo valve. In practice, the pressure can be set with microtorr

precision. However, because of a slow, approximately linear drift of the manometer zero-offset, there is a drift in the true pressure over time. Thus, we monitor the zero offset before and after an experiment.

The liquid delivery system is not as sophisticated as the gas system. Liquid samples are deposited in a narrow test tube which is then attached to the vapor line. To remove air and contaminants in the lines and dissolved in the liquid sample, a freeze-pump-thaw procedure is used. The sample is frozen with liquid nitrogen, the lines are evacuated with a vented diaphragm pump, and then the sample is allowed to thaw. When the pressure reaches a few hundred mtorr, the lines are shut off from the pump. This cycle is usually repeated a few times. The sample is then placed in a temperature-regulated bath in order to produce a constant vapor pressure in the lines. Note that this system also works with other types of samples. For instance, if a gas-phase chemical has a low pressure or is too corrosive for the piezo valve, the liquid system is used.

A needle valve is used to leak vapor into the annihilation cell. In this case, there is no feedback control of the pressure. In spite of this, the pressure is relatively stable. However, one must pay close attention to pressure before, after, and sometimes during the experiment. Liquid species frequently must be run at very low pressures, and so an ion gauge is used to determine the pressure. This can only be done before or after a run. As with the gas system, after finishing with a sample, the vapor lines must be baked for a few days under vacuum to prevent contamination of the next experiment.

3.6 Cold gas cell apparatus

For one set of experiments described in Chapter 5, a cooled gas cell was used. This allows measurements of Z_{eff} as a function of temperature. The apparatus, which is shown schematically in Fig. 3.7 and described in detail in Ref. [64], functions in a manner similar to the 300 K cell discussed above, but has been designed to allow for controlled cooling of the target gas. The ordinary gas cell and back electrode are replaced by electrically isolated, gold-plated copper meshes inside a copper "cold shell." The meshes are used

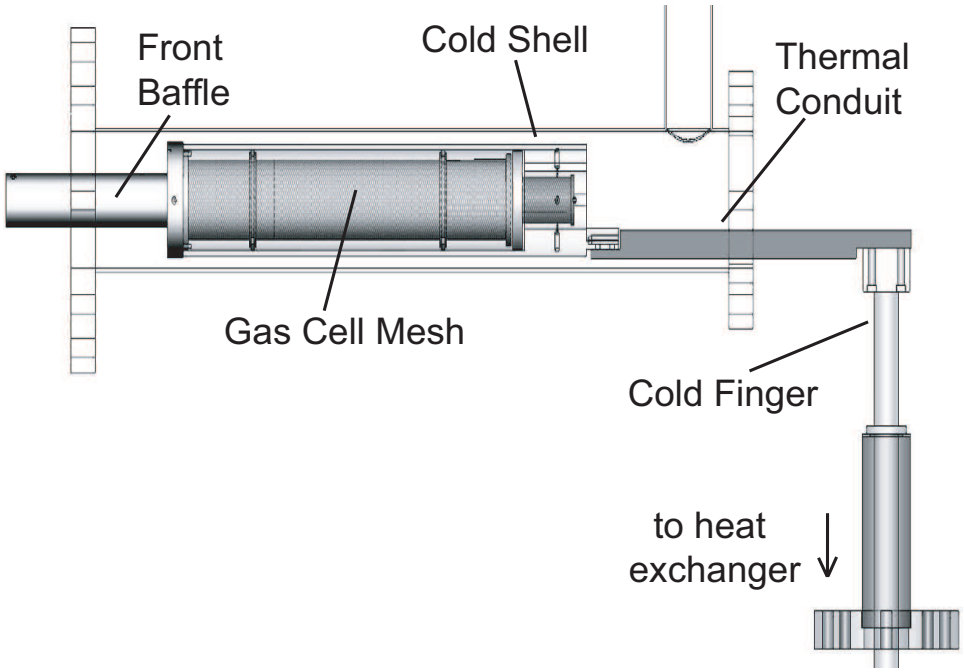

Figure 3.7: Schematic diagram of the cold cell apparatus, expanded in the vertical direction for clarity. For reference, the length of the gas cell mesh is 27 cm.

to set the electrical potential inside the gas cell, while the conduction-cooled, baffled shell contains and cools the test gas. The cold shell rests on stainless-steel standoffs to thermally isolate it from the vacuum chamber and is connected by a copper bar to a thermally insulated vacuum feed through. The feed through is connected to an open-ended heat exchanger outside the vacuum chamber that operates on pulses of liquid N_2 from a supply dewar and exhausts into the atmosphere. As a result, the test-gas cell can be cooled to ~ 100 K with a 10 K to 15 K variation from one end of the cell to the other.

3.6.1 Temperature measurement and constraints

The temperature is measured by a diode on each side of the cold shell and a platinum resistive temperature device (RTD) on the outside of the feed through. The RTD and a PID controller are used to switch on and off the flow of liquid N_2 to maintain a constant (i.e., set-point) temperature.

One of the most important constraints in this type of experiment is the operating range of test-gas temperatures. It is limited by the temperature of liquid N_2 at atmospheric pressure (i.e., 77 K) and the conduction of the copper bar connecting the heat exchanger to the gas cell. Moreover, it is also limited at the low-temperature end by the vapor pressure of the test gas, which decreases with temperature and must be kept higher than the operating pressure in the cell to prevent condensation inside or outside the gas cell. The operating pressure itself must be maintained high enough for good signal to noise, but low enough to keep total scattering low (i.e., below about 15%). Since the vapor pressures and condensation temperatures of alkanes decrease with increasing molecular size, so does the minimum operating temperature. This places a significant constraint on studies of larger alkane molecules.

3.6.2 Pressure measurement and constraints

The pressure of the test gas is measured both by a manometer, connected via a tube to one end of the gas cell and by an ion gauge near the gas inlet outside the back baffle. The manometer provides an absolute measure of the gas pressure after applying an equal-flux temperature correction, namely

$$P_m = P_c\sqrt{T_m/T_c}, \tag{3.4}$$

where the subscripts m and c refer to the manometer and gas cell respectively. While the ion gauge has a gas-dependent correction factor, it has the advantage that it can measure the low operating pressures needed to study alkanes with large Z_{eff}. This correction factor is determined empirically by comparing the manometer and ion gauge readings at several pressures below the vapor pressure of the test gas.

Above the test-gas vapor pressure, liquid starts to condense in the cell and the thermal conduit from the heat exchanger. As a result, the pressure read by the ion gauge in the warm region grows rapidly, while the manometer pressure (which measures the pressure inside the cell) remains relatively constant. In this case, the cold cell is acting as a cryopump. Observation of this phenomenon provides evidence that the test gas is, in fact, making a sufficient number of inelastic collisions to cool to the cell temperature. It is estimated that a large molecule entering the cold cell will make ~ 50 collisions with the cell walls, over the course of ~ 5 ms, before exiting the cell.

3.7 A typical experiment

A typical experiment begins with the growth of a new moderator. The BGT system is then tested to ensure the proper positron trapping. The trap exit voltage V_a is chosen so that the transport energy is below the positronium threshold for the test species.[3] Positrons above this threshold can form positronium with gas outside the gas cell. These positronium atoms, in turn, annihilate readily, producing an unwanted background signal.

The energy distribution of the positrons is determined by doing a cutoff using the gas cell as an RPA. The pulse strength is determined by measuring the charge on the collector plate. The fill time must be adjusted so that the pulse is not too large. Otherwise, annihilation counts could saturate the CsI detector during the experiment.

Annihilation counts are recorded both with a hardware counter and by analyzing the integrated scope signal. To further eliminate noise, both of these inputs are time windowed. Counting begins a set time after the "dump" phase trigger. Typically, this is set to the time that the positrons hit the collector plate when all subsequent potentials in the beam line are grounded. The software counter is flexible in that it allows this window to be chosen after the run is complete.

[3] As described above, this threshold is $E_i - 6.8$ eV, where E_i is the ionization potential of the test species, and 6.8 eV is the binding energy of a positronium atom.

Between 0.1 and 100 μtorr of test gas are introduced into the gas cell. This pressure is chosen so that scattering processes are small enough to be ignored. It is also chosen so that the annihilation rate is large enough to provide good statistics, but not so large that the detector is saturated. Since the annihilation and scattering rates can only be estimated before an experiment, this is inherently a perturbative process.

To determine the annihilation rate at parallel energy, $E_{||}$, the gas cell is set at $V_c - E_{||}/e$, and the back baffle is set a few volts larger than V_c (i.e., to reflect the beam). A positron pulse is then allowed to bounce through the cell several times. Annihilation counts are accumulated for 10 to 25 pulses, in each case within a fixed time window (usually ≈ 15 μs). This process is repeated for all energies between 50 and 500 meV at 10 to 15 meV intervals. This entire process is then repeated a few hundred times, which can take a day or two.

To eliminate the possibility of three-body effects, this protocol is repeated for two or more pressures of the test species. If the absolute Z_{eff} and the shape of the spectrum does not change with a change in presure, the result is accepted. This source of error will be discussed more thoroughly in section 3.9.

3.8 Calculating the annihilation rate

The absolute annihilation cross section can be determined from the number of detected annihilations I_γ, the target gas temperature T, pressure P, positrons per pulse I_0, *integrated* detector efficiency η_D for gas cell of length ℓ, and number of passes through the cell b. This is expressed as follows,

$$\frac{I_\gamma}{I_0 \eta_D} = n(\ell b)\sigma = (P/kT)(\ell b)\sigma \tag{3.5}$$

where n is the density of the target gas and k is Boltzmann's constant. For a single pass through the cell, $b = 1$. For multiple passes through the gas cell, within a fixed time window t_b,

$$b = t_b/\delta t \tag{3.6}$$

and

$$\delta t = \sqrt{m/2}\left[\frac{d}{\sqrt{eV_c}} + \frac{\ell}{\sqrt{eV_c - eV}}\right] \tag{3.7}$$

where d is the distance from the trap to the cell, V is the voltage on the cell, and V_c is the cutoff. All of these values are either known or measured during the course of the experiment.

As discussed in Chapter 2, the cross section, σ, is normalized by the cross section for a free electron gas. The result is a dimensionless factor, Z_{eff}:

$$Z_{\mathit{eff}} = \sigma/(\pi r_0^2 c/v) \tag{3.8}$$

where r_0 is the classical electron radius and v is the impact velocity. As mentioned earlier, it was originally thought that Z_{eff} would represent the effective number of molecular electrons interacting with the positron. However, since Z_{eff} can be orders of magnitude larger than Z, the number of electrons in the molecule, a more sophisticated explanation is required.

3.9 Sources of error

The most common sources of error affect the overall magnitude of the annihilation rate. They are primarily due to changes in the pressure and pulse strength over the course of the experiment. There can also be small drifts in cutoff which affect the absolute energy. In addition, there are less obvious factors which can change the overall shape of the energy-resolved annihilation rate.

3.9.1 Pressure

When using the capacitance manometer and piezo valve, the pressure can only be regulated and measured to within a couple of μtorr of the set-point pressure. This random error increases as the overall pressure decreases. Furthermore, there is a nontrivial drift of the zero point over the course of the experiment. To correct for this, the pressure of the evacuated gas cell is measured before and after the experiment. To lowest order,

this drift is typically linear but can have weak higher order terms. If the drift is a significant fraction of the total pressure, the resulting magnitude is regarded with suspicion. Sometimes, a short second experiment is performed at single annihilation resonance to determine the overall magnitude.

When working with vapors, a needle valve is used. Since there is no feedback, the pressure in the cell can drift over time. In more recent experiments, the pressure is measured at regular intervals during a run. This is not possible at lower pressures, where an ion gauge is required. In this case, the pressure measurement can only be made at the beginning and end of the experiment because the ion gauge takes a long time to stabilize. The ion gauge itself must be calibrated to the manometer to determine the absolute pressure. Even with the calibration factor, the accuracy of the ion gauge is not as good as the manometer.

A small leak or source of impurities can be a significant issue. They can be prevented by making sure the gas and vapor lines can maintain a vacuum and using a residual gas analyzer (RGA) to check the purity of the test species. The RGA is also used to perform a helium leak test. A depression in the ion gauge calibration factor can be a tell-tale sign of a leak, since air has a small ion gauge calibration factor compared to larger molecules.

3.9.2 Pulse strength

The pulse strength can change over the course of the experiment as the moderator decays. In recent experiments, the pulse strength was measured at regular intervals with the test gas present, eliminating some of this error. There is also the issue of attenuation during multi-pass experiments. As the pulse passes back and forth through the cell, some of the beam may be scattered and lost. By aperturing the beam, lowering the pressure, and reducing the number of bounces, this effect can be reduced. We try to run with less than 15% of the beam scattered elastically. Note that the losses due to annihilation with the test gas are typically negligible. All told, the overall systematic error in the magnitude of Z_{eff} from pressure, pulse strength, and other sources is $\sim 10 - 20\%$. The

repeatability of experiments verifies this estimate. However, under properly controlled conditions, the relative error between two similar experiments can be smaller.

3.9.3 Number of passes through the cell

As discussed in section 3.8, the cross section is affected by the number of bounces, b, of the positron pulse through the cell in the time window, t_b. The value of b is, in turn, determined by the time of flight, δt, from the trap to the back baffle of the cell. A simple model potential is used to calculate time of flight. This may differ from the true time of flight by a small amount. However, given the consistency of single and multi-pass experimental results, this effect is likely smaller than the other sources of error [62].

Another issue arises from the fact that the positron beam is bunched in time. This results in a roughly integral number of bounces instead of the non-integral value used in our analysis. Hence, it is possible to slightly over- or under-estimate Z_{eff} when the number of bounces is small and the positron pulses are short in time. This effect is mitigated, for instance, by increasing the positron transport energy or extending the time window to increase the number of bounces. Also, in some cases, one can slow down the "dump" phase to extend the time width of the pulse (i.e. making it "less bunched").

3.9.4 Counting errors

Counting errors can lead to large uncertainties. If the detector receives two 511 keV gammas within a fraction of a microsecond, it can produce a larger pulse which is rejected by the SCA. Even if both are accepted, the software and hardware counters may not properly discriminate them. As a result, the average count rate depends non-linearly on the true annihilation rate. In the extreme case, large peaks are clipped at the top. To avoid such counting errors, the pulse strength and pressure are reduced. Ideally, we run with less than one count in ten beam pulses.

There is also an issue of background radiation. The lead shielding and copper baffles reduce this considerably. There are also inevitable "dark" counts produced by noise in

the detector. This cannot be avoided. However, with the energy and time windows, there are typically less than 1×10^{-9} background counts per positron. With the introduction of a test gas, this background may increase due to scattered positrons annihilating with the wall. This is greatly reduced by aperturing the beam. There is also a problem of positronium formation outside the cell. As discussed above, this can be eliminated by reducing the transport energy below the positronium formation threshold of the target molecule. Usually a margin of at least 0.5 V is maintained. There is also direct positron-molecule annihilation outside the cell, but this is typically negligible. The total background contribution, after accounting for all these factors, is still quite small compared with the other sources of error.

The most obvious source of error is due to counting statistics. For N counts, the uncertainty is $\sigma_N \sim \sqrt{N}$, and the standard error is ~ 1. We represent this standard error by the error bars in our Z_{eff} spectra. For molecules with small Z_{eff}, much longer integration times are required to achieve good signal to noise ratios.

3.9.5 Three body effects

Three body effects are a significant source of error. They occur when the positron scatters from one molecule before annihilating with another molecule. An inelastic collision changes the energy of the positron, allowing it to sample annihilation resonances at a lower energy. This can result in additional, high-energy peaks in the Z_{eff} spectrum.

A more subtle problem is the change in parallel energy following a scattering event. This changes the number of passes through the cell in the bounce window, and it can even prevent positrons from re-entering the gas cell. This, in turn, can differentially reduce the annihilation rate as a function of energy. Usually this is strongest near threshold. For this reason, data below 50 meV are considered suspect and are usually rejected.

As mentioned before, these effects can be inferred by examining Z_{eff} data at different test-gas pressures. If the absolute peak heights change with pressure, the experiment is repeated at a lower pressure. If the Z_{eff} spectrum does not change between two

well-separated pressures, it is assumed that this effect is negligible. Alternatively or additionally, one can compare the result to that produced using time-delayed bounce window.

3.9.6 Errors in energy

The cutoff contains two important pieces of information, the energy and the energy width of the beam. As mentioned earlier, the cutoff only measures when the maximum potential of the cell equals the parallel energy of the positron pulse. As a result, it indicates the minimum parallel energy within the cell for a given electrical bias on the cell. Technically, one would like the *average* total energy in the middle of the cell (i.e., where the detection efficiency is greatest). The average parallel energy over the entire cell can be gleaned from time-of-flight measurements. This differs from the cutoff by up to 10 meV even under ideal conditions. Keep in mind that this measurement also has its problems. The match between the experimental data and the model fit is often not perfect [30]. Furthermore, both measurements ignore the perpendicular energy component. This is inferred indirectly from experiment to be 12 meV [44]. Hence, the systematic error in absolute energy may be as large as 10 meV. Variations of this value can be quantified by performing an experiment with a reference gas like propane, whose C-H stretch resonance occurs at a known energy.

The cutoff itself can drift by $5 - 15$ meV over the course of the experiment (larger deviations usually result in rejection of the data set). If not accounted for, this drift can result in random errors in the peak energies and line widths determined in different experiments. Also, as mentioned above, the parallel energy FWHM ranges between $24 - 30$ meV. For these reasons, there is an implicit error in the empirically determined binding energies of $\sim 5 - 10$ meV.

Chapter 4

VFR in small molecules

Positron binding and the vibrational Feshbach resonance (VFR) mechanism are probably best understood by looking at the annihilation resonances in molecules with only a few degrees of freedom. In this limit, the number of indistinguishable resonances is greatly reduced and more predictive theories are possible.

In this chapter, a number of experiments on small molecules are discussed. The interpretation of these results is aided by a quantitative model for VFR by Gribakin and Lee [65]. This theory successfully predicts exact magnitudes for annihilation resonances in methane-derived species. In particular, it shows that VFR magnitudes in these molecules are largely determined by a factor g which depends only on the positron binding and impact energy [see Eq. (4.2)].

Experiments indicate that the behavior and type of resonances changes as the "size" of a molecule increases, indicating the presence of additional internal dynamics. Some of these changes, like the appearance of multi-mode resonances, can be accommodated by the Gribakin-Lee theory, while others cannot. This distinction will lead to our more narrow definition of "small molecule."

In addition, data for molecules are presented which exhibit no apparent resonances. These results hint at the conditions required for positron-molecule binding and VFR-induced annihilation.

4.1 The halomethanes

Halogen-substituted methane molecules or halomethanes have a number of characteristics that make them amenable to theory. Primarily, they have a small number of vibrational modes. This not only reduces computational complexity, but it also separates the modes by an amount closer to experimental resolution. Each peak can be caused by only a few distinct vibrational modes (all with strong electric dipole transitions, which will later be shown to be important). Thus, one can more easily classify the peaks and their individual magnitudes, thus allowing more stringent tests of theory.

As will be shown shortly, these molecules display the most elemental form of VFR. They have little potential for the complex internal dynamics which likely cause the huge Z_{eff} seen in larger alkanes. Hence, fewer additional parameters are needed to explain changes in Z_{eff}.

Fig. 4.1 shows energy-resolved Z_{eff} spectra for methyl fluoride (CH_3F), methyl chloride (CH_3Cl), and methyl bromide (CH_3Br). Below each spectrum are a series of bars indicating the positions of the vibrational modes according to the NIST webbook [66]. All spectra exhibit clear VFR in the form of two or more peaks. The positions of these peaks correlate strongly with the positions of infrared (IR) absorption resonances, also shown in Fig. 4.1. The high-energy peak is due to the C-H stretch vibration. The stronger low-energy peaks are due to C-H bends and C-X modes (where X is the halogen). The low energy modes are spread further apart in molecules with larger halogens. This results in a broader low energy peak. In CH_3Cl, one can actually distinguish all three classes of modes: C-X, C-H bend, and C-H stretch. Still, in all cases, it is impossible to distinguish the influence of symmetric and asymmetric modes.

As the size of the halogen increases, the peaks increase dramatically in magnitude, particularly between CH_3F and CH_3Cl. In addition, the peaks shift to lower energy, indicating increasing binding. The binding for CH_3Cl is ~ 25 meV and for CH_3Br ~ 40 meV. The binding for CH_3F cannot be determined because the apparent C-H stretch peak is shifted above the position of the C-H stretch energy for a neutral molecule. This

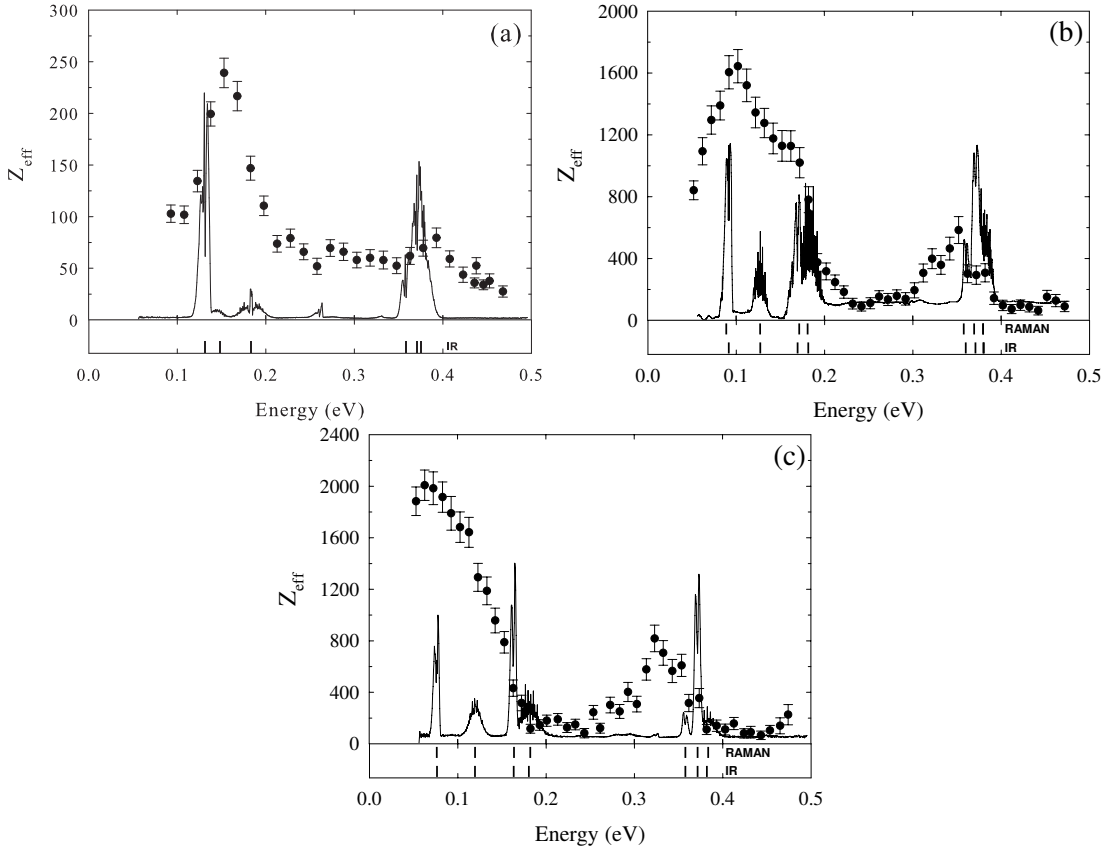

Figure 4.1: (•) Z_{eff} for (a) methyl fluoride (CH_3F), (b) methyl chloride (CH_3Cl), and (c) methyl bromide (CH_3Br). The solid curves indicate normalized infrared absorption spectra, and the vertical bars beneath each plot indicate the positions of the vibrational modes (from NIST [66]).

will be discussed more thoroughly later. For now, a very small positive binding will be assumed for CH_3F to satisfy the requirement for a VFR.

It is easy to speculate why such trends are observed. An increasingly polarizable molecule should attract positrons more strongly. As a result, the positron is more deeply bound. This leads to enhanced overlap with the molecular electrons and higher annihilation rates. There is some support for this intuition. A quantitative theory by Gribakin and Lee says that, for small molecules, binding energy plays a dominant role in determining both the positron-electron overlap and resonant annihilation peak height [44]. This theory is described in greater detail in the next section.

The origin of the bound states and binding energies of the halomethanes is on less stable theoretical ground. Few models are available because of the difficulties of the calculation. Only the most qualitative treatment is available for this specific set of molecules. A more complete discussion of this will be left for a later section.

4.2 Small molecule model

In a recent paper, Gribakin and Lee developed a relatively simple quantitative model which predicts the Z_{eff} spectrum due to infrared-active modes in small molecules [44]. It assumes a spherically symmetric positron wave function and Born-dipole coupling to the nuclear degrees of freedom. The results of their work are the focus of this section.

Gribakin and Lee's model starts with the vibrational Feshbach resonance model discussed in Chapter 2. Resonant annihilation occurs via positron capture followed by positron annihilation, normalized by the sum of all other channels, such as elastic escape. Each vibrational mode, ν, contributes a Breit-Wigner resonance,

$$Z_{eff}^{(res)}(\epsilon) = \frac{1}{kr_0^2 c} \sum_{\nu} \frac{g_\nu \Gamma_\nu^a \Gamma_\nu^e}{(\epsilon - \omega_\nu + \epsilon_b)^2 + \Gamma_\nu^2/4}, \tag{4.1}$$

where atomic units are assumed. The Γs represent the widths of various processes (Γ_ν^a is annihilation, Γ_ν^e is elastic capture, and Γ_ν is the total), ϵ_b is the binding energy, ω_ν is

the vibrational mode energy, g_ν is the mode degeneracy, ϵ is energy and k is the positron momentum.

A number of approximations are then applied to derive these widths. To start, it is assumed that the bound positron has a spherically symmetric wave function identical to that produced by a bound state in a zero-range potential (ZRP). Thus, it has the form [67]:

$$\varphi_0(r) = A\frac{e^{-\kappa r}}{r}. \tag{4.2}$$

This corresponds to a positron scattering length of $1/\kappa$ and a binding energy $\epsilon_b = \kappa^2/2$, with a normalization factor, A $= \sqrt{\kappa/2\pi}$. In the case relevant here, where the positron binding is relatively weak, this describes a positron cloud which is diffuse in comparison to the molecular electrons. Technically, the wave function should drop to almost zero within the electron cloud, since the positrons are strongly repelled by the unshielded nuclei. However, in this situation, it is safe to assume the molecule is point-like [44,67]. Complicated interactions with electrons at the molecular interface are largely ignored. Thus, the positron wave function is regarded as completely independent of nuclear and electronic degrees of freedom.

Calculation of the positron capture width can now proceed using a Born-Dipole approximation for the positron-molecule dipole coupling. The initial state is assumed to be a plane wave, $e^{i\mathbf{k}\cdot\mathbf{r}}$, for the positron and a ground state molecule, Φ_0. The final state is the bound positron wave function, $\varphi_0(r)$, and a vibrationally excited molecule Φ_ν. These states are coupled via a potential based on the dipole operator $\hat{\mathbf{d}}$, namely:

$$A_{\nu\mathbf{k}} = \langle\varphi_0(r)\Phi_\nu|\frac{\hat{\mathbf{d}}\cdot\mathbf{r}}{r^3}|e^{i\mathbf{k}\cdot\mathbf{r}}\Phi_0\rangle = \langle\varphi_0(r)|\frac{\mathbf{d}_\nu\cdot\mathbf{r}}{r^3}|e^{i\mathbf{k}\cdot\mathbf{r}}\rangle, \tag{4.3}$$

where

$$\mathbf{d}_\nu = \langle\Phi_\nu|\hat{\mathbf{d}}|\Phi_0\rangle. \tag{4.4}$$

The dipole moment for vibration ν, $\mathbf{d}_\nu$, can either be taken from infrared absorption data or determined with physical chemistry software such as GAMESS [68]. In particular,

the infrared absorption cross section is proportional to $\omega_\nu d_\nu^2$. The final expression for $A_{\nu\mathbf{k}}$ can be calculated analytically and involves the hypergeometric function, ${}_2F_1$ [44]. The elastic capture width, Γ_ν^e, can then be determined exactly,

$$\Gamma_\nu^e = 2\pi \int |A_{\nu\mathbf{k}}|^2 \delta(k^2/2 - \omega_\nu + \epsilon_b) \frac{d^3k}{(2\pi)^3} = \frac{16\omega_\nu d_\nu^2}{27} h(\xi) \ , \tag{4.5}$$

where

$$h(\xi) = \xi^{3/2}(1-\xi)^{-1/2}[{}_2F_1(\frac{1}{2}, 1; \frac{5}{2}; -\xi/(1-\xi))]^2, \quad \text{with} \quad \xi = 1 - \frac{\epsilon_b}{\omega_\nu}. \tag{4.6}$$

The function $h(\xi)$ has a single maximum of 0.75 at $\xi = 0.89$ and gradually drops to zero at $\xi = 0$ and $\xi = 1$. Thus, Γ_ν^e is essentially proportional to the infrared absorption cross section. Note that other non-dipole entrance channels may be possible but are ignored here since the corresponding widths are more difficult to estimate.

The remaining width to calculate is that of annihilation, Γ_ν^a. This width is ultimately determined by the positron-electron overlap density ρ_{ep}, defined by,

$$\Gamma_\nu^a = \pi r_0^2 c \rho_{ep}, \tag{4.7}$$

where

$$\rho_{ep} = \int \sum_{i=1}^{Z} \delta(\mathbf{r} - \mathbf{r}_i) |\Psi(\mathbf{r}_1, ..., \mathbf{r}_Z, \mathbf{r})|^2 d\mathbf{r}_1 ... d\mathbf{r}_Z d\mathbf{r}, \tag{4.8}$$

with the positron and electron wave function, Ψ, the electron positions $\mathbf{r}_i$, and the positron position $\mathbf{r}$. This basically treats the positron and electrons as free particles that annihilate within the molecule via the 2-γ process. (The 3-γ process has a longer lifetime, and so it is ignored [40].) The key ingredient is the overlap of the positron and electron wave functions at the outer perimeter of the molecule, which cannot be ignored. Gribakin assumes that this overlap occurs within a thin shell of width δR around the molecule [23, 40]. This assumption is, in fact, reinforced by gamma-ray spectroscopy of positron-atom annihilation, which shows that positrons preferentially annihilate on valence electrons [12]. Presumably, the attraction of the electrons is balanced by the repulsion of the nuclear charges. Using the s-wave positron wave function described

above and assuming an electron density $\rho_e(R)$, one gets the following expression for positron-electron overlap:

$$\rho_{ep} = 4\pi\delta R\rho_e(R)\frac{\kappa}{2\pi} \equiv \frac{F}{2\pi}\kappa. \tag{4.9}$$

The factor κ provides an explicit dependence on the binding energy, ϵ_b. In reality, the complex, density-altering interactions between the electrons and the positron cloud at this interface are largely unknown. Hence, in Gribakin's formalism, the unknown thickness δR, radius R, and electron density in the shell $\rho_e(R)$ are absorbed into a single parameter F. Note that this places less restrictions on the geometry of the overlap region. Mitroy *et al.* calculated Γ^a and κ for several atoms using the Stochastic Variational Method, frequently assuming fixed cores [48]. These values appear to be linearly correlated with each other, giving an empirical value for F of 0.66. Gribakin uses this empirical F value to calculate ρ_{ep} in small molecules [40, 69].

At this point, there is sufficient information to calculate the elastic capture and annihilation widths for specific molecules. For example, consider the widths associated with CH_3Cl. As seen in Fig. 4.1(b) from the previous section, this molecule has a positron binding energy of ~ 25 meV. According to Eqs. (4.7) and (4.9), $\Gamma^a = 0.15$ μeV. In contrast, Gribakin found that the elastic capture widths for this molecule were on the order of 0.1 meV [44]. Table 4.1 shows $\Gamma^e_\nu/h(\xi)$ and $h(\xi)$ for each fundamental vibrational mode of CH_3Cl. Note that Γ^e_ν is consistently much larger than Γ^a_ν. The significance of this fact will soon become clear.

Assuming no other channels, the total width, $\Gamma_\nu = \Gamma^e_\nu + \Gamma^a_\nu$, is much smaller than the experimental width of the positron beam (which is about 50 meV FWHM). Hence, when the distribution function of the positron beam, $f(\epsilon)$, is taken into account, the expression for resonant Z_{eff} can be written,

$$\begin{aligned} Z^{(res)}_{eff}(\epsilon) &= 2\pi^2 \sum_\nu \frac{\rho_{ep}}{k}\frac{g_\nu\Gamma^e_\nu}{\Gamma_\nu} f(\epsilon-\epsilon_\nu) \\ &\approx \pi F \sum_\nu g(\epsilon_\nu,\epsilon_b)\frac{g_\nu\Gamma^e_\nu}{\Gamma_\nu} f(\epsilon-\epsilon_\nu) \end{aligned} \tag{4.10}$$

Table 4.1: Physical parameters of CH_3Cl modes used in the calculation of Born-dipole elastic widths for the Gribakin-Lee model based on values from Ref. [44].

mode	symmetry	ω_ν [meV]	g_ν	d_ν [a.u.]	$h(\xi)$	$\Gamma^e_\nu/h(\xi)$ [μeV]
ν_1	a_1	363	1	0.0191	0.73	78.2
ν_2	a_1	168	1	0.0176	0.75	30.6
ν_3	a_1	91	1	0.0442	0.63	105
ν_4	e	373	2	0.0099	0.72	22.0
ν_5	e	180	2	0.0162	0.75	27.9
ν_6	e	126	2	0.0111	0.70	9.09

where

$$\epsilon_\nu = \omega_\nu - \epsilon_b \quad \text{and} \quad g(\epsilon, \epsilon_b) \equiv \kappa/k = \sqrt{\epsilon_b/\epsilon}. \tag{4.11}$$

Since $\Gamma^e_\nu \gg \Gamma^a_\nu$, the ratio $\Gamma^e_\nu/\Gamma_\nu \approx 1$, so there is no dependence on the capture width or dipole moment in the final expression. Thus, the calculated capture width only needs to be correct to within an order of magnitude. *The peak height is determined entirely by the factor $Fg(\epsilon, \epsilon_b)$. This is a key result. It is remarkably useful in interpreting a broad class of experimental results and will be revisited several times in this thesis.*

In addition to the resonant contribution to Z_{eff}, there is a contribution from direct annihilation, $Z^{(dir)}_{eff}$. As described in Chapter 2 and Ref. [23], this process is due to the overlap of the positron and electrons during ordinary elastic scattering and occurs within a thin shell enclosing the molecule. As a result, at low energies, $Z^{(dir)}_{eff}$ can be expressed in terms of the integrated overlap density parameter, F, and the elastic cross section, σ_{el}:

$$Z^{(dir)}_{eff} = F\frac{\sigma_{el}}{4\pi} = \frac{F}{\kappa^2 + k^2}. \tag{4.12}$$

Not included in Eq. (4.2) is the convolution with the experimental beam distribution function, which can be done numerically.

As shown in Fig. 4.2, Gribakin and Lee's final calculation for the methyl halides agrees surprisingly well with the experimental data described in the previous section [45]. The only free parameter in this model is the binding energy, which in some cases can

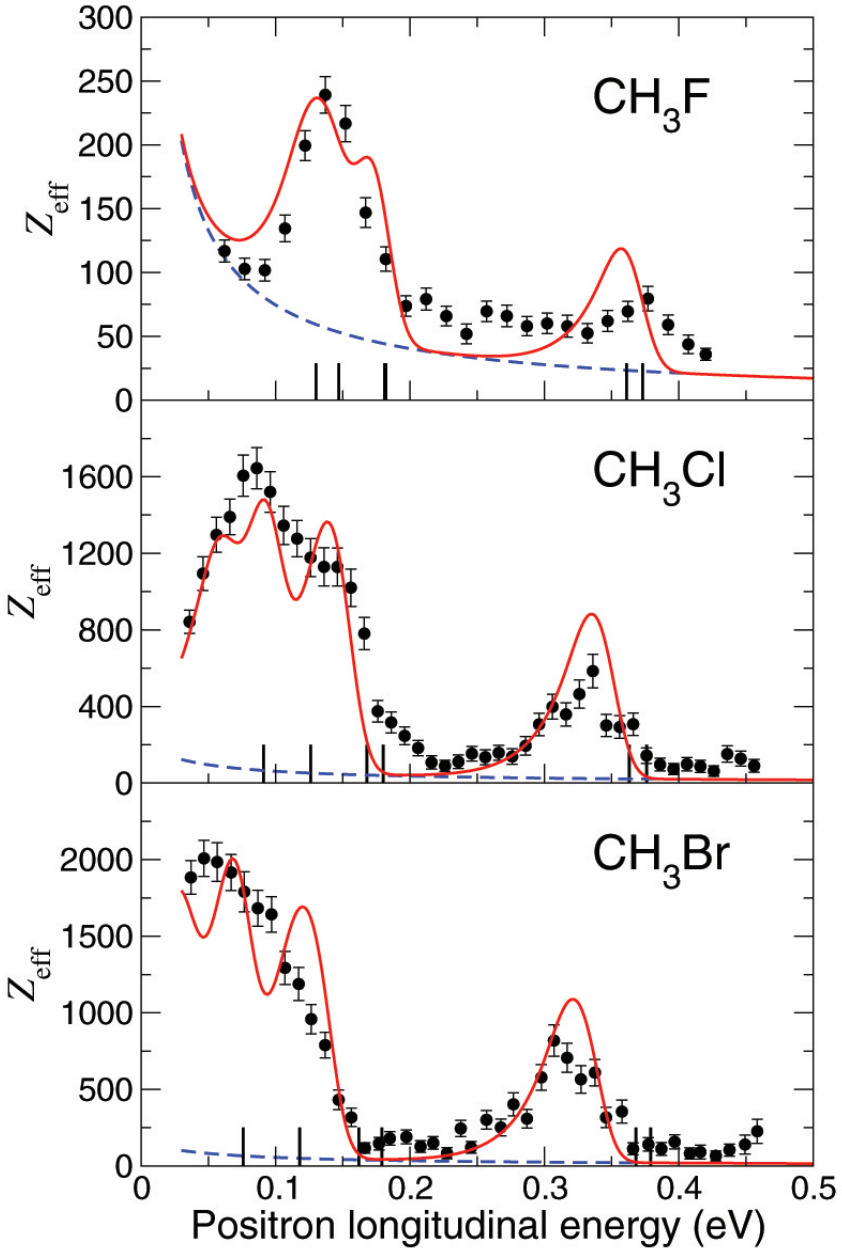

Figure 4.2: Gribakin-Lee model for (a) methyl fluoride (CH_3F), (b) methyl chloride (CH_3Cl), and (c) methyl bromide (CH_3Br), courtesy of [44]. The solid curve represents the model result while the dashed curve represents just the non-resonant (direct) contribution to the result.

be determined empirically from the shift in energy of the peaks. Only CH_3F requires fitting to the peak heights alone. Since the C-H stretch peak in CH_3F occurs above the vibrational mode, its apparent binding is negative (which is impossible for a VFR). Instead, a small binding energy of 0.3 meV was assumed to provide the best fit. For comparison, the empirical binding energy determined from a temperature-dependent measurement of thermal Z_{eff} for CH_3F was 1.4 meV [23]. This ignored the presence of VFR, which were not apparent in the thermal data for Z_{eff}.

Many of the observed trends are consistent with the Gribakin-Lee theory. The fact that the low-energy peaks are taller than the high-energy peaks is due entirely to $g = \sqrt{\epsilon_b/\epsilon_\nu}$. The way Z_{eff} increases with binding is also explained by this factor. The overall magnitude is determined by F.

The cancellation of Γ^e_ν and Γ_ν for infrared-active fundamental vibrations is remarkably fortunate, as it greatly simplifies the calculation of Z_{eff}. Of course, it also means that only a limited amount of information about Γ^e_ν can be gleaned from the Z_{eff} spectra.

The situation changes dramatically when a capture width is less than or equal to the annihilation width. For instance, if $\Gamma^a \gg \Gamma^e$, annihilation is practically guaranteed so that Z_{eff} is proportional to the initial capture rate Γ^e. Fortunately, such channels contribute a negligible amount to Z_{eff}. In essence, Γ^a is the threshold capture width required for "strong" resonances dependent only on g. So far, capture by dipole-excited fundamental vibrations appears to meet this requirement. In later sections, the possibility of additional capture channels, such as those from combination or overtone vibrational excitations, will be discussed.

4.3 The deuterated halomethanes

In order to provide a more stringent test of the Gribakin-Lee VFR model, experiments with *deuterated* methyl halides were performed. While replacing the hydrogen atoms with deuterium atoms lowers the frequency of many vibrations, the ground state electronic wave functions should be unchanged. As a result, the binding energy should be

unchanged. This has been confirmed for a number of hydrocarbons [24,43,62,70]. Thus, if the binding energy from ordinary halomethanes is assumed, the model for deuterated halomethanes is fully constrained.

Figure 4.3 shows the Z_{eff} spectra of CD_3Cl and CD_3Br overlaid with the theoretical predictions. The agreement between experiment and theory is quite good for CD_3Cl. Other than a slight mismatch in the peak positions, the agreement for CD_3Br is also good. The discrepancy for CD_3Br might be attributed to systematic experimental uncertainty in total energy, but this is unlikely to explain all of the observed shift. The peak heights match well in this molecule indicating that the choice of binding energy is probably close to the right value. Overall, these data provide excellent confirmation of the Gribakin-Lee theory using *no* free parameters.

This theory is significant as it provides a robust understanding of the VFR mechanism in small molecules. In the following sections, it will be extended in various ways to explain the Z_{eff} spectra for molecules of increasing size and complexity. Certain aspects of this theory, such as the $g = \sqrt{\epsilon_b/\epsilon_\nu}$ scaling factor, will be used to better understand a broad class of molecules. In particular, it will be shown in the next chapter that g generally determines the dependence of Z_{eff} on binding energy, even in large molecules.

4.3.1 Higher-order shifts in peak position

As mentioned above, the observation of a VFR requires a positive binding energy, ϵ_b. Furthermore, it is assumed that this binding energy does not change with deuteration. In this sense, the relative peak shifts observed in CD_3Br and CH_3F are both anomalous. There are a few ways to achieve higher-order peak shifts: either the modes themselves have changed in energy, the binding depends on mode, or the binding mechanism is more complicated than originally believed. The first option seems the most plausible.

Following positron binding, the overall charge and charge distribution of a molecule is changed. Presumably, the added positive charge, which repels the nuclei and shields some of the negative charge of the valence electrons, could perturb the nuclear dynamics.

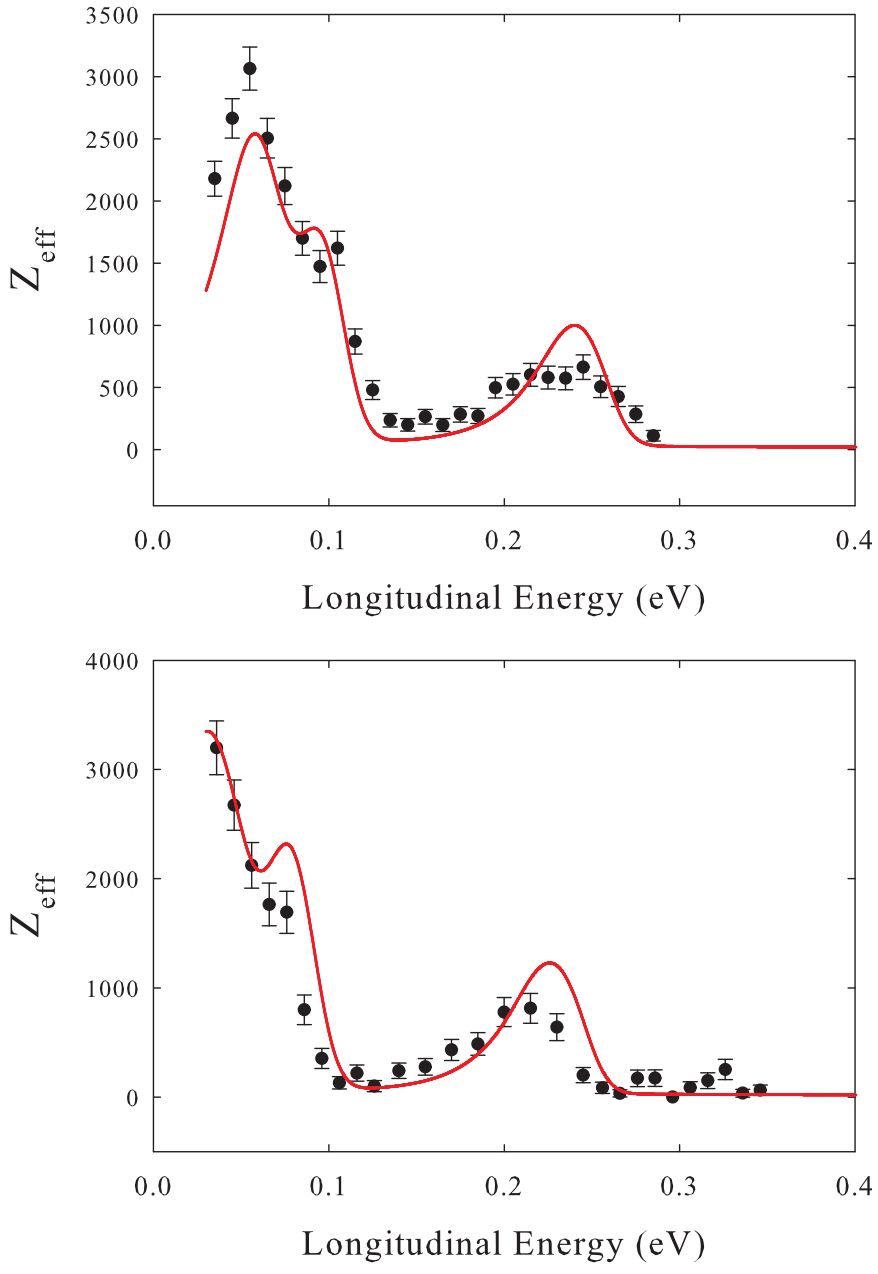

Figure 4.3: Energy-resolved Z_{eff} (•) for (a) deuterated methyl chloride (CD_3Cl) and (b) deuterated methyl bromide (CD_3Br). The predictions of Gribakin-Lee theory from Ref. [71] are shown by the solid curves.

In a recent model for VFR in Kr dimers, which assumes s-wave positron potentials for each atom, small ($\sim 10\%$) shifts in bond length and frequency occurred following positron attachment [65, 72]. In this case, the molecule is only weakly bound by Van der Waals forces. Using several alternative approaches, a similar shift in bond length was found for LiH [73–75]. Presumably, this would also lead to a change in vibrational frequency. It is difficult to judge how strong this effect might be in larger molecules.

At present, molecules with quantitative predictions for ϵ_b tend to have large dipoles and inconveniently low vapor pressures. For instance, there are several calculations of positron binding to alkali metal hydrides and alkali earth oxides such as BeO [53, 73–78]. They all seem to include changes in bond length. To the author's knowledge, the largest molecules with rigorously calculated values for positron attachment are urea and acetone [79,80]. These molecules have bound states but do *not* appear to have significant changes in bond length [75]. It is not clear whether this can be generalized to other polyatomic molecules. Note that there are no experimental data for any of these molecules, and nearly all of them have large dipoles which exceed the threshold conditions for a bound state [81].

Gianturco has suggested that a change in geometry such as an increase in bond length or angle might be *required* to permit binding and VFR in small hydrocarbons [82,83]. This implies that the binding can depend on the type and amount of vibrational excitation. It also implies that a mode could change frequency in response to binding. However, his calculations tend to require very significant deformations for binding. For instance, acetylene requires the C-C-H angle to deform by 16° in order to bind a positron. It is unclear what mechanism could induce such a large change with the limited energy available due to weak positron binding.

The remaining possibility is that resonant positron binding is far more complicated than originally believed. Since binding is so intimately connected to the VFR process, this topic will be revisited in a later section.

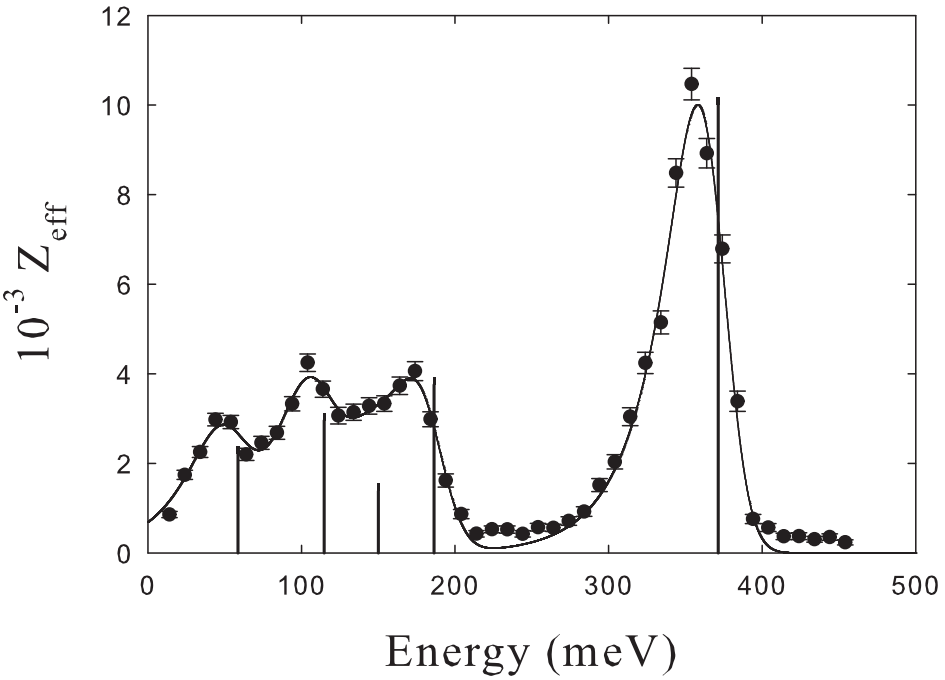

Figure 4.4: Energy-resolved Z_{eff} for propane (•) with a fit (—) produced by convolving five delta functions of arbitrary amplitude and position (vertical lines), with the incident positron energy distribution function. Note that, while the magnitudes of these delta functions exceed greatly the predictions of the Gribakin-Lee theory, they still occur close to fundamental vibrations, after correcting for the ~ 10 meV binding energy.

4.4 Propane, a "large" molecule

While the Gribakin-Lee theory works well for molecules with a few atoms, it breaks down as the number of atoms increases. Molecules such as propane (C_3H_8), shown in Fig. 4.4, have peaks at the fundamental modes which are orders of magnitude larger than that predicted by this "one mode–one peak" VFR theory. Furthermore, the characteristic dominance of the low energy resonances in the halomethanes is replaced by a dominance of the high-energy C-H stretch resonance. In this case, the *relative* Z_{eff} peak heights are no longer determined by the g factor alone.

Clearly, a new mechanism is required to produce the observed enhancement in Z_{eff}. Gribakin has suggested that the number of available VFR states can be effectively increased by intramolecular vibrational redistribution (IVR) [49]. In his model, the energy of the initially excited fundamental vibration, called the "doorway" state, rapidly relaxes into a reservoir of nearly degenerate multi-mode vibrations, called "dark" states. As a result, there are more opportunities for annihilation. Thus, resonant Z_{eff} is enhanced by the local density of "dark" states. This is discussed at length in the next chapter.

Because of its distinct properties, propane is referred to here as a "large" or enhanced-Z_{eff} molecule while the halomethanes are referred to as "small" or Gribakin-Lee molecules. Essentially, the Gribakin-Lee theory is used as a tool to distinguish these two classes. If a Z_{eff} spectrum can reasonably be ascribed to a series of relatively small, mode-based resonances, then the molecule is called "small." If one must invoke IVR or some other enhancement process, then the molecule is called "large." In some cases, it is not clear which classification is correct. Over the next few sections, we consider a variety of intermediate-sized molecules in attempt to better understand this transition in behavior.

4.5 Methanol

4.5.1 Z_{eff} spectrum of methanol

One of these intermediate molecules is methanol (CH_3OH), a substituted methane with the same number of electrons as CH_3F but with one more atom. Experimental Z_{eff} and gas-phase IR absorption spectra for this molecule are shown in Fig. 4.5. Data from a number of experimental runs were averaged to better resolve the feature above the C-H stretch vibrational mode. As a result, the region between 350 and 450 meV may be slightly mismatched with the rest of the data due to systematic errors.

The general shape of the Z_{eff} spectrum is similar to that of the halomethanes except that the C-H stretch peak is a bit broader. There is also a peak at 430 meV which appears to be due to the O-H stretch vibrational mode. This is the first time that a Z_{eff} feature

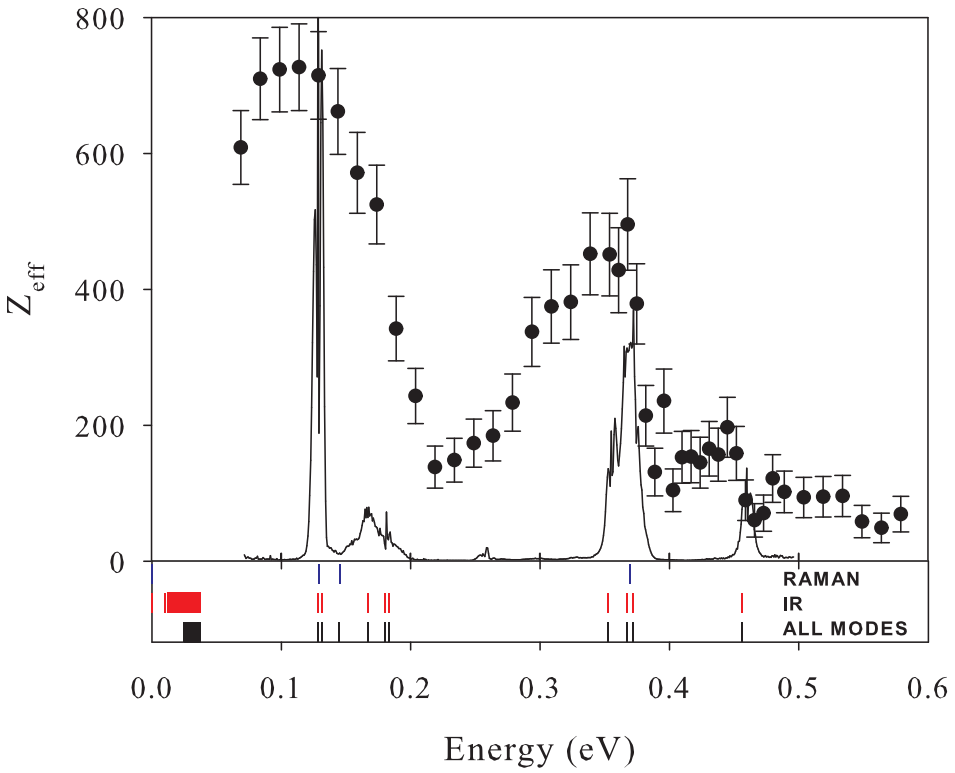

Figure 4.5: Z_{eff} spectrum of methanol. Also shown is the normalized gas-phase IR absorption (—) and vibrational mode energy data (vertical bars) from Ref. [66].

due to a non-carbon-based vibrational mode has been so clearly observed. According to the NIST webbook [66], the theoretical energy of the O-H stretch mode is 456 meV in gas phase. However, comparisons between liquid and gas-phase IR absorption data indicate that the energy of this vibration may be particularly sensitive to the molecular environment. In this way, the presence of a positron may cause a reduction in the O-H stretch mode energy.

The binding energy is difficult to determine from the C-H stretch peak in Z_{eff}, as this peak is broad and occurs within the energy spread of the infrared-active fundamental modes. Perhaps this is to be expected for a molecule so similar to CH_3F. However, whatever process caused the upward shift in the C-H stretch peak position for CH_3F must be absent or suppressed in CH_3OH.

As discussed in the previous sections, the infrared absorption spectrum is expected to be only weakly correlated with the Z_{eff} peak heights. That said, each infrared peak in Fig. 4.5 seems to correlate with a VFR peak. In fact, one might attribute the enhanced Z_{eff} around 250 meV to the overtone/combination mode peak observed in the infrared spectrum. This possibility is discussed further in the next section.

4.5.2 An adapted Gribakin-Lee model

The Gribakin-Lee model was used to calculate the theoretical curves in Fig. 4.6, with some adjustments as described below.[1] To calculate the capture widths, Gribakin used a combination of experimental and theoretical values for the frequencies and dipole moments, shown in Table 4.2.[2] For the dashed curve in Fig. 4.6, only VFR from the fundamental modes are included. This results in a narrow C-H stretch peak that is half the size of the experimental peak. Adjusting the binding energy does not fix this problem. The binding used in the figure is 2 meV. By quadrupling this quantity, the C-H stretch peak is brought up to the experimental height. However, the low energy

[1] Results provided by Ref. [71]

[2] Mode energies, ω_ν, are from Ref. [66]; and dipoles, d_ν, from Ref. [84], except mode 1 (the CH stretch) and mode 10 (the CH_3 d-deform), for which the theoretical values of Ref. [85] were used.

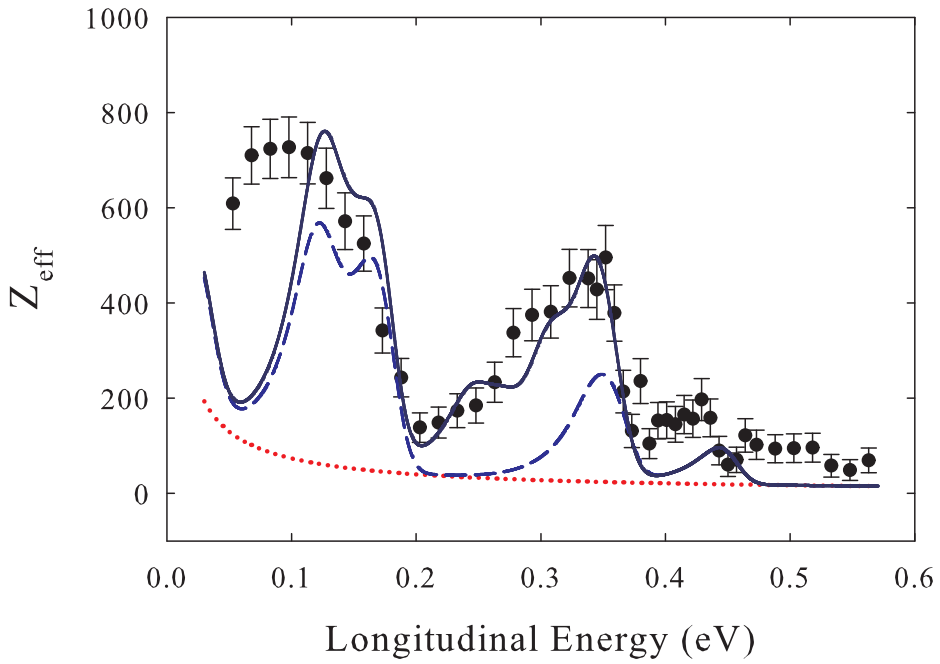

Figure 4.6: Z_{eff} for methanol, with adapted Gribakin-Lee model predictions, assuming 2 meV positron binding energy. The dotted curve represents the non-resonant (direct) contribution; the dashed line represents the total contribution including only fundamental-mode VFRs; and the solid curve represents the total contribution including both fundamental and multi-mode VFRs. Theoretical results were provided by G. Gribakin (private communication). See text for details.

Table 4.2: Energies, ω_ν; mode degeneracy factors, g_ν; dipole moments,d_ν; normalization factor $h(\xi)$ (assuming $\epsilon_b = 2$ meV), and normalized capture width $\Gamma^e_\nu/h(\xi)$ for the vibrational modes of methanol.[1,2] Mode numbers greater than 12 refer to combination modes and overtone excitations. Where possible, a plausible identification for these modes is suggested.

mode	ω_ν [meV]	g_ν	d_ν [a.u.]	$h(\xi)$	$\Gamma^e_\nu/h(\xi)$ [μeV]
ν_1	456.4	1	0.0265	0.31	190
ν_2	369.5	1	0.025	0.39	137
ν_3	351.3	1	0.026	0.35	141
ν_4	183.1	1	0.016	0.44	27.8
ν_5	179.8	1	0.011	0.45	12.9
ν_6	176.3	1	0.040	0.45	167
ν_7	138.3	1	0.026	0.49	55.4
ν_8	128.3	1	0.074	0.5	416
ν_9	365.2	1	0.029	0.34	182
ν_{10}	183.1	1	0.016	0.44	27.8
ν_{11}	134.9	1	0.0087	0.49	6.05
ν_{12}	36.58	1	0.087	0.70	164
$\nu_{13} = 2\nu_5, \nu_4 + \nu_6$	359.6	1	0.027	0.34	155
$\nu_{14} = \nu_5 + \nu_6$	357.1	1	0.012	0.34	30.5
$\nu_{15} = 2\nu_6$	347.8	1	0.024	0.35	123
$\nu_{16} = \nu_7 + \nu_{10}$	321.9	1	0.0086	0.36	14.1
$\nu_{17} = \nu_8 + \nu_{10}$	312.7	1	0.016	0.36	47.4
$\nu_{18} = 2\nu_7$	276.4	1	0.006	0.38	5.89
$\nu_{19} = 2\nu_8$	253.6	1	0.008	0.39	9.61
ν_{20}	161.2	1	0.017	0.46	27.6
ν_{21}	148.8	1	0.018	0.48	28.6

peak then becomes too large.

To reconcile this, Gribakin considered coupling to combination and overtone modes. He used the dipole widths from the experimental IR absorption spectra in Ref. [84]. This adjustment resulted in an enhanced height and width around the C-H stretch peak with little change in the low energy peaks. The agreement at high energies is much better than when only fundamental modes were allowed. The width of the C-H stretch is also

improved.

One discrepancy between model and experiment is the relatively small value of Z_{eff} predicted below 100 meV. Gribakin actually includes the torsion mode at $\sim$ 40 meV, which causes a slight upturn in Z_{eff} near zero energy. However, it does not have sufficient strength and width to bridge the gap to the next peak at higher energy. According to the NIST webbook, the energy of this torsional mode is poorly defined due to a "large coupling between internal and overall rotations" [66]. While this effect might allow a shift or redistribution of this Z_{eff} peak, the overall weight of the peak would still be too small. Gribakin has suggested that perhaps overtones of this mode can contribute, but at present, there is no estimation of their magnitudes [86].

Other than the caveat mentioned above, this adapted theory works surprisingly well. This is significant because it was previously thought that such multi-mode resonances could only be populated indirectly, via single-mode doorways [49,65], instead of directly, as is the case in methanol. Indeed, previous experiments with large molecules indicated that only fundamental modes supported VFRs [24, 43, 45]. As discussed in the next chapter, an exception to this behavior for a large molecule, benzene, was discovered recently. As it turns out, there may be many previously overlooked examples multi-mode VFR in small molecules. They will be discussed at some length in later sections.

4.5.3 Overtone & combination mode VFRs

It is natural to ask why multi-mode VFR are not observed in the Z_{eff} spectra of the halomethanes. The Gribakin-Lee model by itself provides no strong selection rules. Any excitation with a capture width within a few orders of magnitude of the fundamental mode capture width is expected to produce a measurable VFR. In contrast, Table 4.2 shows that the capture widths of some combinations and overtones can be less than an order of magnitude smaller than those of the fundamental vibrations.[3] By this reasoning, multi-mode VFR should be more prevalent. To suppress a VFR in this model, either the

[3]To some degree this is aided by mode-mixing with degenerate fundamental modes.

capture width must be lowered below Γ^a or another exit channel must be introduced. The annihilation width itself cannot be changed as that would result in a change in F, which determines the overall magnitude of all of the resonances.

It is possible that the Born-dipole approximation overestimates the magnitudes of these capture widths. While this approximation does quite well in describing single-mode, vibrationally inelastic scattering for a variety of simple molecules (i.e., within a factor of two) [29], it may well fail when describing resonant vibrational excitation below threshold. Since the final positron state is bound instead of free, the calculation is far from identical. The magnitude of the capture width Γ^e_ν intimately depends upon the details of this bound state, which is poorly understood.[4]

On average, the Γ^e_ν/Γ^a for the fundamental modes in methanol are about five times larger than Γ^e_ν/Γ^a for those modes in CH_3Cl. In other words, the multi-mode capture widths in CH_3Cl are probably five times closer to Γ^a. If the estimates of all the capture widths were too large by a factor of one hundred, multi-mode excitations would likely be VFR-active in methanol, but not in CH_3Cl. Only a direct experimental measurement of Γ^e_ν could determine if this is the case.

An alternate way to suppress multi-mode VFR is to allow inelastic exit channels. For instance, a positron may excite two vibrational quanta, become temporarily bound, then absorb one quantum and be ejected from the molecule. Since single-mode elastic widths should be larger than multi-mode elastic widths, the former should dominate the total width, causing an overall suppression of Z_{eff}. While this is a great hypothesis, as will be shown in the next chapter, it conflicts with the behavior observed in most large molecules. It also conflicts with the results of the a cold-cell experiment discussed in that chapter.

All told, the relative strengths of single and multi-mode VFR seem to indicate a better calculation of the capture width is needed. This will become especially clear in the next section. The other possibilities, such as variations in annihilation width and

[4] In future, it may be possible to directly measure this capture width by looking for resonances in elastic scattering. This will be discussed in the conclusion chapter.

additional escape channels are more difficult to reconcile with the experimental results.

4.6 Two-carbon molecules

As discussed, the Gribakin-Lee theory can clearly be adapted to describe methanol. However, it starts to lose predictive capability with further changes in molecular size and shape. Assorted diatoms do not exhibit VFR. In contrast, "large" molecules, like propane, have greatly enhanced resonances which are orders of magnitude larger than those predicted by this small-molecule theory. The methyl halides sit in a comfortable zone in the middle of this progression, where the Gribakin-Lee theory is most effective. A lot can be learned by looking outside of this zone. The focus of this section is the two-carbon molecules: acetylene, ethylene, ethane, and ethanol. Each of these molecules displays unique properties hinting at some type of transitional behavior.

4.6.1 Acetylene, ethylene, and ethane

Acetylene (C_2H_2), ethylene (C_2H_4), and ethane (C_2H_6) have increasing numbers of vibrational degrees of freedom and decreasing C-C bond strengths. Acetylene has a triple bond, ethylene a double bond, and ethane a single bond. The Z_{eff} spectra for these molecules, measured in our lab by Barnes and Gilbert and reported in Refs. [24, 43, 62], are shown in Fig. 4.7.

At the time of these papers, comparatively little was known about the processes relevant in small molecules. The Gribakin-Lee theory did not yet exist. Recent developments in theory and experiment provide a new context for these previous results. For the sake of completeness, the important features of these two-carbon molecules will be recounted, then given a fresh analysis.

There are a number of features to notice in these molecules. First, there is an unusual change in the shape of the Z_{eff} spectrum with increasing hydrogen saturation. Acetylene is dominated by a low-energy peak with no sign of a C-H stretch peak; ethylene has both peaks; and ethane is dominated by a large C-H stretch peak, with a weaker low-energy

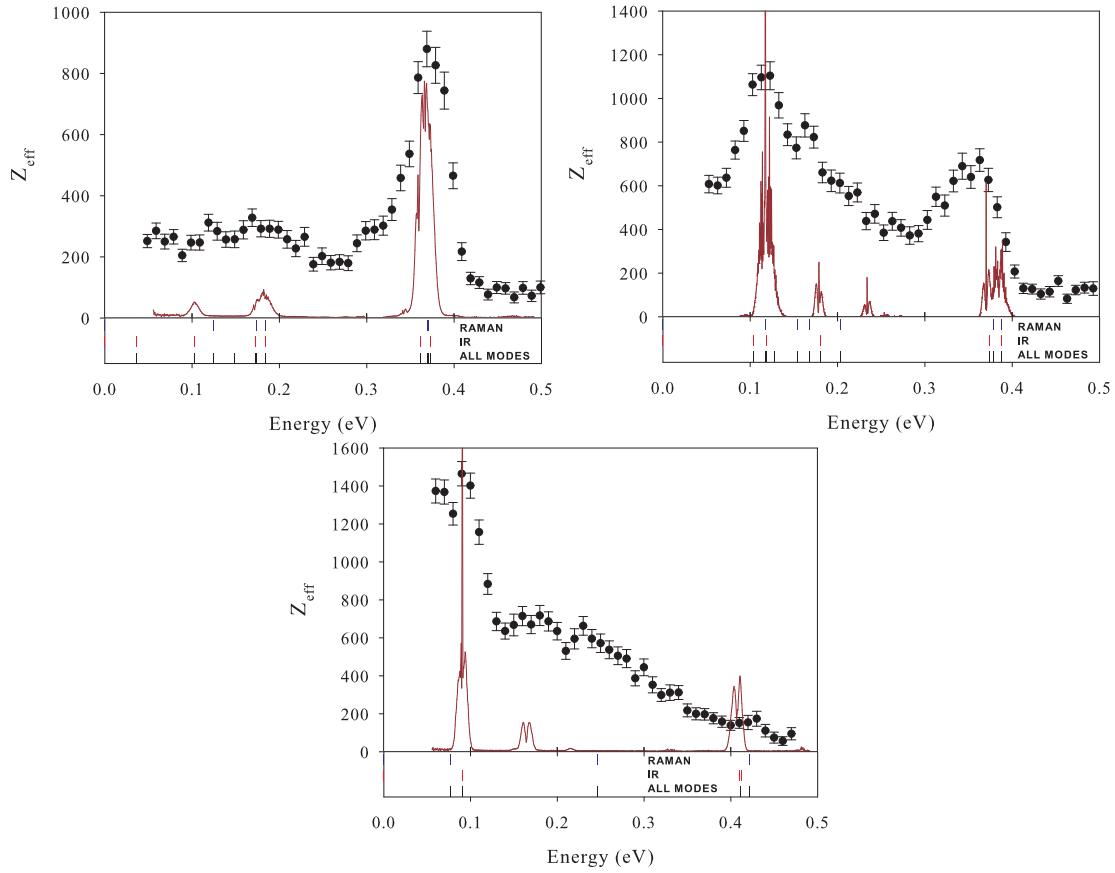

Figure 4.7: Z_{eff} (•) for (a) ethane, (b) ethylene, and (c) acetylene reproduced from Ref. [24]; the solid curves (—) show normalized infrared absorption spectra from Ref. [66], and the vertical bars below each plot indicate the fundamental vibrational modes, also from Ref. [66].

plateau. The Z_{eff} spectra of the latter molecule is closer to the shape observed in propane and other large alkanes. In all three molecules, there is a strong "background" Z_{eff} in the region between the low energy bending modes and the C-H stretch mode. Ethylene seems to have the greatest binding energy of the three.

The original interpretation of these results was that perhaps the type of C-C bond or number of C-H bonds are somehow responsible. One might also point to changes in the infrared absorption spectra which roughly mirror those seen in Z_{eff}. In light of more recent data for small molecules, other patterns can be discerned. Specifically, some behavior can be described by comparing with other molecules of equivalent size. Take for instance ethylene (C_2H_4). It has the same number of hydrogens and heavier atoms as methanol (CH_3OH). Its Z_{eff} spectrum also bears a strong resemblance to methanol, with the exception that it does not have an O-H stretch peak. Like methanol, the low-energy peak is larger than the high energy peak. The ratio of the low and high-energy peak heights is similar (around 1.5 for methanol vs. 1.6 for ethylene). The magnitudes of the peaks in ethylene are slightly larger, but so is the binding energy. The weight in the middle range of energies is likely due to overtone/combination-mode VFR. For instance, the strong multi-mode infrared peak at around 230 meV could produce VFR in that region.

Attempts to reproduce the ethylene spectrum with the Gribakin-Lee model have had limited success. The main difficulty is determining the relative strengths of the many multi-mode and infrared-forbidden VFR, which appear necessary to explain the observed spectrum. It has already been established that the approximate methods described in section 4.2 may be insufficient for these border-line resonances. That said, with the proper elastic coupling parameters, this molecule is probably still consistent with the small molecule VFR model.

Acetylene is actually smaller than methane and its derivatives. The closest molecule with available Z_{eff} data is ammonia (NH_3), which has the same number of atoms. Energy-resolved Z_{eff} for NH_3 can be found in Ref. [62] and is reproduced in Fig. 4.8. As it turns out, the Z_{eff} spectra of acetylene and NH_3 are remarkably similar. In both,

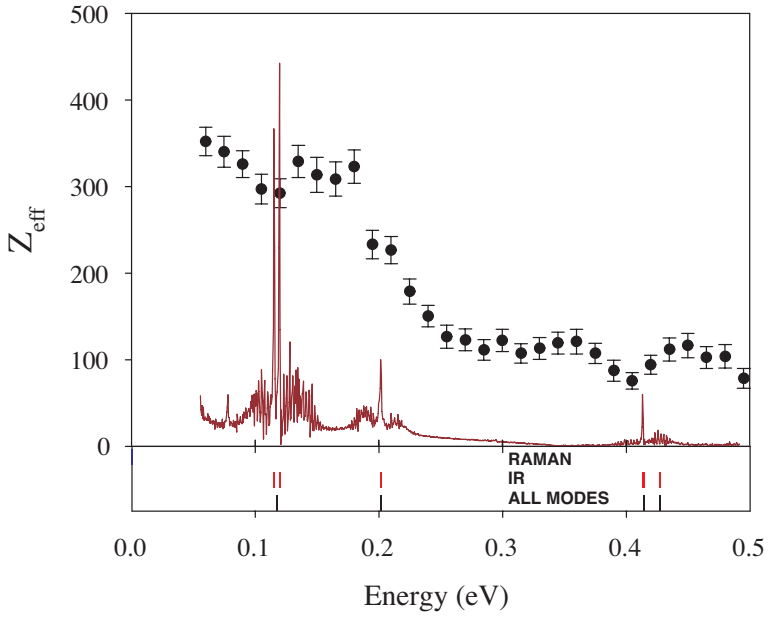

Figure 4.8: Energy-resolved Z_{eff} and infrared absorption spectra for ammonia reproduced from Ref. [62]. The bars below indicate the positions of vibrational modes (from Ref. [66]).

there is a low energy feature, a significant "background" Z_{eff}, and little or no high energy peak. Acetylene has a thermal Z_{eff} of 3160 [12], which is also a strong indicator that low energy VFR might be present (the maximum Z_{eff} for direct annihilation is $\sim 10^3$ [23]).[5] While the thermal and energy resolved Z_{eff} for acetylene is larger than that of ammonia by about a factor of two or more, this might be explained by a difference in the modes and the g factors. For instance, the relative magnitudes could be explained if acetylene had a binding of 5 meV and NH_3 a binding of 1 meV, which is not inconsistent with the available data.

Evidence seems to indicate that both acetylene and ammonia bind a positron to produce Z_{eff} peaks at low energy—yet neither have peaks from high energy modes.

[5]The contribution from direct Z_{eff} may in fact be close to this maximal value because of a low-lying virtual or weakly bound state [87]

Maybe some symmetry selection rule is responsible. In addition, both seem to have a strong "background" Z_{eff} which is likely due to overtone/combination mode resonances. In fact, the infrared spectrum of acetylene, shown in Fig. 4.7(c), has resonances around 170 meV and 210 meV, both of which are due to overtones. There is also an infrared-inactive mode around 245 meV. Here again, difficulties in calculating borderline capture widths make it difficult to include these effects in a quantitative model for Z_{eff}.

The largest molecule in this series is the alkane, ethane. Like the other molecules discussed in this chapter, ethane has a significant "background" Z_{eff}, especially around 250 meV, where there are no fundamental modes. This is likely due to multi-mode VFR. However, ethane also has many characteristics in common with larger alkanes, such as propane or pentane. The signature feature of these molecules is an unusually large C-H stretch peak and a weak low energy plateau, presumably due to C-C and C-H bend modes. This Z_{eff} spectrum is virtually impossible to achieve using the small molecule theory. In particular, one would expect the peak heights to be proportional to the degeneracy and the factor $g = \sqrt{\epsilon_b/\epsilon}$. This factor should result in a C-H stretch peak which is *smaller* than the lower energy peaks, as it is in the methyl halides. Like CH_3F, the binding energy of ethane is close to zero, significantly reducing the predicted magnitudes of all VFR. In fact, its low energy Z_{eff} is as weak as that of CH_3F, which has a model-fitted binding energy of 0.3 meV.

The C-H stretch peak has clearly been enhanced in some way. The observed enhancement, using CH_3F for comparison, is about a factor of five above the Gribakin-Lee prediction (taking into account the 50% increase in number of C-H stretch modes). In other words, there are effectively 30 states contributing to the C-H stretch peak in ethane, even though this molecule has only six C-H stretch modes.[6] This is likely the same VFR-enhancing phenomenon observed in larger alkanes like propane. As mentioned in section 4.4, this enhancement is probably caused by IVR (intramolecular vibrational relaxation), a process which effectively increases the resonant states populated by posi-

[6] In fact, there are only 18 fundamental vibrations in ethane.

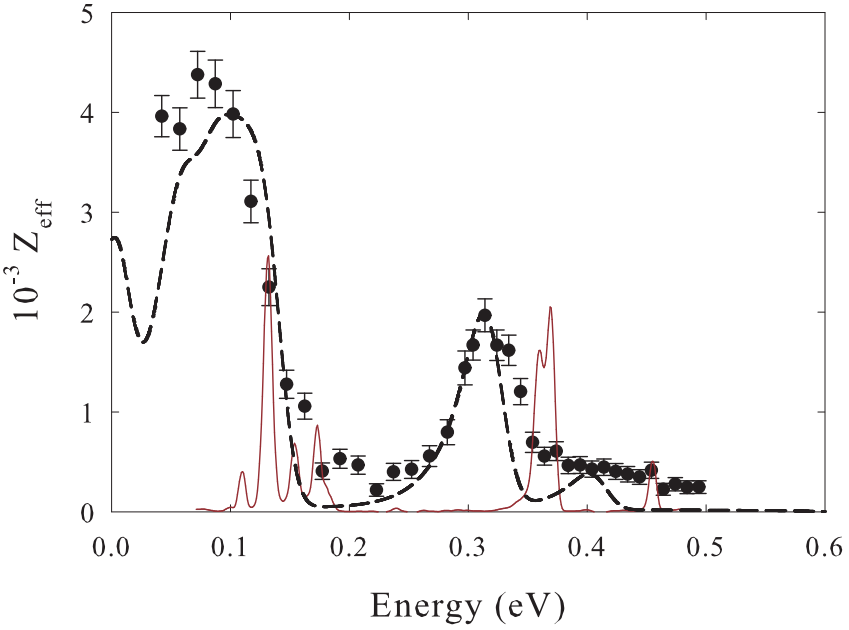

Figure 4.9: Experimental Z_{eff} for ethanol (•), with Gribakin-Lee model (- -) and normalized infrared absorption (—) from NIST [66].

tron capture near a VFR-active vibration [49]. Thus, those "extra modes" in ethane are probably combination and overtone modes accessed via IVR.

4.6.2 Ethanol

The final molecule in this set is ethanol (C_2H_5OH), whose energy-resolved Z_{eff} spectrum is shown in Fig. 4.9. This molecule has more degrees of freedom than the other two-carbon molecules yet it does not have the same enhanced-Z_{eff} behavior of ethane or the larger alkanes. Like methanol, it has a terminal -OH group, which may be connected to its different behavior.

The primary characteristic of ethanol is the dominance of the low energy peak over the C-H stretch peak. This behavior is more like that of smaller molecules like the

halomethanes and ethylene. The huge enhancement of the C-H stretch peak observed in ethane is absent. Also absent is a clear O-H stretch peak, which was weak to begin with in methanol. Instead, there is a smeared-out feature between 350 and 450 meV. In addition, the "background" Z_{eff} between peaks is relatively small.

It appears that this larger molecule is acting like a "small" molecule. The binding energy is around 40 meV, similar to CH_3Br, but the low energy peak has a Z_{eff} of $\sim$4500, more than twice that of CH_3Br. Since ethanol has more than twice as many vibrational degrees of freedom, it appears to be acting exactly according to the Gribakin-Lee small molecule model. In fact, if all fundamental modes are assumed active, the predictions of the model agree surprisingly well with the data. This is also shown in Fig. 4.9. Something is suppressing or preventing the expected enhancement of Z_{eff} at the C-H stretch peak. A similar suppression is observed in the Z_{eff} spectra of large, fluorine-substituted alkanes like 1-fluorohexane and 1-fluorononane [24, 43, 45]. This chemical sensitivity is discussed at length in the next chapter.

4.7 Propane and cyclopropane

In this section, propane (C_3H_8) is compared to its cyclic analogue, cyclopropane (C_3H_6). Cyclopropane is formed by removing two of the terminal hydrogens in propane and joining the ends of the molecule together. The structures of both molecules are shown in Fig. 4.10. As can be seen in Fig. 4.11(a), propane displays the typical Z_{eff} shape of large alkanes, with a dominant C-H stretch peak and a low energy plateau of C-H bend and C-C peaks.

The Z_{eff} spectrum of cyclopropane, shown in Fig. 4.11(b), has a number of features which distinguish it from that of propane. Its C-H stretch peak is half as large as that of propane, while it has 3/4 as many C-H stretch modes. The value of Z_{eff} in the low energy region is about the same as that of propane (i.e. $\sim$ 4000) but only in a narrow region. The binding energy for both these molecules is small, i.e., $\sim 10-15$ meV. While the uncertainty in binding may result in differing g factors, this alone cannot provide a

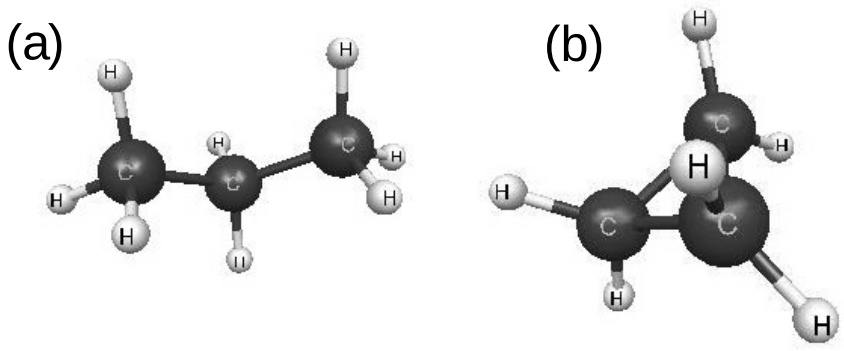

Figure 4.10: Structures for (a) propane and (b) cyclopropane.

consistent explanation of the observed effects.

In both cases, the small molecule VFR theory would predict a relatively weak C-H stretch peak, especially for the small binding energies of these molecules. Hence, both molecules exhibit "large" molecule VFR behavior, as defined in section 4.4. In this context then, the reduction in the C-H stretch peak height is not very surprising. As will be shown in the next chapter, the scaling of the resonant Z_{eff} in molecules larger than ethane is highly nonlinear.

The broad plateau in propane becomes a single peak in cyclopropane. This is probably due to a reduction in VFR-active bending and C-C modes in cyclopropane relative to propane. Since these modes are distributed more sparsely than the C-H stretch modes, the magnitudes of the VFR peaks remains the same, but the number of peaks changes. The fact that Z_{eff} does not change for these peaks suggests that the Z_{eff} enhancement process is unaltered.

When comparing the Z_{eff} and infrared absorption spectra in these molecules, one finds some parallels but no absolute proportionality. This is consistent with the Gribakin-Lee theory for small molecules in which the magnitude of Z_{eff} depends on the number of dipole-allowed modes but not the magnitude of the coupling. As is discussed in Ref [45]

and the next chapter, this intuition seems to hold for other large molecules.

In the Z_{eff} spectrum of cyclopropane, there is a small feature at 250 meV, in the valley between the C-H bend and C-H stretch peaks. As pointed out by G. Gribakin, this feature occurs in the same region as enhancements in the infrared absorption [88]. The conclusion is that this feature in Z_{eff} is likely due to combination-mode VFRs. If this is the case, it is interesting that these peaks are so weak. Their magnitudes are more like those of a VFR in a small molecule. Perhaps large-molecule Z_{eff}-enhancement processes do not occur as effectively for these types of resonances. This would explain why multi-mode VFR are so rare in larger molecules [24, 43, 45]. Indeed, the magnitude of Z_{eff} around 250 meV in propane is similar to that in cyclopropane. This indicates that these features may persist in larger molecules but only with tiny relative magnitudes. It is not understood why this is the case.

4.8 Comparison of "small," "large," and "suppressed" molecules

With more examples to draw from, it is possible to reexamine the distinction between "small" VFR-active and "large" VFR-active molecules. We regard the substituted methanes, acetylene, and ethylene all as "small" molecules. While there are some issues about which modes are counted, none deviate too far from the Z_{eff} magnitudes allowed by the Gribakin-Lee theory. On the other hand, we regard ethane, cyclopropane, and all alkanes with three or more carbons as "large" molecules. Their Z_{eff} magnitudes are enhanced by some process not accounted for by this simple, mode-based VFR theory. Presently, the best explanation for this enhancement is some kind of IVR process, as described in Ref [49]. This process will be considered in depth in the next chapter, which focusses exclusively on large molecules.

There is another important class of molecules: "suppressed" VFR-active molecules. These molecules have a nontrivial binding energy and a size and structure similar to that of "large" molecules, but have unusually weak Z_{eff} compared to other "large" molecules.

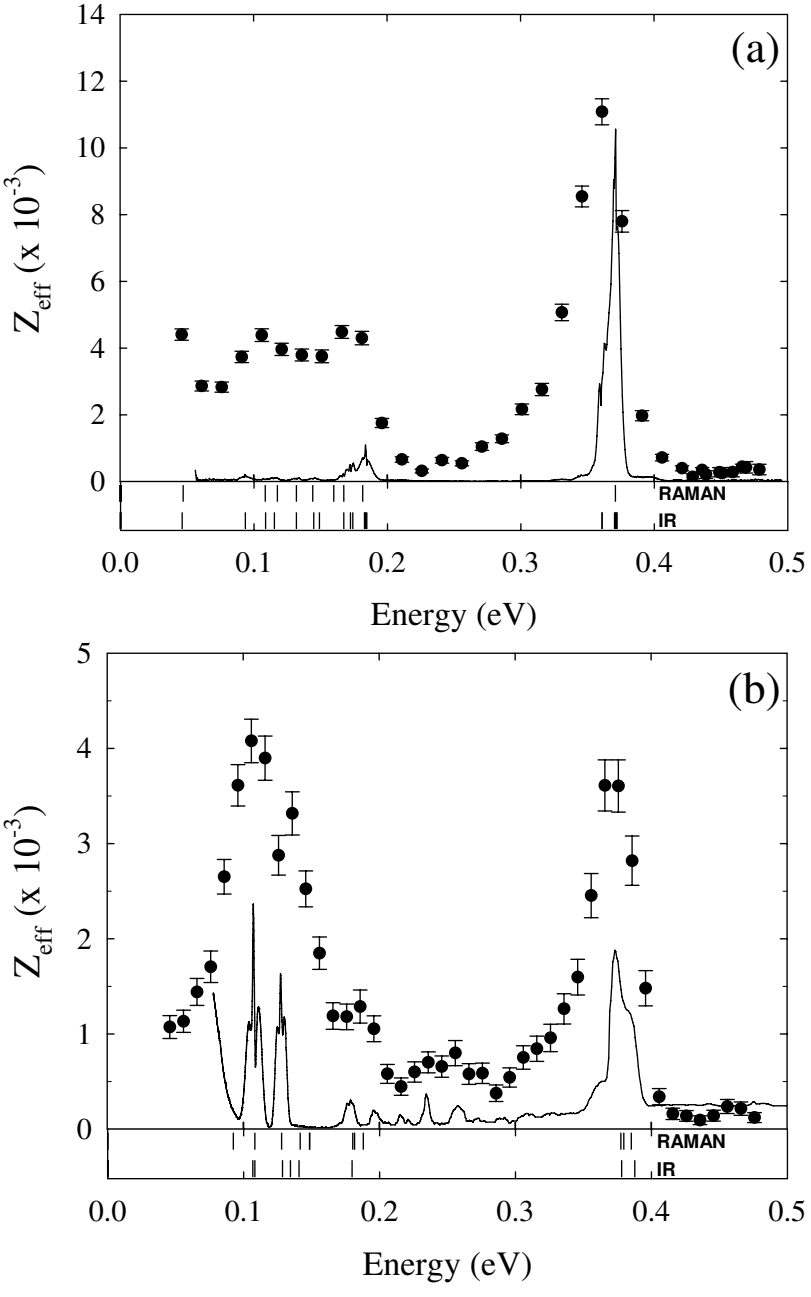

Figure 4.11: Energy-resolved Z_{eff} (•) for (a) propane and (b) cyclopropane. The solid curve (—) represents normalized IR absorption and the vertical bars below each plot show the active vibrational mode energies, both from Ref. [66].

Ethanol might be grouped into this class, as it is derived from ethane, which acts like a "large" molecule. Other "suppressed" molecules, like 1-fluorononane, have a strongly suppressed C-H stretch peak, but also have an overall Z_{eff} which exceeds Gribakin-Lee VFR predictions by orders of magnitude [43, 45]. These "suppressed" species will be considered more thoroughly in the next chapter.

4.9 VFR-weak or inactive molecules

There is one final class of molecules, those with little evidence of VFRs. This means that either the VFRs do not exist or they are too weak to be detected. In some cases, there are hints of weak structure. However, that structure is not like any VFR observed to date. Frequently, only a small change in structure is required to make such a molecule VFR-active. For instance, while CH_3F has VFR peaks, CH_4 (methane) does not [43]. This can be seen in Fig. 4.12. In this section, new data for CO_2 and H_2O are presented, demonstrating that they belong to this broadly-defined class of molecules with little or no VFR.

4.9.1 CO_2 and H_2O

Water and carbon dioxide are among the smallest molecules studied to date. The original reason for looking at these molecules is that both have a relatively small number of electronic and nuclear degrees of freedom, which is expected to simplify theoretical calculation of their positron binding energies and VFR magnitudes. However, as seen in Fig. 4.13, neither of these molecules appear to exhibit VFR, so there is no way to empirically determine their binding energy (or virtual state energy, as the case may be).

Fig. 4.13 (a) shows the energy resolved Z_{eff} of CO_2 as well as the infrared absorption and mode data from NIST [66]. Ignoring the considerable noise, the Z_{eff} spectrum is relatively smooth and has a baseline value of ~ 35. Since $Z = 22$, this is not too far from that of the uncorrelated electron gas prediction. At low energies, $Z_{\mathit{eff}}^{(dir)}$ should be dominated by annihilation due to positron overlap during elastic scattering [23]. This

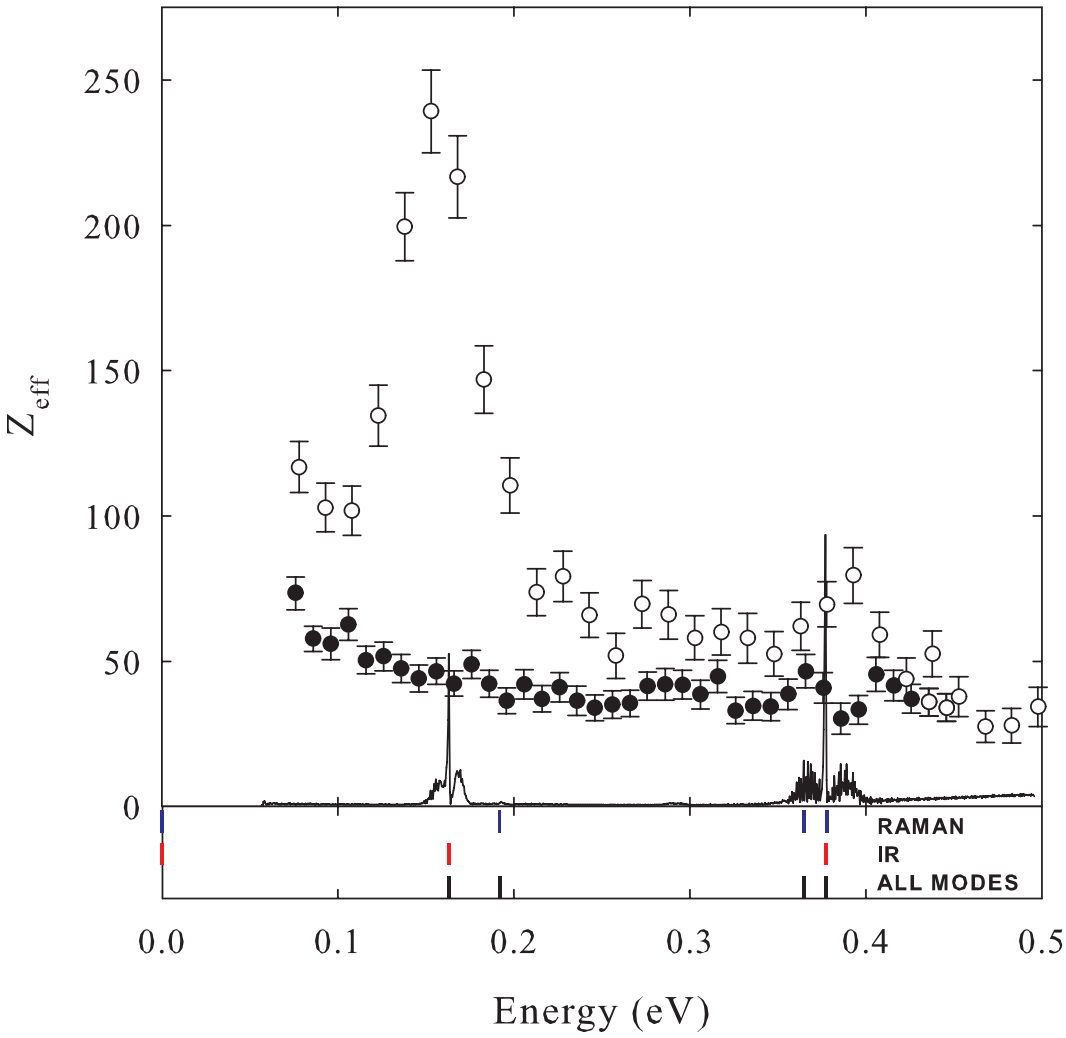

Figure 4.12: Energy-resolved Z_{eff} for (•) CH_4 and (◦) CH_3F from Ref. [43]. The solid curve (—) represents normalized IR absorption for CH_4 and the vertical bars below this plot show the active vibrational mode energies for CH_4, both from Ref. [66]. Note the lack of VFR in CH_4 as compared to CH_3F.

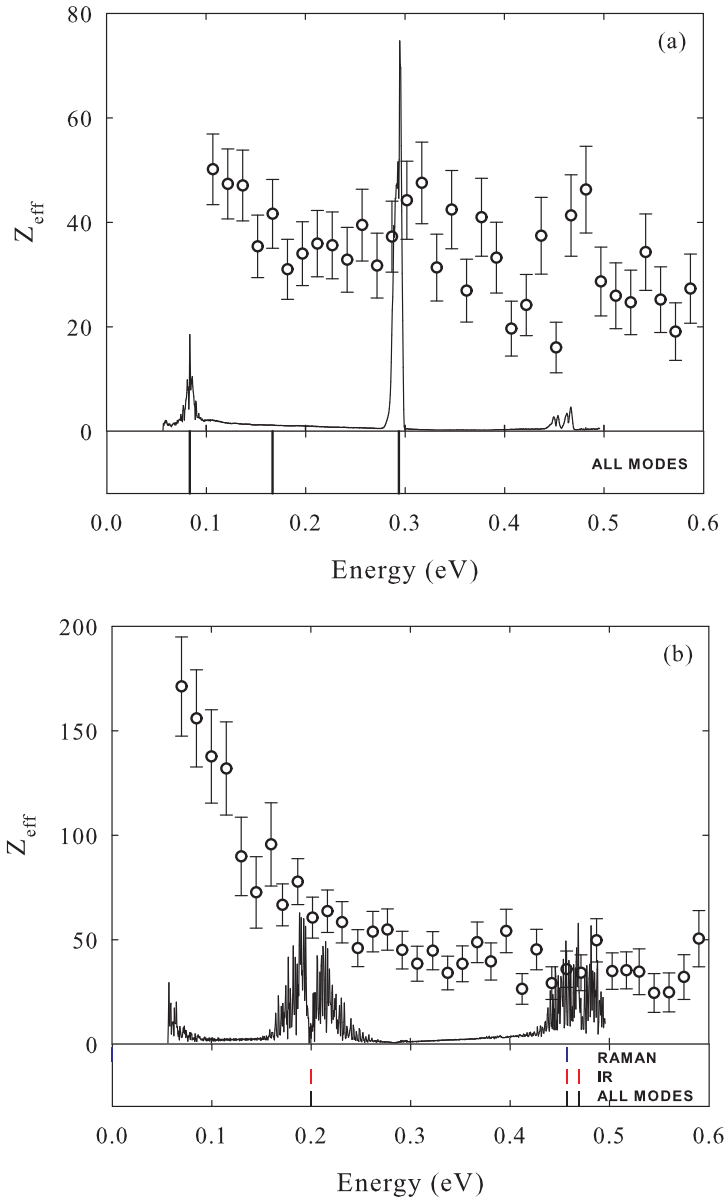

Figure 4.13: Energy-resolved Z_{eff} (○) for (a) CO_2 and (b) H_20. The solid curve (—) represents the normalized IR absorption spectrum and the vertical bars below each plot show the active vibrational mode energies, both from Ref. [66].

could explain the slight rise in Z_{eff} as the positron energy approaches zero. The thermal value of Z_{eff} is 54.7 [1]. The fact that there are no VFR evident near the IR absorption peaks seems to indicate that there is no bound state. A fixed nuclei calculation by Gianturco *et al.* predicts a relatively flat spectrum with no resonances and $Z_{eff} \sim 50$ [89]. This relatively good agreement occurs with few assumptions in the model. It helps that there are no resonances to take into account.

Fig. 4.13 (b) shows data for water. The results are similar to CO_2. The spectrum is smooth and has a slightly higher baseline Z_{eff} of ~ 50. It also has a much larger upswing near zero energy, approaching $Z_{eff} \sim 175$. Indeed, the thermal value of Z_{eff} is 319. This is suggestive that binding and VFR might be present. However, a virtual state near zero energy could also produce a large direct Z_{eff} near threshold (up to ~ 1000, assuming room temperature positrons) [23].

4.9.2 Spectra for CO_2 and H_2O with increased signal-to-noise

A second dataset for CO_2 and water was taken in which the positrons were allowed to bounce back and forth through the gas cell for 40 μs instead of 15 μs. These results are shown in Fig. 4.14 (a) and Fig. 4.14 (b) respectively. While the count rate is improved, various sources of systematic error are still present, if not enhanced.

Scattering can alter both the direction of the incident positrons and, in the case of inelastic scattering, their total momentum. In the first situation, the positron momentum along the gas cell axis is reduced, so the number of bounces through the cell within a fixed time window is reduced, thus suppressing Z_{eff}. Also, if the scattering occurs outside the cell, the positron may not have enough parallel energy to enter the gas cell at its elevated potential, thus preventing further interactions. In the second situation, annihilation can occur at an energy significantly lower than the initial energy. Since these processes may have various thresholds and resonances, they can add additional structure to the observed Z_{eff}. While these effects are usually small, tripling the size of the bounce window can amplify them.

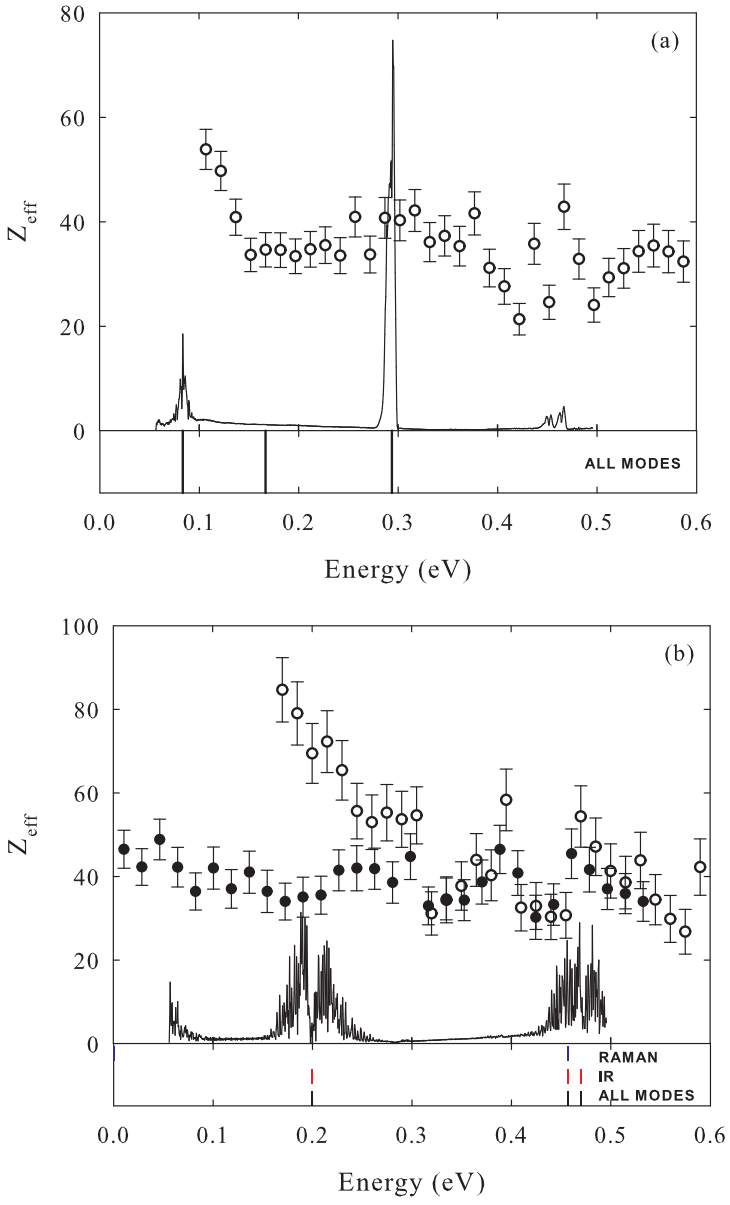

Figure 4.14: Energy-resolved Z_{eff} (○) for (a) CO_2, and (b) H_20, using an extended 40μs bounce window. Note the emergence of new features. The solid curve (—) represents the normalized IR absorption, and the vertical bars below each plot show the active vibrational mode energies, both from Ref. [66]. Also shown in (b) is the Z_{eff} spectrum for CH_4 (•) with rescaled energy $\epsilon' = 1.8\epsilon - 0.27$ eV (see text for details).

That said, some interesting features appear in these longer bounce-window datasets. In CO_2, a small but distinct feature occurs at 450 meV. The infrared absorption spectra from NIST [66] indicate a peak at precisely this energy, which seems to be a combination of the symmetric and asymmetric stretch modes. Contamination due to hydrocarbons can be ruled out in this case, because the dominant feature occurs far above the C-H stretch energy.

The shape of this feature is unlike a VFR, and it occurs where one might expect a multi-mode excitation to be. Thus, we are led to consider other possibilities. For instance, the direct annihilation can have features which parallel those in the elastic scattering cross section. A resonance which enhances the scattering wave function also enhances the pick-off annihilation rate due to positron-electron overlap; this does not even require binding.

There are also various interference terms between direct and resonant annihilation which are usually omitted [23]; they have the form,

$$Z_{eff}^{(int)} = 2\sqrt{\frac{\pi}{k}} Re\left[\sum_{\nu} \frac{\sqrt{\Gamma_\nu^e}\rho_{ep}^{\nu(int)}}{\epsilon - \omega_\nu + \epsilon_b + i\Gamma_\nu/2}\right], \tag{4.13}$$

where

$$\rho_{ep}^{\nu(int)} = \langle\varphi_0(r)\Phi_\nu|\sum_{i=1}^{Z}\delta(\mathbf{r}-\mathbf{r}_i)|e^{i\mathbf{k}\cdot\mathbf{r}}\Phi_0\rangle. \tag{4.14}$$

This produces a feature for each mode which usually cancels with neighboring terms and is washed out after averaging over the experimental line width. However, in the situation described here, the mode spacing is much larger than the experimental line width. If the VFR magnitude is finite but smaller than the direct annihilation, the interference can be comparable to or larger than the VFR. The resulting feature is typically called a Fano resonance [86]. At present, it is not possible to distinguish the origin of the 450 meV feature in CO_2.

Invoking such unusual effects is especially tempting for the Z_{eff} spectrum of water, shown in Fig. 4.14 (b). In this molecule, there is a distinct reduction in Z_{eff} between 300 and 500 meV with a small spike at 400 meV. The center of this feature is below the

OH stretch mode by nearly 80 meV. It is closer to C-H stretch mode energy in alkanes, although no alkane VFR has that kind of structure. A similar feature occurs in the Z_{eff} spectrum of methane (CH_4) at a lower energy. In Fig. 4.14 (b), the feature in methane has been arbitrarily shifted and rescaled in energy to align with the feature in water. The fact that the Z_{eff} features from two different molecules have such a similar shape seems to indicate a common origin. Calculations by Gianturco indicate that water has a reasonably strong vibrational excitation cross section with sharp onsets [90]. These may either directly or indirectly affect the observed Z_{eff} spectra. More measurements will be required to verify and better understand these effects.

4.10 Bound and virtual states

Previous sections in this chapter focussed on the magnitude of the VFR in various small and intermediate-sized molecules. Since ultimately these resonances depend on the existence and magnitude of a bound state, it is worth discussing this crucial molecular property. For weak binding, the binding energy is best understood in terms of the positron scattering length, $1/\kappa$. If $1/\kappa$ is positive, there is a bound state with binding energy, $\epsilon_b = \kappa^2/2$, and VFR with magnitudes proportional to $g = \sqrt{\kappa/k}$, where k is the positron momentum. If $1/\kappa$ is negative, the bound state is replaced by a virtual state in the continuum. In both cases there is a contribution from direct annihilation proportional to $(\kappa^2 + k^2)^{-1}$ [23, 40]. However, because of the broad energy width of the positron beam, it is difficult to extract binding energies from the direct annihilation alone.

Binding energies derived from VFR positions and other data for a variety of small and medium-sized molecules are summarized in Table 4.3. In the cases where there are VFR peaks but the binding energy is too small to measure, the binding energy is given a place marker value of ~ 0. On the other hand, when there is no evidence of VFR, no assignment is made. In this case, positrons either form barely bound or virtual states. Immediately, one can discern some rough trends when comparing the binding

energy to the available physical parameters. To lowest order, binding tends to increase with molecular size. Larger molecules such as propane (C_3H_8) are more likely to bind positrons than small molecules like N_2. That said, there is significant variation of binding with molecular structure.

Another potentially relevant parameter is the permanent dipole moment of the molecule. It has been shown that all molecules with a dipole above 1.625 Debye should be able to support a bound state with an electron or positron [80, 81]. Indeed, all the molecules which meet this criterion in Table 4.3, with the exception of water, do appear to have bound states. Still, this parameter apparently has little influence on the magnitude of the binding energy. Furthermore, there are plenty of molecules with no dipole moment that nonetheless have bound states.

Additional insight can be obtained by comparing with calculations of binding in atoms. According to a simplified model by Mitroy *et al.* for atoms with one valance electron (i.e., alkali atoms), the positron dynamics are determined entirely from the polarizability α (or equivalently, the ionization potential E_i) [48]. In this model, the positron interacts only with the valence electron, which acts in the potential of the core atomic charge. This technique works reasonably well compared to more rigorous fixed-core variational methods or configuration-interaction calculations. Binding appears to increase with increasing polarizability or decreasing ionization potential. Furthermore, the minimum polarizability required to bind a positron is ~ 2.9 Å^3, while the maximum ionization energy is ~ 13.5 eV.

As can be seen in Table 4.3, molecules with no clear VFR [i.e. those with null (–) binding] tend to fall short of these threshold conditions. Conversely, molecules with measurable binding energy or large resonant Z_{eff} (e.g. ethane) more than meet these conditions. One can even attribute the increasing binding in the halomethanes to increasing polarizability. For either parameter, the dividing line between VFR-active and VFR-inactive molecules is not strict. For instance, the VFR-active molecule CH_3F has a polarizability below threshold and below that of CF_4. At the same time, CH_3F has a smaller ionization potential compared to the threshold value and CF_4. Methane meets

Table 4.3: Positron binding energy, ϵ_b; polarizability, α; ionization energy, E_i; and permanent dipole, μ; in assorted medium-sized molecules. Physical parameters are from Ref. [1]. Molecules with no clear VFR have been assigned a null (–) binding energy. 'Threshold' indicates the minimum α and maximum E_i needed for binding in alkali atoms, according to Ref. [48]. It also indicates the minimum dipole moment for which a bound state is required, assuming a point-like potential [81].

Species	ϵ_b [meV]	α [Å^3]	E_i [eV]	μ [D]
threshold	>0	>2.9	<13.5	>1.625
H_2O	–	1.47	12.61	1.85
N_2	–	1.94	15.98	0
CH_4	–	2.6	12.7	0
CO_2	–	2.66	13.77	0
CF_4	–	2.86	16.25	0
NH_3	~ 0	2.26	10.19	1.47
C_2H_2	~ 0	3.33	11.41	0
CH_3F	~ 0	2.39	12.89	1.85
CH_3OH	~ 0	3.28	10.85	1.70
CH_3Cl	25	4.43	11.22	1.87
CH_3Br	40	5.55	10.54	n/a
C_2H_4	20	4.23	10.51	0
C_2H_6	~ 0	4.44	11.52	0
C_2H_5OH	45	5.11	10.1	n/a
C_3H_8	10	6.29	11.14	0.08

both threshold conditions but has no apparent VFR. A more consistent formulation probably requires both physical parameters. This will be discussed in the next chapter.

4.11 VFR precursors

It is worth asking what happens when a molecule just barely falls short of the conditions for a VFR. What kind of features can one expect in the Z_{eff} spectrum? In the section above discussing the 40 μs bounce window data for CO_2 and H_2O, a number of suggestions were made in this vein. The "pick-off" annihilation of a scattered positron accounts for most of the direct (non-resonant) annihilation at low energies. Thus, it is reasonable to expect that strong resonances in total scattering should also be represented in Z_{eff} in some manner. Furthermore, there are structures like Ramsauer-Townsend minima which may be more clearly visible. Unfortunately, at present, there are few measurements with sufficient resolution and signal-to-noise to test these ideas.

As the binding is reduced, the VFR peaks shrink. According to the Gribakin-Lee model, even the capture width will decrease if the binding energy is very close to zero [44]. In this limit, the VFR peak will then decrease proportional to the capture rate. As mentioned earlier, when the VFR peak is very small, interference terms could start to dominate, such as that between the resonant and direct Z_{eff}. This should produce Fano resonances which may or may not be completely washed out when averaged over a broad beam distribution.

At some point the positron bound state disappears and is replaced by a virtual state. The dynamics in this case are much different. Other than the structure in direct annihilation, there are no sharp resonances as VFR are forbidden. At best, broad enhancements are possible. According to Gianturco, a virtual state may lead to long-lived intermediate states during vibrational de-excitation collisions [91]. These states can last several vibrational periods and result in enhanced Z_{eff} at very low energy. They can be described using complex-valued scattering lengths to account for inelastic channels. Presently, there is no experimental evidence that such states exist for positrons.

Another possibility to consider is a shape resonance. In this case, the positron tunnels through a barrier in the molecular potential and becomes temporarily trapped, enhancing its annihilation rate. The lifetime of this state is limited by the probability that the positron can escape by tunneling back out through the barrier. As a result, a shape resonance should manifest itself as a fairly broad peak in Z_{eff} (electron shape resonances can be a few eV wide). Furthermore, they can occur in the absence of a true positron-molecule bound state or an active vibrational mode. This should be distinguished from a vibrational Feshbach resonance, in which the positron is trapped in a true bound state because its kinetic energy has been resonantly transferred into the nuclear degrees of freedom. That process results in a much sharper peak in Z_{eff} with a well-defined energy.

One could also envision a "vibrationally-enhanced" shape resonance, in which a potential barrier temporarily traps the positron following inelastic excitation of a vibrational mode. These states are known to occur in electron scattering, where they manifest themselves as broad resonances in the vibrational excitation cross sections [92]. In the positron case, this process could produce broad annihilation resonances associated with each vibrational mode, even without a true bound state.

The problem with positron shape resonances (vibrationally-enhanced or not) is that it is difficult to produce the required barrier in the potential. Often, this is fulfilled by some sort of centrifugal barrier. However, the low energy positronic states are thought to have angular momentum $\ell = 0$, precluding such an effect. To date, there is a dearth of experimental evidence that such states exist. In the total scattering cross sections of a number of diatomic molecules, there are no shape resonances [93]. In Z_{eff}, there are at best a few cases where Z_{eff} has a broad enhancement in the "background," such as in ammonia or acetylene. However, these features are usually interpreted to be due to combination or overtone mode VFR or additional direct annihilation. There is a prominent prediction that shape resonances should occur in positron-C_{60} interactions due to both centrifugal barrier states and cage states [94]. There is also a recent prediction of a large p-wave shape resonance at $\sim$130 meV in Mg [95]. Future experiments in our lab aim to test these hypotheses.

4.12 Concluding remarks

Small molecules are, in principle, an ideal target for studying positron attachment and annihilation processes. As shown in this chapter, while there is considerable variety in the observed behaviors, theory and experiment are beginning to converge. Gribakin and Lee developed an excellent, quantitative model for VFR-induced annihilation in small molecules with only infrared-active vibrational modes. The best examples are the halomethanes and deuterated halomethanes. However, as the size of the molecule increases and resonances with weak dipole coupling are introduced, the Z_{eff} spectrum becomes more difficult to predict. As discussed, the Gribakin-Lee model can be adjusted to include infrared-active overtones and combination vibrations as well as modes with different symmetries. This works well for methanol, but only qualitatively for acetylene and ethylene. In these cases, at present, one must make arbitrary decisions as to what proportion of these additional resonances should be counted.

A transition in behavior occurs at ethane. This molecule has a large C-H stretch resonance whose height exceeds greatly any reasonable prediction within the framework of the Gribakin-Lee model. For this reason, we classify it as a "large" molecule, governed by additional dynamics which result in larger enhancements in Z_{eff}. Propane and cyclopropane are also in this class, as are all the molecules in the next chapter.

We also included examples of molecules with no identifiable VFR features, such as water and CO_2. These were termed VFR-weak/inactive molecules. It seems likely that their lack of strong resonances results from a lack of positron binding. Measurements to date appear to exhibit some tantalizing structure which may be a precursor to VFR. Various possibilities, including resonances in the pick-off annihilation, VFR-direct interference terms, and vibrationally-enhanced shape resonances might explain these features. However, further experiments are needed to determine whether any of these possibilities are correct.

One continuing puzzle is the origin of the positron binding energy in molecules. By comparing to a model for alkali metal atoms [48], it is possible to determine the rough

conditions for binding to molecules. Thresholds in polarizability and ionization energy seem to give a crude idea as to which molecules have bound states and which do not. Beyond these empirical rules, there are still no rigorous calculations of positron binding that can be compared with the available experimental data.

Chapter 5

VFR in Large Molecules

Positrons interact differently with large molecules than with small molecules. As shown in the previous chapter, VFR annihilation peaks in large molecules such as propane can be significantly larger than those in small molecules. In the alkanes, Z_{eff} rises exponentially with the number of carbons [24, 37, 43]. As a result, the quantitative Gribakin-Lee model can only describe a tiny fraction of the observed effects. One goal of this chapter is to better understand the nature of the enhancement process in large molecules.

Experimentally, large molecules are capable of much deeper positron binding than small molecules. In general, binding appears to grow with molecular size [43]. Alkanes with 12 or more carbons can even support a second, positronically-excited bound state [45]. However, as we will discuss, size alone does not determine binding. Some molecules, such as benzene, have binding similar to that found in much larger molecules. Another goal of this chapter is to understand more completely the factors that influence positron binding.

To achieve these goals, positron annihilation is studied for a large selection of hydrocarbons. Frequently, small changes in molecular structure are found to cause significant changes in behavior. A number of parameters are used to quantify annihilation in these molecules. In the past, the main parameter studied was $Z_{eff}^{(th)}$, the thermal Z_{eff}. How-

ever, this samples the magnitude of a VFR only at threshold, i.e. where the binding and vibrational energy are nearly equal. It is now clear that Z_{eff} varies significantly with the vibrational mode being excited. As discussed in the previous chapter, a particularly prominent feature in "large" hydrocarbons is the C-H stretch peak. We will use Z_{eff} at this peak as a common benchmark of VFR-enhanced annihilation, and frequently use the terms Z_{eff} and $Z_{eff}^{(CH)}$ interchangeably.

Another important parameter is the positron binding energy, ϵ_b, which can be discerned from the shift of the C-H stretch peak relative to the C-H stretch mode energy. Occasionally, other characteristics will be used, such as the overall Z_{eff} shape, the magnitude of the low energy Z_{eff} plateau (which is usually due to C-H bend and C-C modes), or the non-resonant background, $Z_{eff}^{(dir)}$.

These measured annihilation parameters will be compared with a number of physical characteristics, such as number of atoms in the molecule or details of the molecular structure. A number of interesting trends emerge from these analyses, that will provide new insights into the underlying mechanisms behind positron binding and enhanced Z_{eff}. For instance, it will become clear that Z_{eff} depends only weakly on ϵ_b via the scale factor, $g = \sqrt{\epsilon_b/\epsilon}$, just as in small molecules [70]. Furthermore, once this factor is normalized out, the magnitude of the C-H stretch peak Z_{eff} obeys a universal scaling as a function of the number of vibrational degrees of freedom in the molecule. Qualitative explanations for these trends, such as the "doorway state" IVR model, will be discussed.

A significant exception to this scaling is the class of "suppressed"-Z_{eff} molecules, such as 1-fluorohexane and 1-fluorononane. These molecules have unusually weak C-H stretch peaks as compared to their non-fluorinated analogues. It will be shown that a strong inelastic channel is likely responsible for the observed suppression.

A few other interesting phenomena will be discussed. For instance, the aromatic molecules, benzene and naphthalene, have unusually deep binding *and* exhibit unusually strong multi-mode VFR in their Z_{eff} spectra. Also, in alkanes with twelve or more carbons, the positron-molecule attraction is so strong that a *second*, positronically bound state is observed. This manifests itself as a second peak closer to the C-H stretch mode

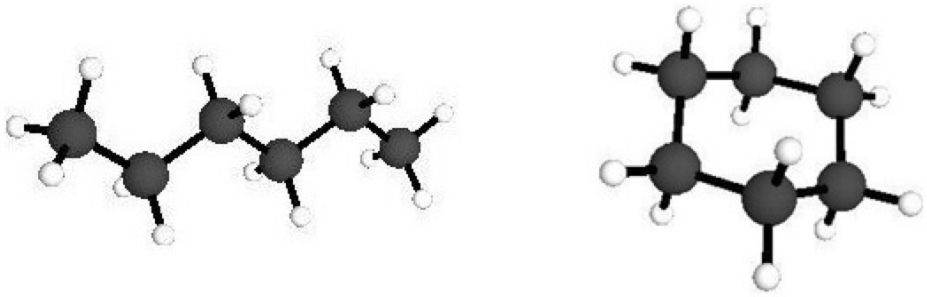

Figure 5.1: Molecular structures of (left) hexane and (right) cyclohexane.

energy in the Z_{eff} spectrum. The relative magnitude of this peak is determined, yet again, by the g factor.

5.1 Hexane and cyclohexane

Hexane (C_6H_{14}) is a six-carbon alkane whose carbon backbone has a "zig-zag" shape. Cyclohexane (C_6H_{12}) is a ring formed by removing two terminal hydrogens from hexane and joining the terminal carbons together. The structures of both molecules are shown in Fig. 5.1. As shown in Fig. 5.2, the energy-resolved Z_{eff} spectrum of cyclohexane is very similar to that of hexane except it is smaller by a factor of two. Both have the same binding energy of 80 meV. The number of C-H stretch modes has been reduced from 12 to 14, which also seems pretty minor.

Previous experiments have shown that, in alkane molecules, both the thermal and peak Z_{eff} values rise rapidly with the number of carbons [24,33,37,43]. As will be shown shortly, this trend can easily be generalized to the total number of atoms or the number of vibrational degrees of freedom in any hydrocarbon. In this context, the change in Z_{eff} magnitude between cyclohexane and hexane is not surprising.

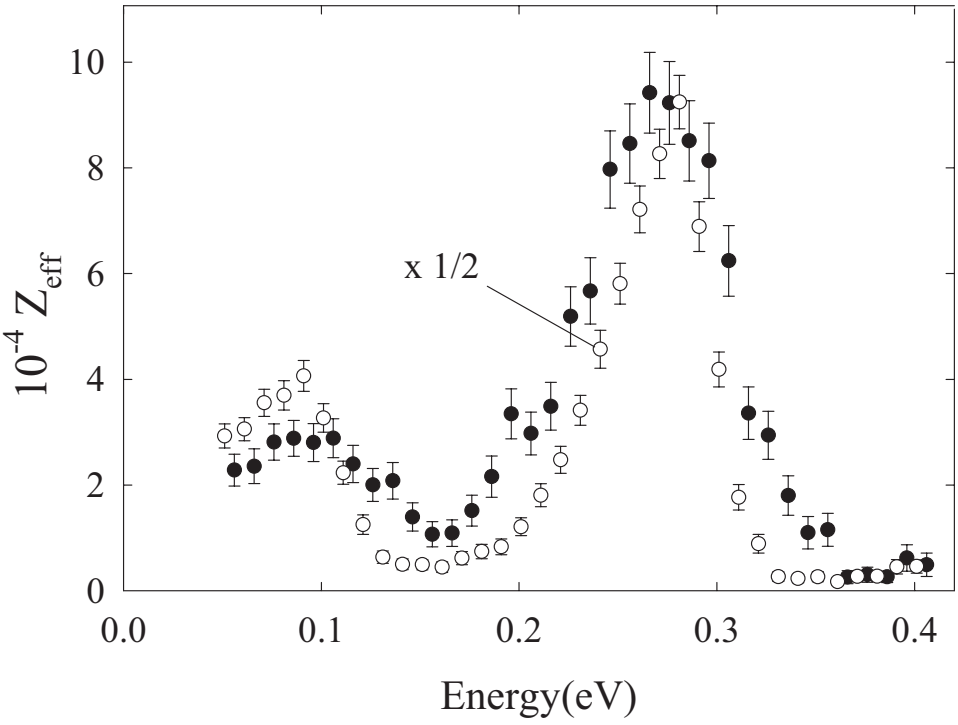

Figure 5.2: Z_{eff} spectra for (○) hexane, scaled by 1/2, and (●) cyclohexane.

5.2 Benzene and d-benzene

Benzene (C_6H_6) also has some interesting behaviors. This molecule is a flat, ring-shaped hydrocarbon. Since there are two equivalent ways to share three double bonds between the six carbons, this molecule is frequently described as being in a superposition of these two states. As a result, the carbons form a perfect hexagon, and the valence π electrons form a delocalized ring above and below the molecule.

Shown in Fig. 5.3 is a recent measurement [70] of the energy-resolved annihilation spectrum for benzene. A broad background present in a previous measurement [45] has been eliminated by lowering the transport energy to prevent positronium formation outside the gas cell. Both the previous spectrum and that in Fig. 5.3 exhibit a sig-

nificant feature at an incident positron energy $\epsilon \sim 230$ meV. The C-H stretch modes that usually produce the dominant resonance in hydrocarbons occur as a collection of modes centered near 380 meV in benzene [66]. Associating these modes with the benzene peak would imply a positron binding energy of 150 meV, which is much larger than the value of 80 meV observed in the analogous 6-carbon alkane molecule, hexane. To identify this peak, the annihilation spectrum of fully deuterated benzene (benzene-d6) was also measured. Since deuterated and non-deuterated species have nearly identical electronic properties, a common binding energy is assumed, which is consistent with previous observations in other hydrocarbons [24].

The Z_{eff} spectrum for benzene-d6, shown in Fig. 5.3, is dominated by a single peak at 148 meV with a plateau on the low-energy side. These data show that the peaks in both benzene and benzene-d6 are due to the C-H (C-D) stretch mode, indicating a common binding energy of 150 meV. In particular, upon correcting for this value of binding energy, the ratio of the energies of the peaks is 1.28, which is very close to the value 1.34, the expected ratio of the C-H stretch mode energies.[1] Making these adjustments in the energy scale for benzene-d6 and adjusting the height by 0.78 results in a curve strikingly similar in magnitude and spectral shape to that of benzene (i.e., the dashed curve in Fig. 5.3). The height scaling of 0.78 is the inverse ratio of positron impact momenta at the C-H and C-D stretch peaks. In other words, it is proportional to the ratio of the g factors for the two molecules, where $g = \sqrt{\epsilon_b/\epsilon}$ is the energy scaling found in small molecules [65, 70]. The significance of this result will be discussed in a later section.

The binding in benzene is as large as that in nonane (the nine carbon alkane), in spite of the former having only six carbons like hexane ($\epsilon_b = 80$ meV), and one more atom than propane ($\epsilon_b \sim 10$ meV). Note that benzene has a relatively small Z_{eff} which is somewhere between that of butane and pentane. Thus, benzene deviates strongly from the behavior seen in alkanes.

[1] The small discrepancy of 15 meV is close to experimental resolution but might be evidence of a positron-induced energy shift or a difference in binding energy such as that observed in CD_3Br.

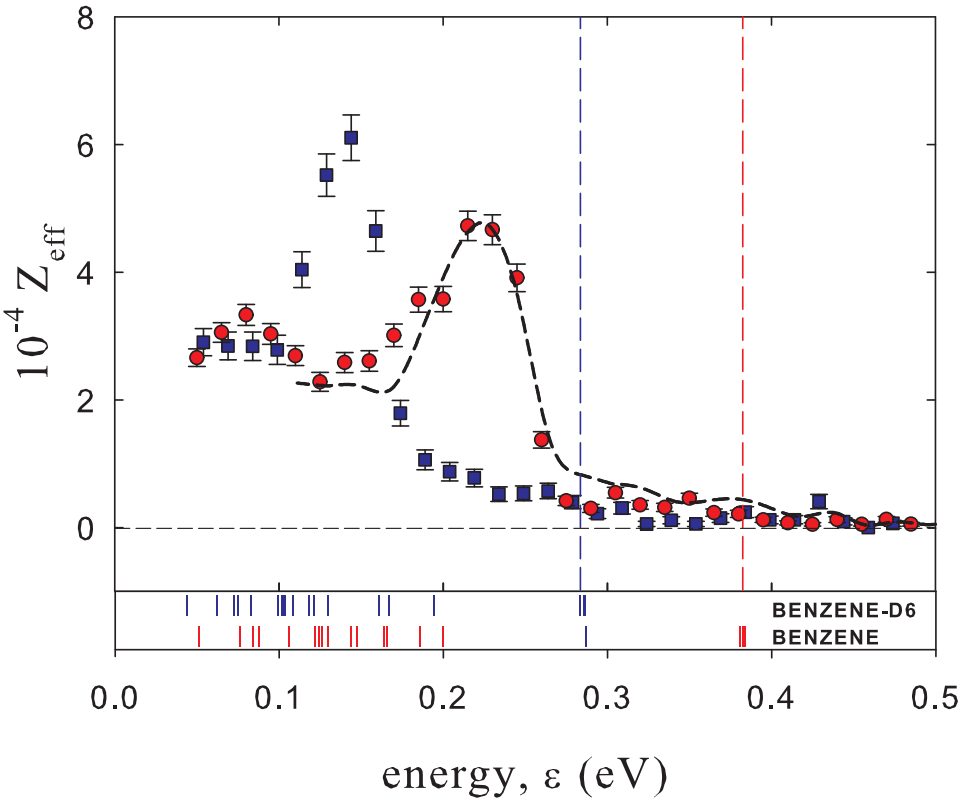

Figure 5.3: Z_{eff} spectra for (red ∘) benzene and (blue □) benzene-d6 from [70]. The dashed line is the benzene-d6 spectrum with the derived mode energy, $\epsilon_v = \epsilon - \epsilon_b$, scaled by 1.28, assuming $\epsilon_b = 150$ meV; and the height scaled by 0.78. The lower panel indicates the positions of the vibrational modes in benzene and benzene-d6 from Ref. [66].

In chapter 4 and in Ref. [48], the possibility that positron-molecule binding can be described as a function of ionization energy, E_i, or polarizability, α, was discussed. Smaller E_i or larger α should lead to deeper binding. As it turns out, the ionization energy of benzene is 9.25 eV [1], which is even smaller than that of dodecane. In other words, the positron feels relatively little repulsion as it penetrates into benzene's delocalized cloud of electrons. This could explain the deeper binding. Benzene's polarizability is a more modest 10.4 Å^3 [1], closer to that of pentane, implying a slightly weaker long range attraction. Thus, α appears to have a much smaller affect on the binding of a positron to this molecule.

5.3 1-Chlorohexane

The Z_{eff} spectra for 1-chlorohexane and hexane from Ref. [70] are shown in Fig. 5.4. The former has binding energy of 175 meV and a C-H stretch mode peak height of 5.2×10^5. Both of these parameters are substantially larger than those in hexane ($\epsilon_b =$ 80 meV; $Z_{eff}^{(CH)} = 1.8 \times 10^5$), even though the number of atoms is the same, and the number of valence electrons is similar.

This result is significant for a number of reasons. To start, the C-H stretch peak Z_{eff} of hexane increases with a single chlorine substitution, while it decreases significantly with fluorine substitution [43, 45]. As will be discussed in a later section, this strong chemical sensitivity may be explained by differences in the strength of their inelastic channels.

It is also intriguing that the binding energy is increased significantly. To some degree, one might attribute this increased attraction to the polarizability. For 1-chlorohexane $\alpha = 13.6$ Å^3; while for hexane $\alpha = 11.8$ Å^3; and for heptane $\alpha = 13.7$ Å^3 [1,96]. Judging from this parameter alone, one might expect that the binding energy of 1-chlorohexane would be close to that of heptane. However, heptane has a more modest binding energy of 105 meV. Furthermore, the ionization energy of 1-chlorohexane is 10.3 eV, slightly larger than that of hexane, which would tend to *reduce* the binding. Of course, 1-chlorohexane

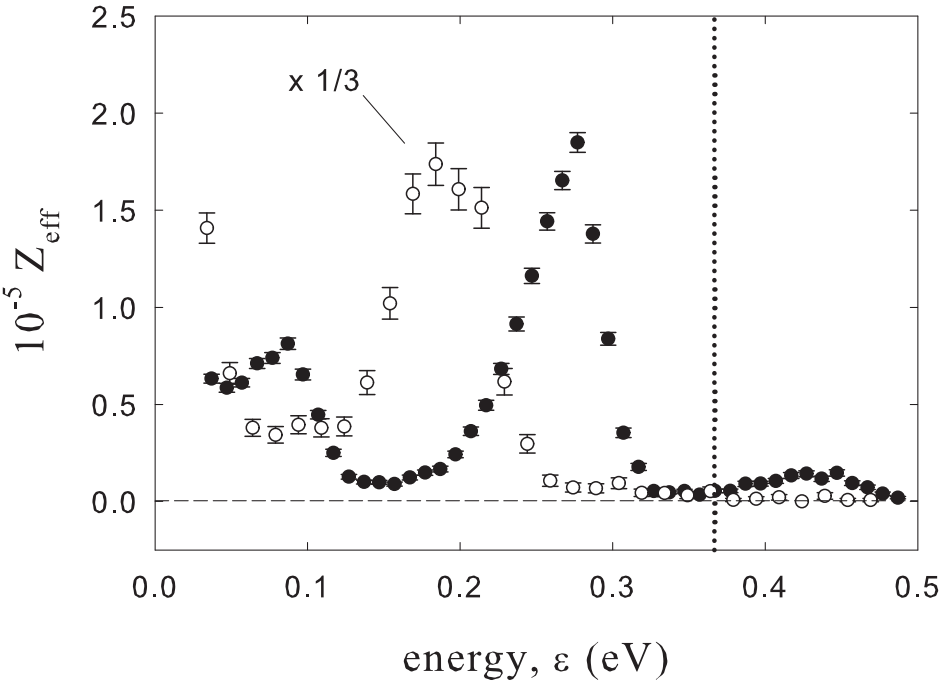

Figure 5.4: Z_{eff} spectra for (○) 1-chlorohexane scaled by 1/3 [70], and (●) hexane [43]. Note the large increase in binding energy in the chlorinated compound.

also has a non-trivial permanent dipole, which may contribute. This mystery will be revisited in a later section where broad trends in binding energies are discussed.

Also worth further examination is the enhancement of Z_{eff} in response to the increased binding in 1-chlorohexane. A similar behavior was observed in methyl chloride and other small molecules. In the next section, it will be shown that this fits into a much broader trend in hydrocarbons.

5.4 The atom trend

It is useful to consider these data for annihilation in large molecules in light of the general theory of resonant annihilation with energy-averaged parameters [23, 49],

$$Z_{\mathit{eff}} = \frac{2\pi^2 \rho_{ep}}{k} \frac{\Gamma^{(e)}(\epsilon)}{\Gamma(\epsilon)} \rho(\epsilon + \epsilon_b), \tag{5.1}$$

where $k \propto \sqrt{\epsilon}$ is the positron momentum, ρ_{ep} is the electron-positron contact density in the bound state, $\Gamma^{(e)}$ is the positron resonance elastic (i.e. capture) width, Γ is the total resonance width at positron energy ϵ, and $\rho(\epsilon+\epsilon_b)$ is the density of accessible vibrational states. Theory and experiment indicate that the binding energy ϵ_b is the same for all modes of a molecule [23, 43]. In a simple s-wave model of the positron wave function, $\rho_{ep} \propto \sqrt{\epsilon_b}$ [40]. In this case, the "kinematic" dependence of Z_{eff} on ϵ and ϵ_b is through a simple scale factor,

$$g = \sqrt{\epsilon_b/\epsilon}. \tag{5.2}$$

Beyond this factor, Z_{eff} involves the unique dynamics between the positron, nuclei, and electrons.

Fig. 5.5(a) shows Z_{eff} at the C-H stretch peak *vs* binding energy for alkanes and several other species including 1-chlorohexane and benzene. It is clear that this parametrization is insufficient, since many molecules differ from the trend of the alkanes. However, when the dependence on ϵ and ϵ_b predicted by Eq. (5.2) is taken into account, the situation is dramatically different. Fig. 5.5(b) shows Z_{eff}/g *vs* the number of atoms, which is a clear improvement. Data for a variety of species including several of those shown in Fig. 5.5(b) are presented in Table 5.1. A more complete compilation is presented in Appendix A. [Not shown in either Fig. 5.5(b) or Table 5.1 is the second bound state of dodecane due to large uncertainties in $1/g$ caused by a near zero binding energy]. In this normalized representation, CH_3Cl and CH_3Br peak heights are nearly identical, as expected. The normalized benzene and benzene-d6 peak heights are also nearly identical.

In general, Fig. 5.5(b) and Table 5.1 indicate that hydrocarbons with similar numbers of atoms tend to have similar normalized C-H stretch peak heights. When 1-chlorohexane

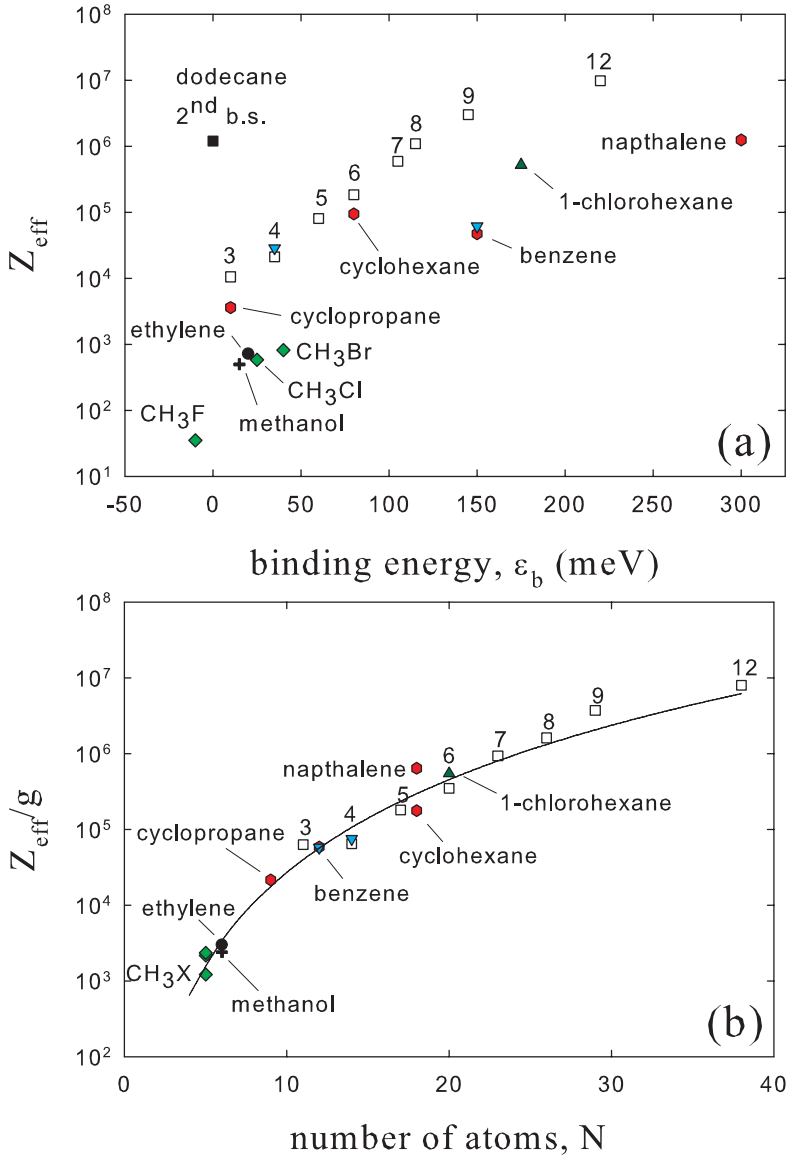

Figure 5.5: (a) Z_{eff} at the C-H stretch peak *vs* binding energy, ϵ_b, for alkanes, C_nH_{2n+2} (□); rings (red hexagons); halomethanes (green ⋄); ethylene (•); methanol (+), 1-chlorohexane (dark green △); and deuterated species (cyan ▽). (b) Z_{eff} at the C-H stretch peak normalized by the factor $g = \sqrt{\epsilon_b/\epsilon}$ *vs* the number of atoms, N, in the molecule. For alkanes, the number of carbon atoms, n is indicated. In (b), the solid line shows the fit, $Z_{eff}/g = 2.3\ N^{4.1}$, described in the text. This plot demonstrates that Z_{eff} is insensitive to positron binding beyond the weak dependence, g, which is predicted by theory.

Table 5.1: C-H stretch peak values, Z_{eff}, normalized by $g = \sqrt{\epsilon_b/\epsilon}$ for various molecules. The number of atoms per molecule N is provided for comparison. Data are from both new and previous experiments [24, 43, 45]. The binding for CH_3F is from a theoretical prediction [44]. Absolute Z_{eff} for $C_{14}H_{30}$ and $C_{16}H_{34}$ are unknown, and so these values are multiplied by arbitrary common factors 'x' and 'y'.

Species	N	ϵ_b [meV]	Z_{eff}	Z_{eff}/g
methyl fluoride (CH_3F)	5	0.3	35	1200
methyl chloride (CH_3Cl)	5	25	585	2160
methyl bromide (CH_3Br)	5	40	820	2300
cyclopropane (C_3H_6)	9	10	3,600	21,500
propane (C_3H_8)	11	10	10,500	63,000
benzene (C_6H_6)	12	150	47,000	58,000
benzene-d6 (C_6D_6)	12	150	61,000	57,500
pentane (C_5H_{12})	17	60	80,000	180,000
cyclohexane (C_6H_{12})	18	80	94,000	180,000
hexane (C_6H_{14})	20	80	180,000	340,000
1-chlorohexane ($C_6H_{13}Cl$)	20	175	$5.2 \cdot 10^5$	$5.4 \cdot 10^5$
nonane (C_9H_{20})	29	145	$2.9 \cdot 10^6$	$3.6 \cdot 10^6$
1-fluorononane ($C_9H_{19}F$)	29	145	$9.3 \cdot 10^5$	$1.15 \cdot 10^6$
dodecane ($C_{12}H_{26}$)	38	220	$9.8 \cdot 10^6$	$8.0 \cdot 10^6$
tetradecane ($C_{14}H_{30}$)	44	260	$11x$	$6.8x$
2^{nd} B.S.	44	50	$2.8x$	$7.0x$
hexadecane ($C_{16}H_{34}$)	50	310	$15y$	$6.4y$
2^{nd} B.S.	50	100	$4.0y$	$6.5y$

and hexane are normalized in this way, the ratio of the C-H stretch peak height, while not unity, is reduced from 2.8 to 1.6 (c.f., Table 5.1). Unlike in Fig. 5.5(a), benzene is no longer an outlier. Other molecules such as cyclohexane and cyclopropane, which have relatively small Z_{eff} values [45], are also close to the trend line of the alkanes. The best empirical fit to this trend is a simple power law, $Z_{eff}/g = 2.3\ N^{\eta}$, where N is the number of atoms and $\eta = 4.1$.

Not shown in Fig. 5.5(b) are tetradecane, the 14-carbon alkane, and hexadecane, the 16-carbon alkane. The absolute Z_{eff} values for these wax-like compounds are uncertain due to difficulties in determining the absolute test-gas pressure. As will be shown later, these molecules exhibit C-H stretch resonances due to both first and second (i.e., positronically excited) bound states. As shown in Table 5.1, the scaled values, Z_{eff}/g, from their first and second C-H stretch peaks are nearly identical, providing further support for this normalized representation.

The only major exceptions to this trend, of which we are aware, are the fluorine-substituted compounds such as 1-fluorohexane and 1-fluorononane [not shown in Fig. 5.5(b)] [43, 45]. Here, the addition of a fluorine reduces Z_{eff} by a factor two or more (c.f., Table 5.1), but leaves the binding energy unchanged. It will be argued in the next section that this is due to an unusually effective inelastic escape channel that results from C-F stretch modes with their associated strong dipole coupling.

The fact that Z_{eff}/g depends so strongly on the number of atoms, N (or essentially the number of vibrational degrees of freedom, $3N-6$) has interesting implications. In the past, it has been suggested that the rapid growth of Z_{eff} is due to the fact that single-mode vibrational resonances act as "doorways" [49] whose energy may be transferred into a large reservoir of higher-order multi-mode vibrational excitations. This process, called intramolecular vibrational relaxation (IVR), results in an enhancement of Z_{eff} roughly proportional to the density of nearby states, which in turn, is expected to grow exponentially with the number of degrees of freedom. While experiments show that the growth of Z_{eff} is not proportional to the total vibrational mode density, as this simple model would predict [49], the fact that Z_{eff} does grow rapidly with the number

of vibrational degrees of freedom suggests that some form of IVR is occurring.

The lack of dependence of Z_{eff} on ϵ_b beyond that in the factor g is particularly interesting. A bound positron may not escape via de-excitation of a mode of energy ϵ_v if $\epsilon_v < \epsilon_b$. Thus, increasing ϵ_b should block escape *via* these inelastic channels, resulting in an additional enhancement of Z_{eff} and a deviation from the 'universal' curve. However, there are few outliers to this curve. Note that, in this regard, the second bound state results for tetradecane or hexadecane should show a very large effect. Tetradecane has a factor ~ 6 difference in binding energy between its ground and first-excited states, but this produces virtually no change in Z_{eff}/g. Also, 1-chlorohexane has only a modest residual deviation from hexane after normalization. *Thus, it appears that in most cases, inelastic escape channels with more than a small amount of energy loss are inactive.*[2]

In summary, large annihilation rates are not strongly correlated with positron-molecule binding energies. This provides evidence that inelastic escape channels are relatively unimportant in most molecules. The most important parameter appears to be the number of atoms in the molecule (i.e., the number of vibrational degrees of freedom). In the future, studies of other non-alkane hydrocarbons as well as additional (e.g., second) bound states can be expected to clarify further this effect.

5.5 The temperature dependence of Z_{eff}

In principle, thermally excited modes can also stimulate positron detachment, contributing to the overall inelastic width and suppressing Z_{eff}. In the simplest picture, the probability that a given degree of freedom has sufficient energy to unbind the positron decreases exponentially with binding energy at a rate proportional to the Boltzmann factor, $exp(-\epsilon_b/k_BT)$, where k_B is the Boltzmann constant and T is the temperature. As T decreases, so does the probability of thermal detachment, which should result in an increase in Z_{eff} determined by the binding energy and the mode density.

L. D. Barnes noticed that in alkanes, $Z_{eff} \propto (2n+2)e^{(\epsilon_b/\epsilon_0)}$ where $\epsilon_0 = 26$ meV [62].

[2] In a later section, we discuss one striking exception to this behavior.

This scaling looks remarkably similar to an inverse Boltzmann factor, which suggests that Z_{eff} resonances could increase dramatically in magnitude if the temperature of the target gas were lowered.

5.5.1 Z_{eff} of cold alkane molecules

Using the cold gas cell described in Chapter 3, we measured Z_{eff} as a function of temperature for two alkane molecules, pentane (C_5H_{12}) and heptane (C_7H_{16}) [64]. Pentane was measured at 153 K and 15.5 μtorr and heptane at 195 K and 1.34 μtorr. For reference, the "peak desorption temperature" for these molecules, which is the temperature at which the surface sticking coefficient goes to zero, is 168 K and 211 K, respectively, on a Cu(111) surface [97]. As a result, these molecules have an appreciable probability (e.g., $\geq$ 50 %) of sticking and thermalizing to the cold electrodes upon each collision [97–99].

The resulting energy spectra for Z_{eff} are shown in Fig. 5.6, where they are compared with spectra measured at test-gas temperatures of 300 K. For both molecules, there was relatively little change in the magnitude or shape of Z_{eff} in response to the significant change in temperature. Most of the change in Z_{eff} that did occur was observed at lower positron impact energies. Specifically, at low temperature and smaller values of positron energy, Z_{eff} increased by $\sim$ 30% in pentane and $\sim$ 50% in heptane.

We note that, in Fig. 5.6, there is a slight broadening of the Z_{eff} peaks compared with previous measurements (e.g., Fig. 5.2 and Refs. [24, 43]). Since this occurs consistently for both the room- and low-temperature measurements in both targets, it is likely due to a broader positron energy distribution within the gas cell. It could be caused either by positron scattering or by variations in electrical potential due to the metal mesh inside the cell. Also note that the positions of the Z_{eff} peaks are unaltered when the temperature is changed, indicating that there is little change in the binding or vibrational-mode energies. The preciseness of the match between the high and low temperature measurements, both in magnitude and energy spectrum, indicates that the relative systematic errors between high- and low-temperature measurements are small. This is nontrivial, because a

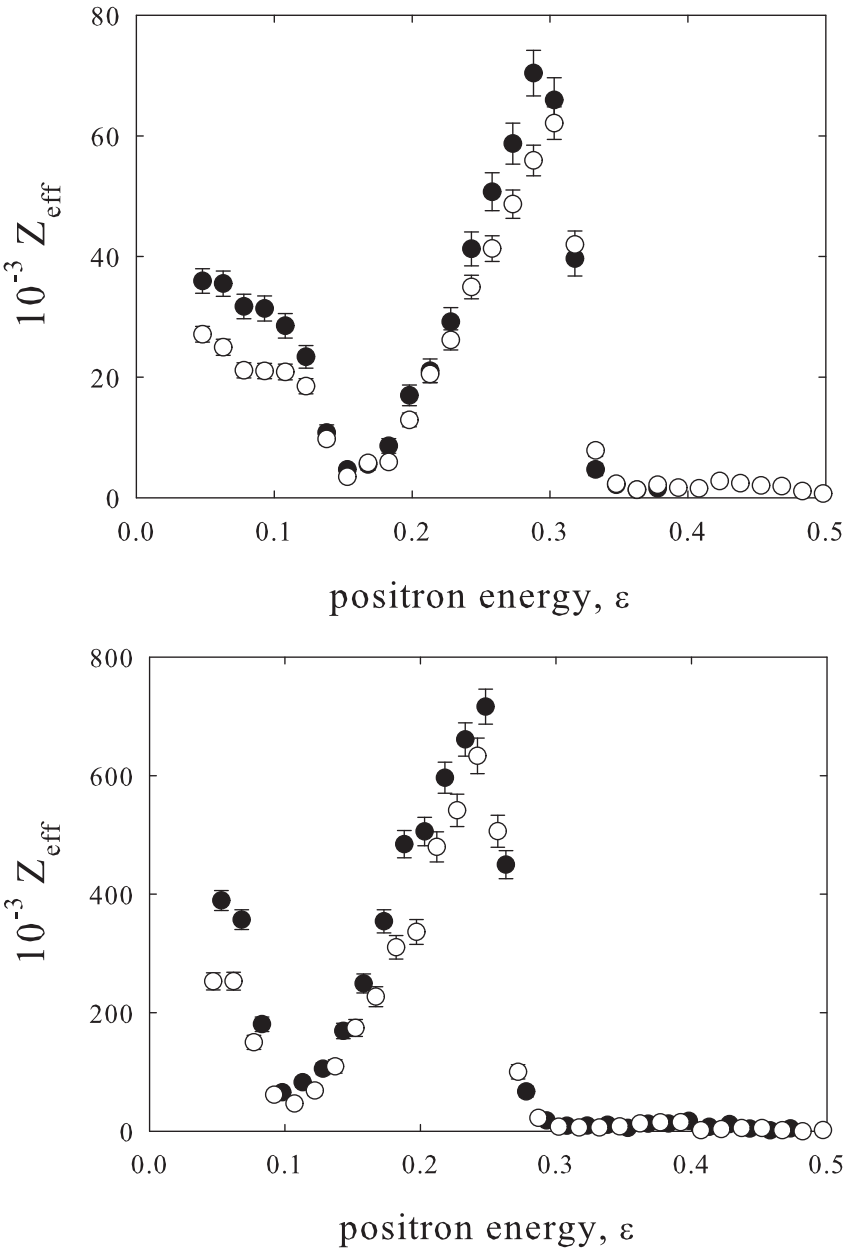

Figure 5.6: Energy-resolved Z_{eff} for (a) pentane (C_5H_{12}) at (○) 300 K and (●) 153K; and (b) heptane (C_7H_{16}) at (○) 300 K and (●) 195K.

different calibration factor for density and particle flux must be used at each temperature.

The spectra of Z_{eff} for propane (C_3H_8) and butane (C_4H_{10}) were also measured at temperatures of 133K and at 151K respectively. Unfortunately, at these temperatures, the probability that these molecules stick to copper is infinitesimal [97–99]. For this reason, it is more difficult to guarantee that these molecules are completely thermalized in the cold cell. That said, the spectra for both targets showed no change in Z_{eff} with temperature within the measurement errors, which were similar to those shown in Fig. 5.6 for pentane and heptane. Again, this is non-trivial considering that temperature-dependent calibration factors were used to derive the absolute values of Z_{eff}. Thus, although it was not possible for us to corroborate, these molecules may well have thermalized by a combination of collisions with the irregular copper-oxide layer on the gas-cell walls and adsorption on the colder thermal conduit before entering the gas cell.[3]

5.5.2 Analysis of the cold cell data

This lack of a strong temperature dependence of Z_{eff} eliminates the postulated Boltzmann-like scaling of Z_{eff} with binding. If that scaling were correct, the C-H stretch peak in pentane should have grown by a factor of ten as the temperature was lowered by the amount indicated. In general, inelastic positron detachment by thermal modes appears to be a relatively weak process in these molecules.

The temperature-independence of the binding energy apparently rules out one model of positron binding. In particular, it was suggested that a change in the bond geometry might be required for a positron to bind to a molecule (i.e., also required for VFR-mediated annihilation) [82, 83]. For example, it was predicted that a change in the C-C-H bond angle of 19° would be required for binding to acetylene (C_2H_2) [82]. As a result, binding could occur only if the molecule were in a highly excited vibrational state. One way to control the level of vibrational excitation is to change the temperature (i.e., "hot" molecules would be expected to have deeper binding than "cold" molecules).

[3]It is estimated that a large molecule entering the cold cell will make $\sim$ 50 collisions with the cell walls, over the course of $\sim$ 5 ms, before exiting the cell.

By extension, hot molecules would also be more likely to have VFR annihilation peaks (or have larger peaks). The cold-cell data presented here show no evidence of this effect, namely the binding energy is constant over approximately a factor of two change in molecular temperature.

The results described here place important constraints on theories of positron-molecule annihilation. The positron-molecule binding energy does not change with molecular temperature. Explicit thermal detachment processes are shown to be relatively weak. This conclusion, that inelastic channels seem to be generally weak or inactive in large molecules, is also consistent with the weak scaling of Z_{eff} with positron binding energy described in the previous section and Ref. [70].

5.6 Fluoroalkanes

There is a class of large hydrocarbons for which Z_{eff} is unusually small. We refer to them as "suppressed"-Z_{eff} molecules. A good example is 1-fluorononane, reproduced in Fig. 5.7(a). These molecules have C-H stretch peaks which are smaller by a factor of two or more than their non-substituted alkane counterparts [24,43,45]. To better understand this phenomenon, further experiments on fluoroalkanes were performed.

A previous experiment on 1-fluorohexane was found to be in error, likely due to an air leak into the vacuum system. The experiment was repeated, and the results are shown in Fig. 5.7(b). At low energies, this Z_{eff} spectrum is consistent with a previous measurement of thermal Z_{eff}, which indicates that Z_{eff} is 269,000 at threshold [1].[4] For reasons which are presently unclear, there is *significant* variability in the measured magnitude of the C-H stretch peak for 1-fluorohexane – a problem that does not occur for the other fluorinated compounds studied here. As a result, we only trust the magnitude of the 1-fluorohexane data to within $\sim 50\%$. For the purposes of this discussion, this accuracy is sufficient. The important facts are that the C-H stretch peak in 1-fluorohexane (and 1-fluorononane) is two to four times smaller than in hexane (nonane) while the low energy

[4] Based on the vibrational mode spectrum of 1-fluorohexane, there is probably a VFR at ~ 25 meV.

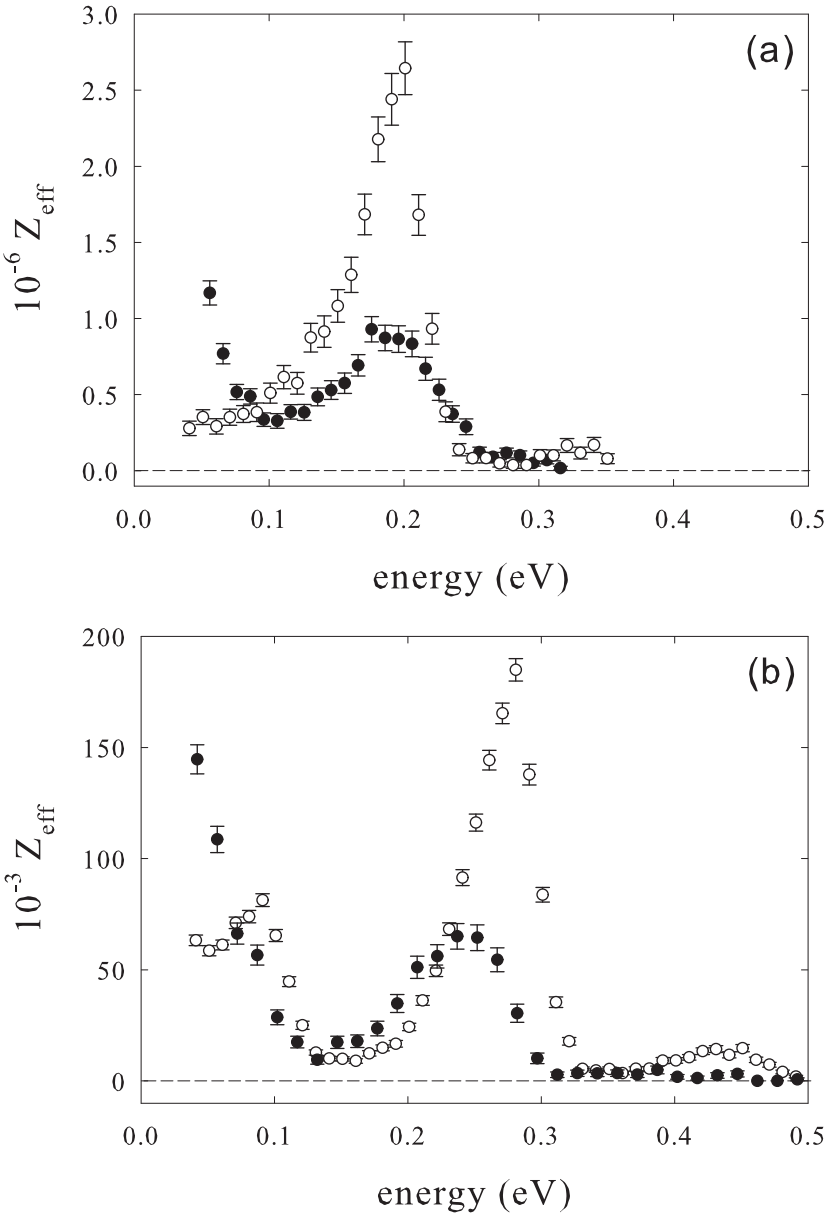

Figure 5.7: (a) Z_{eff} spectra for (•) 1-fluorononane and (○) nonane from Ref. [43]. (b) A recent measurement of Z_{eff} spectra for (•) 1-fluorohexane compared to (○) hexane from Ref. [43]. Note that there is likely a $\sim 50\%$ error in the C-H stretch peak height of 1-fluorohexane. See the text for details.

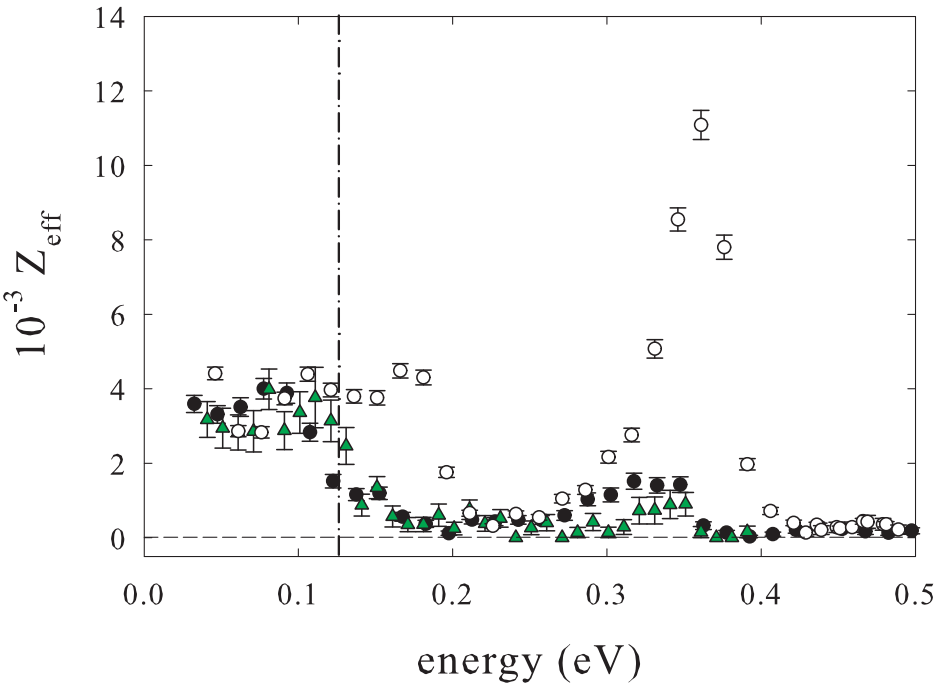

Figure 5.8: Z_{eff} spectra for (○) propane and (●) 1-fluoropropane (present work), and (green △) 2,2-difluoropropane from Ref. [24]. The vertical dot-dash line (-·-) indicates the empirical position of an inelastic threshold – roughly where the Z_{eff} magnitude is reduced to half of its low energy value, averaged between the two fluorinated species. This is explained in a later section.

peaks are clearly larger than in hexane (nonane).

5.6.1 1-Fluoropropane

The Z_{eff} spectra of propane (C_3H_8), 1-fluoropropane (C_3H_7F), and 2,2-difluoropropane ($C_3H_6F_2$) are shown in Fig. 5.8. A number of interesting characteristics are apparent. Like 2,2-difluoropropane, 1-fluoropropane has a much suppressed C-H stretch peak. It is smaller than that of propane by a factor of five. Also as with 2,2-difluoropropane, 1-fluoropropane has low energy peaks with $Z_{eff} \sim 4000$, the same magnitude as those in propane. These peaks drop in magnitude by a half above ~ 120 meV in 1-fluoropropane

and 2,2-difluoropropane while they persist until 200 meV in propane. This apparent "threshold" is indicated by the vertical dot-dash line in Fig. 5.8.

These Z_{eff} spectra indicate that the positron binding energies of propane, 1-fluoropropane, and 2,2-difluoropropane are 10 meV, 35 meV, and 25 meV respectively. The slight extra reduction in the C-H stretch peak in 2,2-difluoropropane relative to 1-fluoropropane can be attributed to 2,2-difluoropropane's smaller binding and slight reduction in C-H stretch modes. The molecules 2,2-difluoropropane and 1-fluoropropane appear to exhibit VFR very similar to small molecules. Indeed, their peak magnitudes are quite similar to those in ethanol, which was shown in Chapter 4 to conform quite well with the Gribakin-Lee model. Their binding energies are slightly smaller than those of ethanol but they have 40% more C-H stretch modes. In both, it appears that the enhanced-Z_{eff} dynamics are *strongly* suppressed.

5.6.2 1-Fluorobutane

The molecule 1-fluorobutane (C_4H_9F) continues the trend observed in the other fluoroalkanes. As shown in Fig. 5.9, its C-H stretch peak is depressed by a factor of five relative to butane. It has a binding energy of 70 meV, which is larger than butane's by 35 meV.

Like in 1-fluoropropane and 2,2-difluoropropane, the Z_{eff} suppression in 1-fluorobutane seems to end below a "threshold," indicated approximately by the vertical dot-dash line in Fig. 5.9. In fact, the low-energy Z_{eff} of 1-fluorobutane is ∼18,000, which is ~ 2.5 times *larger* than that for butane. It turns out that there are hints of low energy enhancement in many other fluoroalkanes. For instance, the spectrum for 1-fluorononane has an upward swing above nonane below 100 meV [43, 45]. Both 1-fluorohexane and 2,2-difluoropropane have significantly larger thermal Z_{eff} than their non-substituted analogues [1, 45].

This seems to indicate that the Z_{eff} suppression mechanism affects only a particular set of modes or range of energies. For some reason, low energy modes are not suppressed.

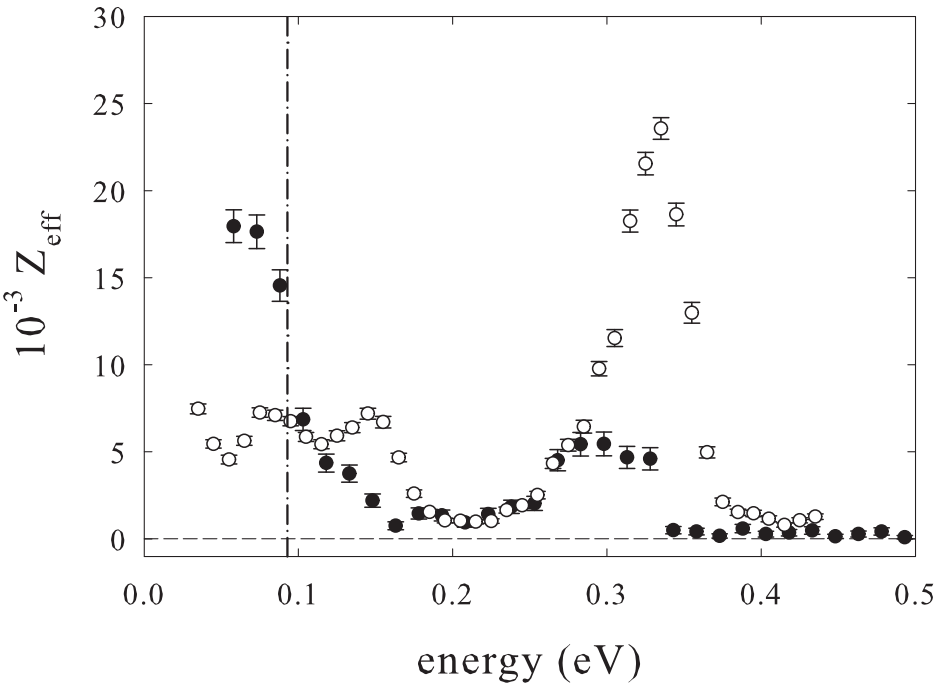

Figure 5.9: Z_{eff} spectra for (○) butane and (●) 1-fluorobutane. The vertical dot-dash line (-·-) indicates the empirical position of a inelastic threshold (explained in a later section).

They may even be enhanced. It should be recognized that the fluorine substitution also results in additional lower energy C-F modes. When Z_{eff}-enhancing mechanisms such as IVR are considered, these additional low-energy states could be nonlinearly enhanced.

5.7 The origin of "suppressed" Z_{eff}

Figure 5.10 shows how these partially fluorinated hydrocarbons fit into the normalized Z_{eff} vs. atom representation discussed in section 5.4. The 1-fluorohexane datum has been given large error bars to account for the experimental uncertainty. All of these molecules fall below the trend-line for the other molecules. The suppression seems largest for the smaller molecules and gradually decreases to a factor of ~ 2.5 in 1-fluorononane. As

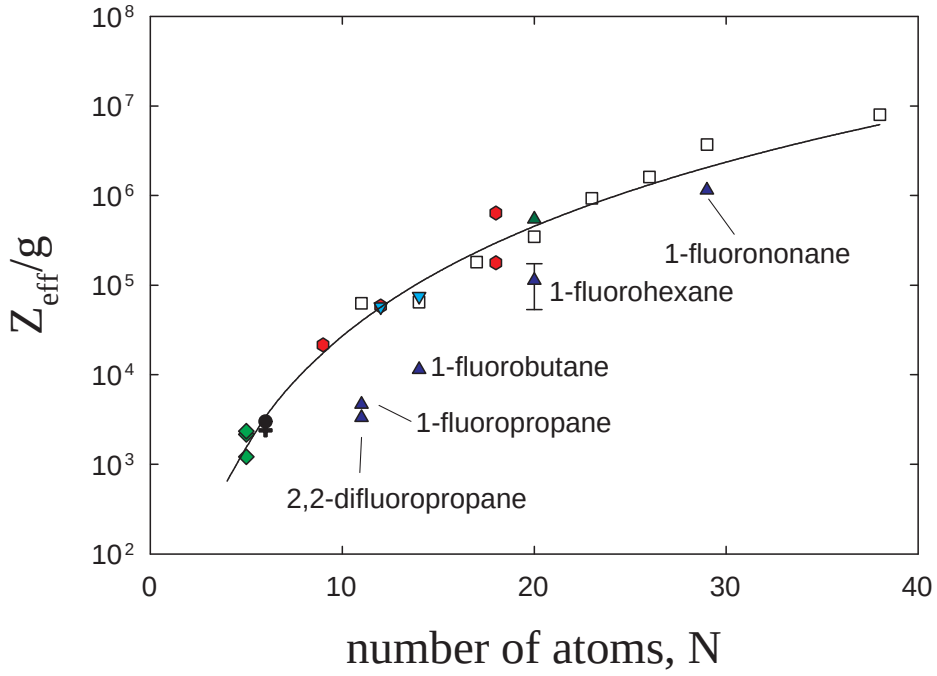

Figure 5.10: Normalized Z_{eff} at the C-H stretch peak *vs* number of atoms for a variety of species (similar to Fig. 5.5), including (blue △) suppressed-Z_{eff} molecules. The error bars on 1-fluorohexane indicate the unusually large uncertainty in this datum. The solid line shows the previously described $Z_{eff}/g = 2.3\ N^{4.1}$ fit for non-suppressed molecules.

discussed below, we expect this ratio to decrease to unity in larger fluoroalkanes.

As mentioned earlier, the presence of additional, inelastic escape channels could be responsible for the observed reduction in Z_{eff}. Gribakin has pointed out that the C-F stretch mode may provide a particularly strong inelastic escape channel [88]. On a related note, the vibrational inelastic excitation cross section for the asymmetric C-F stretch mode in CF_4 is as much as an order of magnitude larger than the inelastic cross sections in other small molecules [29].

5.7.1 Inelastic escape channels

Inelastic processes can best be understood as an adjustment to the basic VFR equation last described in section 5.4. Ignoring the density of "dark" states,

$$Z_{eff}^{(res)} \propto \frac{1}{k} \sum_{\nu} \Gamma_{\nu}^{e} \frac{\Gamma_{\nu}^{a}}{\Gamma_{\nu}^{e} + \Gamma_{\nu}^{a} + \Gamma_{\nu}^{i}}. \tag{5.3}$$

Essentially, the positron is captured at rate Γ_{ν}^{e}, then it annihilates at rate Γ_{ν}^{a}. However, this annihilation must be normalized by the total rate of all possible processes such as elastic re-emission (also Γ_{ν}^{e}) or inelastic re-emission Γ_{ν}^{i}. If one ignores the latter term and assumes that Γ_{ν}^{e} is the dominant factor, the terms cancel and $Z_{eff} \propto \Gamma_{\nu}^{a}/k \propto g$. However, if the $\Gamma_{\nu}^{i} > \Gamma_{\nu}^{e}$, there will be step-like reductions in Z_{eff} above the thresholds for each inelastic channel [23]. This is qualitatively consistent with the behavior observed in the fluoroalkane experiments. In 1-fluoropropane, there is an abrupt reduction in Z_{eff} for the low-energy peaks above a certain energy.

There are two types of inelastic processes that could be involved: resonant excitation and de-excitation. The former leaves the molecule with one more quantum of energy, ω_i, and is similar to the non-resonant inelastic excitation collisions described in Ref. [29]. The latter leaves the free positron with energy $\omega_i - \epsilon_b$, and the remaining energy with the molecule. These processes can be represented in the following way, where ω_ν represents the energy of the initial excitation (e.g., the C-H stretch mode) and M is the molecule:

$$e^{+}(\omega_\nu - \epsilon_b) + M(0) \rightarrow e^{+}(\omega_\nu - \omega_i - \epsilon_b) + M(\omega_i) \quad \text{(resonant excitation)} \tag{5.4}$$

$$e^{+}(\omega_\nu - \epsilon_b) + M(0) \rightarrow e^{+}(\omega_i - \epsilon_b) + M(\omega_\nu - \omega_i) \quad \text{(resonant de-excitation)} \tag{5.5}$$

To determine which process is dominant, one must consider the relative sizes of their inelastic widths. In the Born-Dipole approximation, this width should simply be proportional to the square of the dipole moment for the vibrational transition [65]. Technically, in the harmonic approximation, both inelastic processes are dipole-forbidden, since there is at least a two-quantum change between the VFR-excited and final molecular states. However, if there is a strong coupling $\gamma_{\nu x}$ between the initial excitation ν and an *intermediate* multi-mode excitation x which contains the mode of interest, the dipole transition

has a simple form:

$$\mathbf{d}_{(\nu\to\mu)} \sim \gamma_{\nu x} d_\mu, \quad \text{where} \quad \gamma_{\nu x} = \sum_x \langle \Phi_\nu | \Phi_x \rangle \text{ and } d_\mu = \langle \Phi_\mu | \hat{\mathbf{d}} | \Phi_0 \rangle. \tag{5.6}$$

This means that the inelastic width is modulated by $\gamma_{\nu x}$, which likely decreases with energy, for a given molecule, due to the reduced density of vibrational states. It also means that, for resonant inelastic *de-excitation* of the C-F stretch mode, the capture width is proportional to the strong, dipole-allowed C-F stretch transition. For this reason, *de-excitation of the C-F stretch seems likely to be the cause of the observed effects in the fluoroalkanes.* The experimental data for the fluoroalkanes support this hypothesis.

In this scenario, all VFR due to vibrational modes with energies above that of the de-excitation escape mode should be suppressed. Judging from the location at which the Z_{eff} drops by a factor of two in the smaller fluoroalkanes, the energy of the de-excitation escape mode is $\sim$ 155 meV. The empirical thresholds used in this estimate are marked by dot-dashed lines in Figs. 5.8 and 5.9. Suppression can only occur if the positron can escape, i.e. $\epsilon_b < 155$ meV. Both 1-fluorohexane and 1-fluorononane have binding energies less than 155 meV (the latter has a binding of 145 meV). As a result, both have a suppressed C-H stretch resonance, consistent with the aforementioned inelastic escape condition. It seems likely that this inelastic channel is due to the C-F stretch mode, although it occurs at a slightly higher energy than expected.[5]

This explanation is significant because it resolves the long standing question as to why fluoroalkanes behave differently than alkanes [43, 45]. It suggests that these molecules have a strong, C-F stretch-mediated resonant inelastic channel that causes suppression of Z_{eff} above a certain energy. It also provides evidence for resonant coupling between the C-H stretch mode and an "intermediate," multi-mode vibration, required for this inelastic channel. In a sense, the presence of this state is indirect evidence that mode-mixing processes like intramolecular vibrational relaxation (IVR) are possible. The only difference here is that this "intermediate," multi-mode state may not be part of the final

[5] According to Ref. [100], the C-F stretch mode energy in 1-fluoropropane is 120 meV

set of "dark" multi-mode states. Instead, it may represent an intermediate step between the doorway state and the reservoir of "dark" states. The latter possibility is considered in a later section.

5.7.2 Suppression in other substituted alkanes

It was hypothesized earlier that ethanol is also a suppressed molecule. One might note that the C-O mode occurs at around the same energy as the C-F mode. This could bring necessary intermediate states into resonance. According to Ref. [29], the molecule CO_2 has a fairly large vibrationally inelastic cross section. If the C-O dipole coupling is similar in alcohols, they could act as inelastic escape channels similar to the C-F modes in the fluoroalkanes. Tests with larger alcohols could confirm this.

In the context of inelastic de-excitation, 1-chlorohexane may be an example of what happens when the escape mode $\omega_\mu < \epsilon_b$. In this case, there should be no suppression at any energy, because the vibration μ does not have enough energy to kick the positron off the molecule. The binding energy of 1-chlorohexane is 175 meV, which is greater than the empirical C-F stretch mode threshold of 155 meV; and this in turn, should be larger than the C-Cl stretch threshold. With this is mind, it should not be surprising that there is no suppression in the C-H stretch peak Z_{eff} of 1-chlorohexane in comparison to hexane. Perhaps smaller chloroalkanes are suppressed.

5.8 Other perturbations to the magnitude of Z_{eff}

Even ignoring the fluoroalkanes, there are still some moderate deviations from the universal scaling, $Z_{eff}/g \propto N^{4.1}$, described in section 5.4, such as 1-chlorohexane. It is easiest to explain these effects in the context of the doorway-state IVR model [49]. In this model, the initial vibrational excitation is strongly coupled to a highly degenerate bath of "dark" states, with the latter usually inaccessible by direct VFR. This effectively increases the number of available positron-molecule states and thus increases the opportunities for annihilation. As a result, Z_{eff} should rise with the density of vibrational

Table 5.2: Thermal Z_{eff} for partially deuterated benzenes from Refs. [1, 37, 101]

Species	Formula	$Z_{eff}^{(th)}$
Benzene	C_6H_6	15,000
Benzene-d	C_6H_5D	36,900
Benzene-1,3,5d_3	$C_6H_3D_3$	43,800
Benzene-d_6	C_6D_6	30,500

states. Presumably, this explains the strong power-law scaling of Z_{eff} with the number of atoms or vibrational degrees of freedom [70]. If so, higher-order changes in Z_{eff} may result from changes in the density of dark states or changes in the coupling to these dark states.

5.8.1 Dark states

Both 1-chlorohexane and the large fluoroalkanes show signs of enhanced Z_{eff} compared to similarly-sized alkanes; for the fluoroalkanes, this occurs only below the inelastic threshold, but for 1-chlorohexane, it seems to occur at all energies. This enhancement is likely due to an increased density of dark states. In both cases, a few high energy C-H modes are converted into lower energy C-X modes where X is a halogen, resulting in a higher density of vibrational states.

Other molecules may also exhibit this behavior. It is expected that further deviations in structure from the alkanes may amplify this effect. Namely, these molecules may have larger deviations from the $Z_{eff}/g \propto N^{4.1}$ scaling.

5.8.2 Partially Deuterated Benzenes

The partially deuterated benzenes stand out as a significant deviation from the expected universal scaling. Table 5.2 shows measurements of thermal Z_{eff} by Koji Iwata [1, 37, 101]. These molecules show some unusual behavior which cannot be ex-

plained by darks states or inelastic channels alone. Measurements of energy-resolved Z_{eff} spectra for benzene and benzene-d_6, shown in Fig. 5.3, indicate that all of these molecules should have the same binding energy. The only differences are in the vibrational mode spectrum. Deuteration decreases the energy of all the C-H modes, and this increases the density of vibrational states (and presumably the density of dark states). Thus, the number of enhanced VFR at thermal energies should increase monotonically with deuteration. As a result, thermal Z_{eff} should also increase monotonically. Instead, it peaks at benzene-1,3,5d_3. This is possibly evidence of a new effect.

5.8.3 A tiered IVR model

The behavior observed in the deuterated benzenes can be cast in terms of a tiered IVR model. In such a model, an initial vibration may couple sequentially through ever larger collections of vibrational states [102]. For instance, it was shown by Yamata *et al.* that in phenol-d1 (benzene with a deuterated -OH group), there is at least one tier of intermediate states between the initial excitation and the final bath of "dark" states [103]. Using a picosecond infrared laser to pump the initial state and then a tunable UV probe pulse to initiate 2-photon ionization, a fascinating time progression was revealed. In phenol-d1, there is an oscillation between the initial OD stretch and two intermediate vibrations, in addition to the slow decay into a broad spectrum of dark states. Of particular interest is the change in this IVR decay time when phenol-d1 is completely deuterated. Instead of getting shorter, because of the increased density of dark states, it gets several times longer. The proposed explanation is that, by altering the energies of the vibrational modes, the intermediate states shift out of resonance with the initial excitation, thus preventing full relaxation into the bath of dark states.

While the IVR pathways in infrared and positron-induced excitations may be different, experiments like this reveal how complicated the internal vibrational dynamics can be. To return to the present context, a change in the vibrational mode structure due to a chemical substitution (e.g. adding a deuterium) may displace an important

intermediate channel, reducing the IVR and thus reducing Z_{eff}. Because each VFR has different intermediates associated with it, some peaks may be reduced while others may be enhanced. Further alterations in structure may reverse these effects. This process may explain the unusual variation in the deuterated benzenes. In general, it might also explain some of the observed spread in Z_{eff} values for similarly sized molecules.

5.9 Multi-mode VFR

Before proceeding to larger molecules, it is important to discuss a previously ignored feature in the Z_{eff} spectrum of benzene. As shown in Fig. 5.11, there is a sizeable feature which, after correcting for binding, corresponds to a vibration at $\sim$ 235 meV. While there are no fundamental modes at this energy, there is a pair of dipole-active combination modes at 227 meV and 244 meV. These modes produce strong peaks in the infrared spectrum, which are shown in Fig. 5.11. Essentially, the observed feature in Z_{eff} feature appears to be due to strong, multi-mode VFR. (One might also argue that the small bump at 450 meV is due to such a VFR.) This is unusual since multi-mode VFR-mediated annihilation is typically not observed in large molecules [24, 43, 45]. The only other evidence of combination or overtone VFR is in small and intermediate-sized molecules, such as methanol, where there is little or no IVR (e.g., see chapter 4).

The Gribakin-Lee theory allows for such resonances [44] in the sense that a mode with reasonably strong infrared intensity can produce a VFR just as strong as that of a fundamental mode, assuming the inelastic escape channels are closed. For some reason, though, these multi-mode VFR almost never exhibit enhanced Z_{eff} in large molecules.[6] In this context, it is not clear why benzene is an exception.

[6]For instance, the multi-mode VFR apparent in cyclopropane are weak compared to other VFR in that molecule (see chapter 4).

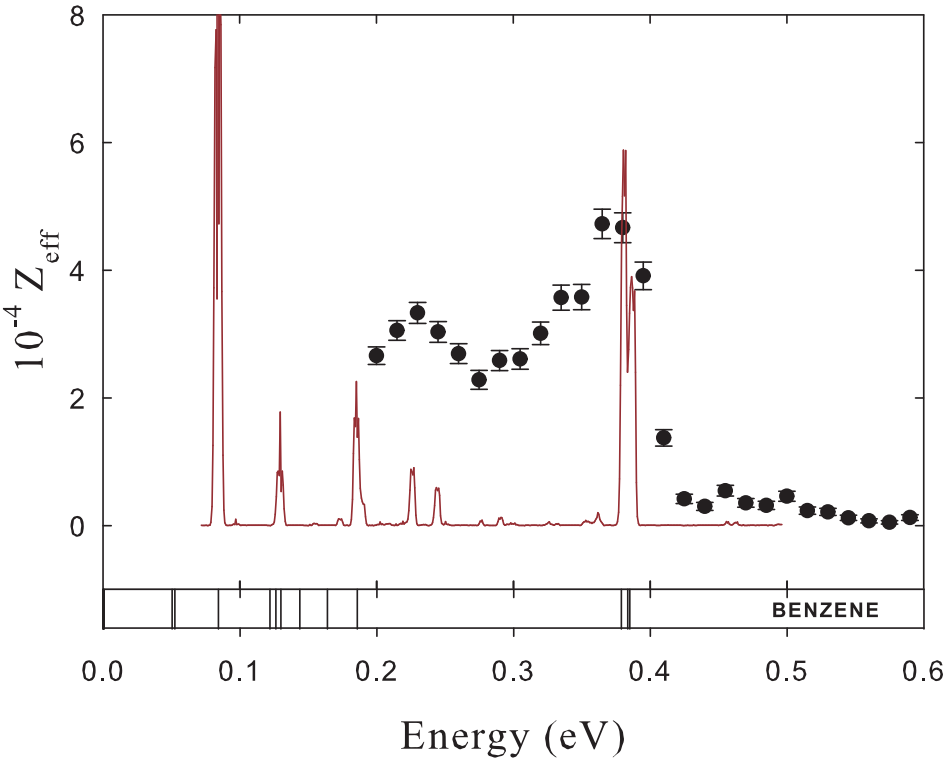

Figure 5.11: Energy-resolved Z_{eff} (•) and infrared absorption (—) for benzene. The Z_{eff} has been shifted upward by the binding energy $\epsilon_b = 150$ for direct comparison. The IR absorption, from Ref. [66], is arbitrarily normalized. The lower panel indicates the positions of the vibrational modes in benzene from Ref. [66].

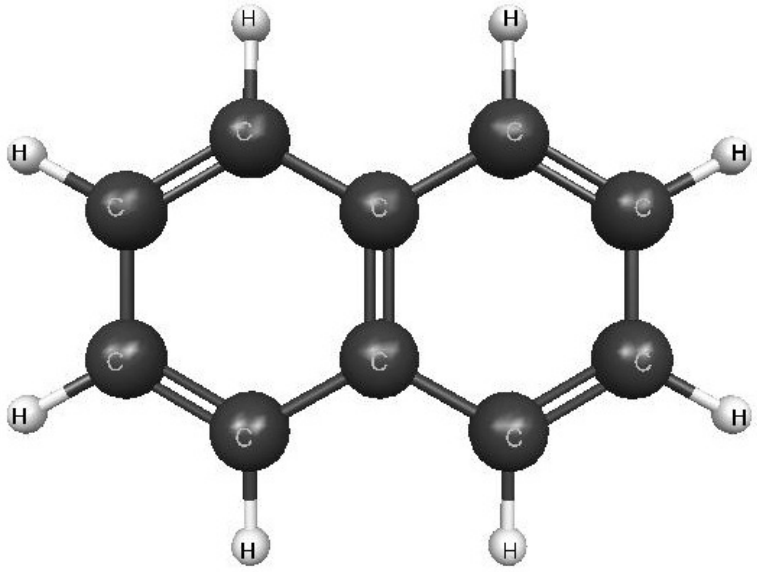

Figure 5.12: Molecular structure of naphthalene. Note that the π electrons in the double bonds are shared in a delocalized cloud across all carbons, similar to benzene.

5.10 Naphthalene and d-naphthalene

Naphthalene ($C_{10}H_8$) is the active ingredient in some brands of moth balls and is another aromatic molecule like benzene. As shown in Fig. 5.12, naphthalene is essentially two benzene rings with a common side. It is the smallest of a class of molecules termed polycyclic aromatic hydrocarbons (PAHs). For this reason, it is expected to share many characteristics with benzene, such as deep positron binding and multi-mode VFR.

Since naphthalene is solid at room temperature, the procedure for measuring Z_{eff} was different than that for other large molecules. The sample was prepared by crushing it into a fine powder so it could fit into the narrow test tube used for liquid samples. It was then attached to the vapor injection system and pumped at low temperatures to purge impurities. Since it has a smaller vapor pressure than many of the volatile liquids studied, a coarser needle valve was used to leak vapor into the gas cell. To further boost

the vapor pressure, the sample test tube was allowed to sit in a room temperature bath instead of a cooled bath.

For various reasons, it is difficult to get accurate gas cell pressure measurements for this molecule. The experiments required a pressure of 1 μtorr or less to avoid saturating the gamma-ray detector. Since this pressure is below the range of the capacitance manometer, which can only measure pressures down to a few μtorr, the ion gauge was used. Since this gauge can only produce relative pressures, one usually compares it to the manometer at higher pressures of the test species to get a calibration. For this particular setup, it was barely possible to get naphthalene in this common range, and unexplained behavior near the noise floor of the manometer cast doubt on the thus-measured calibration factor of ~ 12. Instead, a rough calibration factor of 6 was used as an estimate, based on the measured value of 6.3 for the thermal positron apparatus described in Koji Iwata's thesis [1].[7]

The energy-resolved Z_{eff} spectrum for naphthalene is shown in Fig. 5.13. Note that a large uncertainty in the overall magnitude should be assumed because of the aforementioned uncertainty in pressure. That said, the magnitude of the single peak at 80 meV is 1.2×10^6, similar to the C-H stretch peak of octane. It is natural to associate this peak with the C-H stretch mode since there are no strong peaks at higher energy. This implies that naphthalene has a huge binding energy of 300 meV – larger than that of tetradecane and twice that of benzene. This is reminiscent of the deep binding in benzene. The ionization energy of naphthalene is more than 1 eV smaller than benzene and nearly 2 eV smaller than dodecane [1], indicating that it is significantly easier for the positron to approach a valence electron.

The black line in Fig. 5.13 shows the Z_{eff} spectrum for naphthalene rescaled in energy and magnitude in accordance with the change in energy and g of the C-D stretch vibration. This indicates that the C-D stretch mode peak in deuterated naphthalene should occur at or slightly below threshold, leaving a mostly barren annihilation spectrum. To

[7] Other calibration values in his thesis correlate well with those measured for the energy-resolved annihilation experiment.

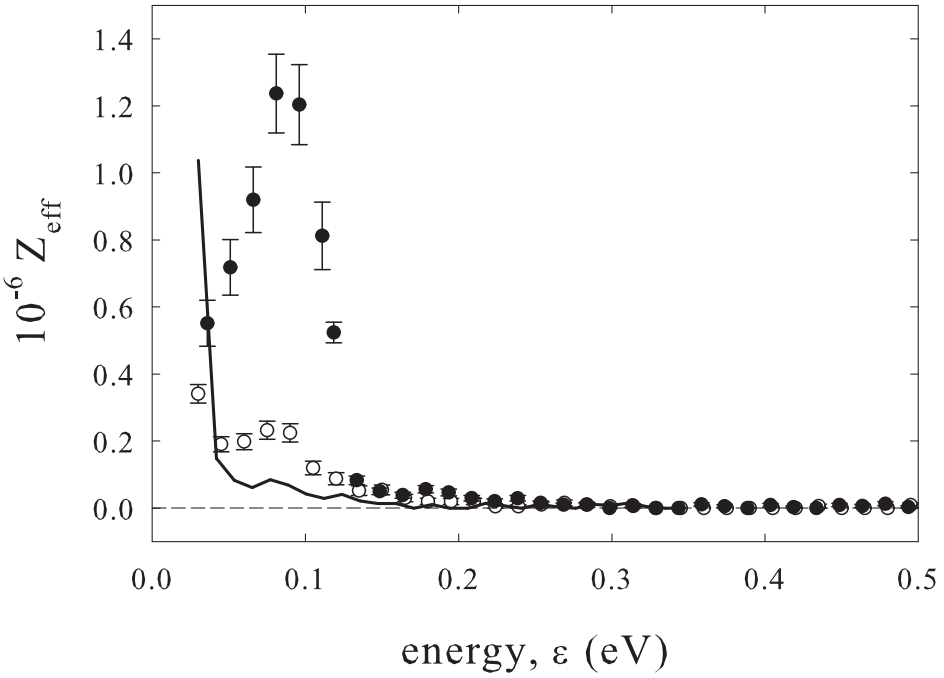

Figure 5.13: Energy-resolved Z_{eff} for (•) naphthalene, (○) deuterated naphthalene, and (—) scaled naphthalene. In the last case, the energy is scaled by the ratio of C-H and C-D stretch mode energies (after correcting for binding), and the magnitude is scaled by the ratio of resulting g factors. Note that only the tail of the C-H stretch peak can be seen after this scaling.

verify this, the Z_{eff} spectrum of deuterated naphthalene was measured and is shown in Fig. 5.13. Here we assume similar ion gauge calibration factors for the protonated and deuterated molecules, so that absolute comparisons can be made. As predicted, there is a significant upswing in Z_{eff} at low energy, which is absent in naphthalene, and is likely due to the C-D stretch mode.[8] There is also another peak around 80 meV with a modest Z_{eff} of 2.5×10^5. One might attribute this feature to a 10% contamination of non-deuterated naphthalene – although there was a two day vacuum bake between these experiments and the purchased sample of naphthalene-d8 had 99% purity. One could also interpret this feature to be an enhanced, multi-mode VFR, which parallels a feature in the rescaled naphthalene spectrum, also shown in Fig. 5.13.[9]

5.11 12, 14, and 16-carbon alkanes

As discussed in Refs. [45, 70], alkanes with twelve or more carbons have some of the largest binding energies and peak Z_{eff} ever measured. The measurements by Barnes *et al.* for dodecane ($C_{12}H_{26}$) and tetradecane ($C_{14}H_{30}$) are reproduced in Fig. 5.14. In addition, a recent measurement for hexadecane ($C_{16}H_{34}$) is included from Ref. [70]. Because of the difficulties measuring pressure, similar to that for naphthalene, the absolute magnitudes of the tetradecane and hexadecane spectra could not be determined. In this case, there were no comparable ionization gauge data, and so the affected Z_{eff} spectra are scaled arbitrarily.

The Z_{eff} for dodecane is huge, almost 10^7. Note also the nearly linear downward shift of the dominant C-H stretch peak with increasing molecular size. This continues the trend of binding increasing with molecular size that was observed in smaller alkanes [24, 43]. An interesting new feature is the second, weaker peak just slightly below the C-H stretch mode. This peak shifts downward and increases in size as the size of the

[8] Note that this occurs at an energy where measured Z_{eff} may be artificially *reduced* due to scattering and reduction of positron flux.

[9] Measurements of Z_{eff} at different pressures indicate that this feature is probably not a spurious three-body effect.

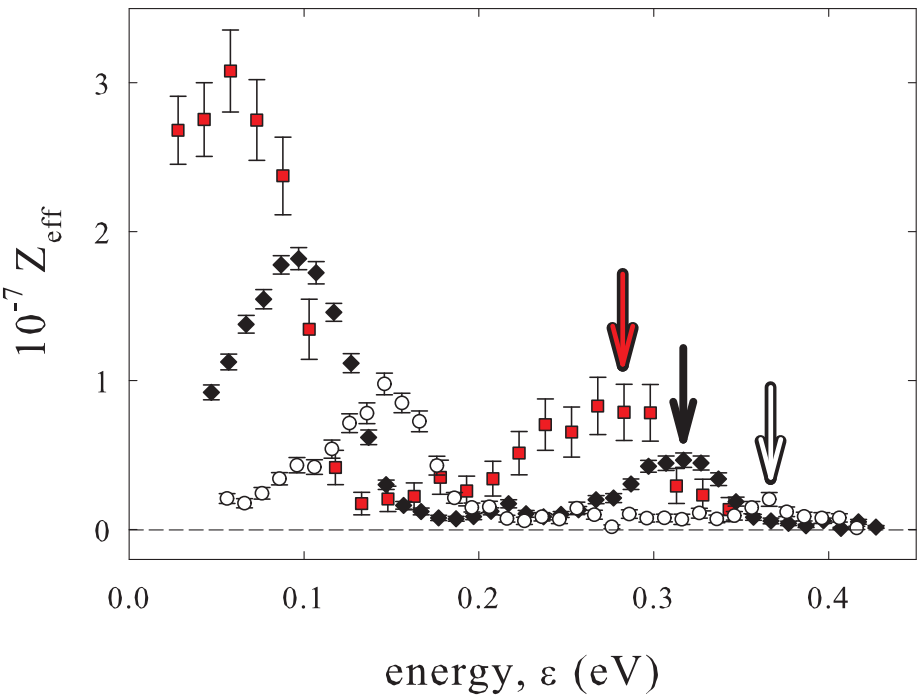

Figure 5.14: Z_{eff} spectra for (○) dodecane, (◊) tetradecane, and (□) hexadecane. The vertical arrows indicate the positions of small C-H stretch mode VFR for the second bound state in each molecule. Because of difficulties measuring absolute Z_{eff} for tetradecane and hexadecane, their spectra are have been arbitrarily normalized (see text for details). The larger peaks at lower energy are the C-H stretch mode VFR for the first bound states (i.e. the positronic ground states).

Table 5.3: Binding energy and Z_{eff} data for molecules with second bound states. The values $\epsilon_b^{(1)}$ and $\epsilon_b^{(2)}$ refer to the energies of the first and second bound states; $Z_{eff}^{(1)}/Z_{eff}^{(2)}$ is the ratio of first and second bound state C-H stretch mode peak heights; and $g^{(1)}/g^{(2)}$ is the ratio of the g scaling factors. For reference, naphthalene is included although it does not have a second bound state.

Species	$\epsilon_b^{(1)}$ [meV]	$\epsilon_b^{(2)}$ [meV]	$Z_{eff}^{(1)}/Z_{eff}^{(2)}$	$g^{(1)}/g^{(2)}$
dodecane ($C_{12}H_{26}$)	220	~ 0	8.17	–
tetradecane ($C_{14}H_{30}$)	260	50	3.94	3.79
hexadecane ($C_{16}H_{34}$)	310	100	3.83	3.69
naphthalene ($C_{10}H_8$)	300	–	–	–

alkane increases. A careful measurement of Z_{eff} as a function of pressure eliminated the possibility that this new peak is a spurious three-body effect. A multi-mode VFR is theoretically possible but unlikely. The best explanation is that this peak is the C-H stretch VFR associated with a second, positronically-excited bound state [45]. In essence, the positron-molecule potential has become deep enough to support another bound state above the ground state. Excited positron bound states have been predicted in calcium and berylium atoms using configuration-interaction methods [104]. They also appear in a less rigorous zero range potential (ZRP) model for binding in alkanes [65], which will be discussed in the next section.

As discussed in section 5.4, the Z_{eff} peak height can be described in terms of an explicit energy-dependent factor, $g = \sqrt{\epsilon_b/\epsilon}$, which comes from the small molecule theory [44]. In that section, it was shown that the ratio of the first and second bound state peaks in tetradecane, $Z_{eff}^{(1)}/Z_{eff}^{(2)}$, is nearly equal to the ratio of their respective g factors, $g^{(1)}/g^{(2)}$. With the addition of data for hexadecane, one can further test this scaling and start to investigate further trends in these second bound states.

Data for first and second bound states are shown in Table 5.3. As can be seen in this table, the binding energy of both the first and second bound states grow by $25-30$ meV per carbon, which continues the trend observed in smaller alkanes [24]. Furthermore,

$Z_{eff}^{(1)}/Z_{eff}^{(2)} = g^{(1)}/g^{(2)}$ for hexadecane as well as tetradecane. In order for this equality to work for dodecane, the binding of the second bound state should be ~ 8 meV, which is within our experimental error. Thus, the g factor provides a robust description of the VFR energy scaling, even for binding energies of 300 meV.

5.12 A zero-range potential model

Gribakin and Lee recently used zero-range potentials (ZRP) to model positron binding energies in alkanes [65]. This approximation is described in Refs. [38,67,72]. In their model, the positronic potential for each atom or monomer is considered point-like, with a reciprocal scattering length κ_i. The boundary condition for the positron wave function ψ as it approaches an atom at $\mathbf{R}_i$ is given by,

$$\frac{1}{r_i\psi}\frac{d(r_i\psi)}{dr_i}\bigg|_{r_i\to 0} = -\kappa_i, \tag{5.7}$$

where

$$r_i = |\mathbf{r} - \mathbf{R}_i|. \tag{5.8}$$

Atomic units are assumed here and elsewhere in this section. The trial positron wave function for a molecule with N ZRP centers is given by:

$$\psi = \sum_{i=1}^{N} A_i \frac{e^{\kappa|\mathbf{r}-\mathbf{R}_i|}}{|\mathbf{r}-\mathbf{R}_i|}. \tag{5.9}$$

The positron-molecule inverse scattering length κ, and thus the binding energy $\epsilon_b = \kappa^2/2$, can be determined by satisfying the boundary conditions, described above. The problem can then be reduced to finding the positive roots of the expression,

$$\det\left[(\kappa_i - \kappa)\delta_{ij} + \frac{e^{-\kappa R_{ij}}}{R_{ij}}(1-\delta_{ij})\right] = 0, \tag{5.10}$$

where $R_{ij} = |\mathbf{R}_i - \mathbf{R}_j|$.

The trick then is to determine the appropriate input values for κ_i. These can be inferred from experiment or obtained from more rigorous theoretical calculations. In Ref. [65], Gribakin and Lee attempt to calculate binding energies for the alkanes. In order

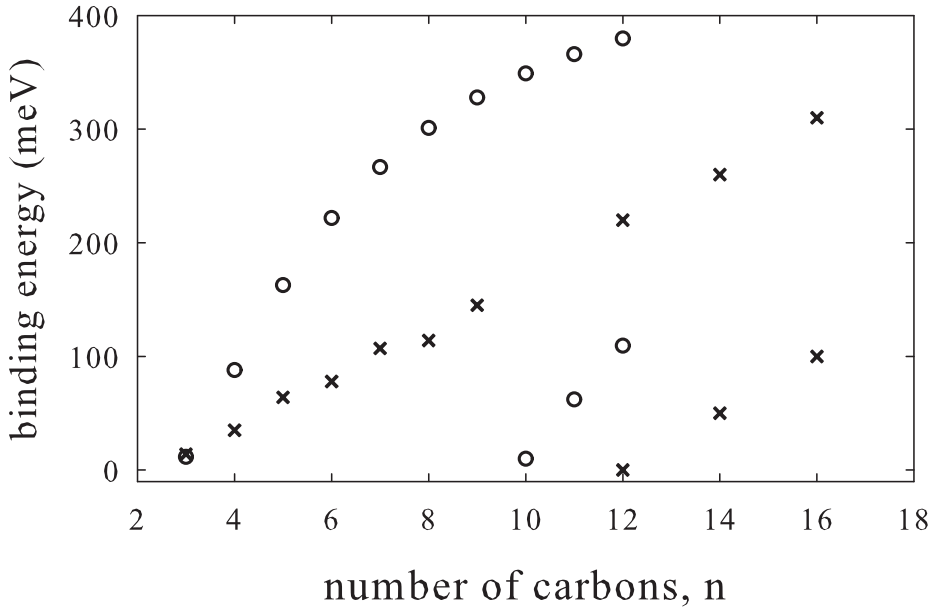

Figure 5.15: ZRP model for binding energy in alkanes (C_nH_{2n}) as a function of the number of carbons, n (reproduced from Ref. [65]). This plot shows the theoretical binding energies ($\circ$) for a chain of ZRP monomers as well as experimental binding energies ($\times$) for the first and second bound states in alkanes [43, 45, 70].

to reproduce the molecular structure of an alkane, they used "zig-zag" chains of ZRPs with center-to-center distances given by the C-C bond length. Each ZRP represents a carbon-based monomer, and is assigned a reciprocal scattering length, $\kappa_i = -1.5$, which is chosen so that the theoretical binding for propane is close to that measured experimentally.

The results of this calculation are shown in Fig. 5.15. The theory reproduces qualitatively the features seen in experiment. The binding energy increases with the number of carbons; and there is a second bound state, whose theoretical onset is at ten carbons, which is not too far from the experimental onset at twelve carbons. The theoretical binding energies are too large by a factor of two, and the ground-state theory curve is

moderately nonlinear with the number of carbons, while the experiment is linear. A more recent ZRP calculation (not shown) yields much better agreement for the larger molecules, including the second bound state, by using a different choice of monomer scattering length. In this case, however, the smallest alkanes are no longer bound.

According to the ZRP model, as the binding energy grows, the positron wave function draws closer to the molecule and becomes oblong. The binding energy of heptane is 105 meV which means $1/\kappa \sim 11\ a_0$. This is smaller than the length of the carbon chain, which is $\sim 15\ a_0$. This may explain the nonlinearity of ϵ_b with N for large N. Also note that, while the first bound state is fully symmetric, of s-wave type, the second bound state has a node, and thus it is of p-wave type. According to the Gribakin model for VFR, these effects should cause changes in both the capture width and the annihilation width [44]. In spite of this, even the largest alkanes obey the g-factor scaling.

5.13 Trends in binding energy

The ZRP model reproduces some qualitative trends; but it ignores important effects like polarization and dipole moment, and it depends on knowing the parameters κ_i. This makes it difficult to predict positron binding energies for other molecular species. In order to gain further insight into the underlying mechanisms governing positron-molecule binding, we plot the binding energy of a variety of species against various physical parameters.

Fig. 5.16 shows binding energy *vs* molecular polarizability, α, for a variety of species. At large distances, the polarizability produces an attractive potential $-\alpha e^2/2r^4$ in response to the positron charge. Thus, ignoring short-range repulsion, it is expected that binding should grow with polarizability.

As expected, binding energies roughly increase with polarizability. This is most clear for the alkanes and their second bound states. Other hydrocarbons studied to date are all slightly above the alkane curve. The most significant outliers are benzene, naphthalene and 1-chlorohexane. These are precisely the molecules that had unusually

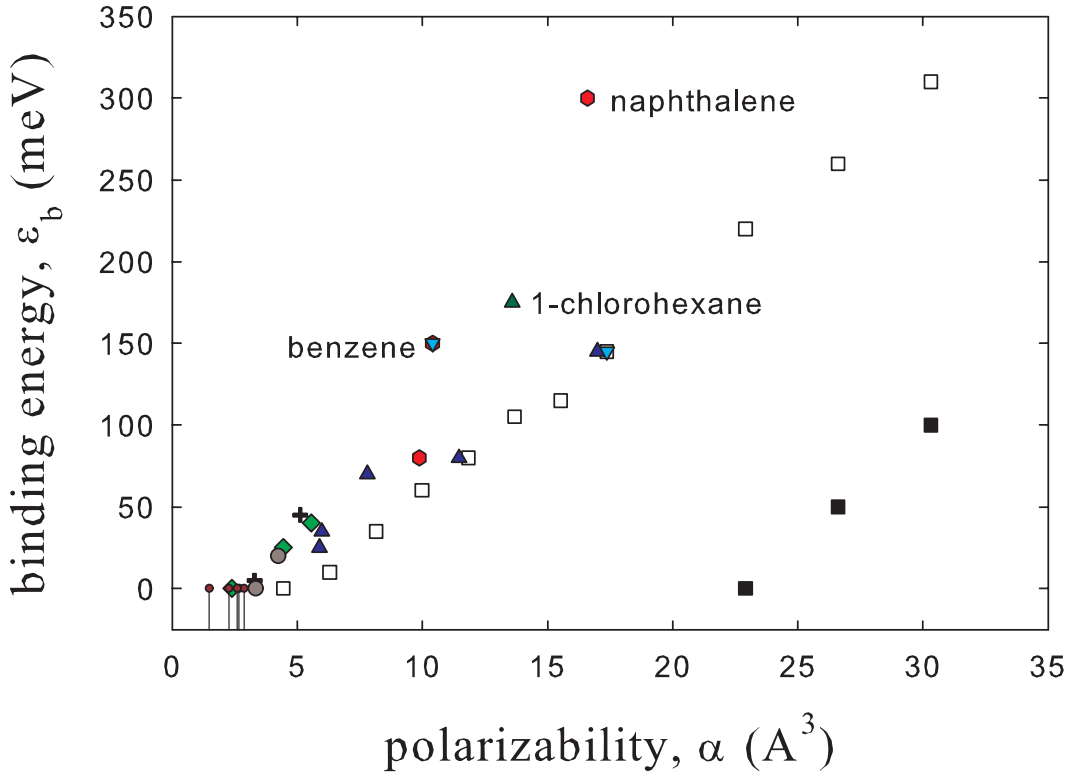

Figure 5.16: Binding energy *vs* polarizability for alkanes (□); alkane second bound states (black □); rings (red hexagons); halomethanes (green ◇); acetylene and ethylene (grey •); alcohols (+), 1-chlorohexane (dark green △); fluoroalkanes (blue △); and deuterated species (cyan ▽). VFR-weak/inactive species (small red ○) have a drop line to indicate possible 'negative' binding energies (i.e., virtual states). See Table 4.3 for details.

large binding energies for their sizes. As mentioned earlier, benzene and naphthalene have significantly lower ionization potentials than comparably-sized molecules, which may result in reduced repulsion at short distances. The molecule 1-chlorohexane does not, however, have this advantage. Perhaps the additional attraction due to its static dipole enhances the binding in this molecule.

The ionization energy E_i is a much weaker predictor of positron binding energies in large molecules. Simple alkanes with six or greater carbons have an ionization potential

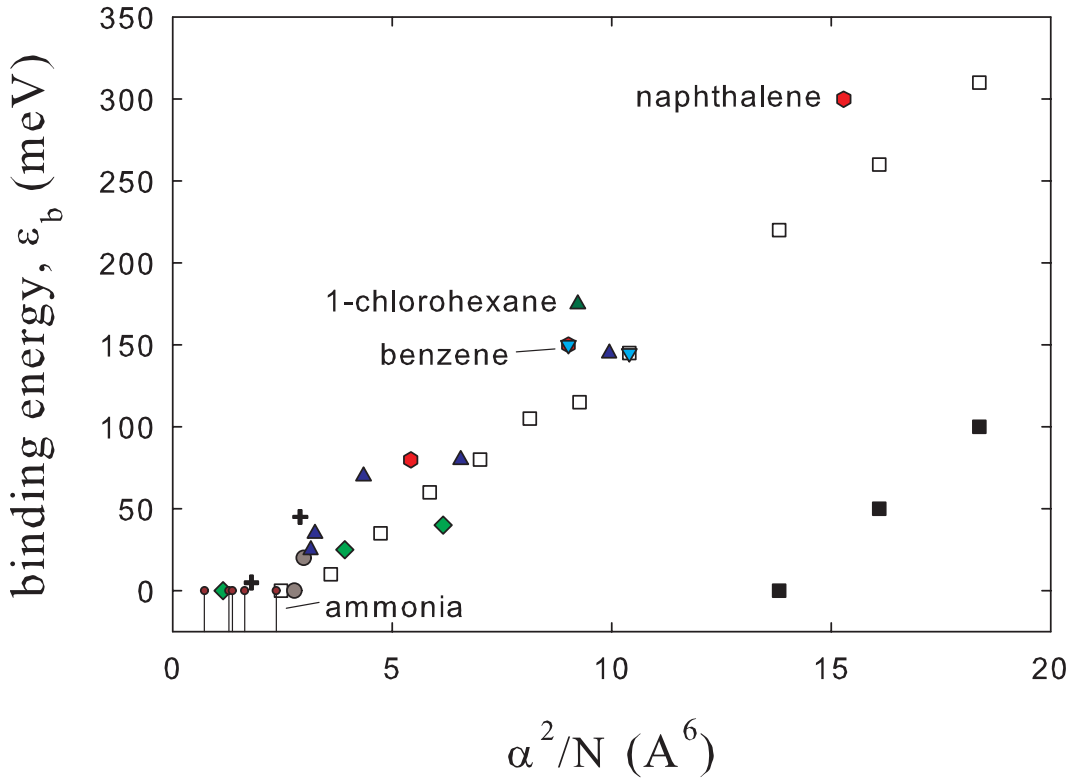

Figure 5.17: Binding *vs* α^2/N for a number of species. See Fig. 5.16 for symbol definitions. Note how there are fewer strong outliers to this trend.

more or less converged at 10 eV. Only especially high or low ionization energies seem to affect binding. Deeply bound species like benzene and naphthalene have unusually small ionization energies (9.25 eV and 8.12 eV respectively). Perfluoroalkanes have unusually high ionization energies, possibly indicating that they do not form bound states.[10] This would explain why their thermal Z_{eff} values barely exceed 1000 [1].

It is possible to get stronger, more linear correlations by finding the optimal combination of the various physical parameters. As shown in Fig. 5.17, there is a better

[10]Technically, the ionization energies for perfluoroalkanes do not meet the threshold ionization energy needed for binding. This threshold is based on the toy model for binding in alkali metal atoms by Mitroy *et al.* [48] (see chapter 4).

correlation between binding energy and α^2/N where N is the number of atoms. In a weak binding model, this would imply that $\kappa \propto \alpha/\sqrt{N}$.

The idea behind Fig. 5.17 is that molecular size matters. Since the polarization potential is $V_{pol} \sim \alpha e^2/(2r^4)$, all other things held equal, the attraction at the surface of a large molecule should be less than the attraction at the surface of a small molecule. Furthermore, one might imagine that the polarizability per electron might affect the short-range positron-electron interactions.

Looking at the binding data, it is tempting to devise some sort of empirical addition law similar to those used for predicting polarizabilities in molecules [96]. In such a scheme, each bond, atom, or monomer is assigned a characteristic value. Calculating the polarizability for a molecule then involves tabulating some mathematical combination of these characteristic values. To some degree, this is similar to using the ZRP model to calculate binding energy. In the ZRP case, the characteristic values are the κ_i. However, simpler addition rules are possible. In the alkanes, for instance, one could assign each single-bonded carbon a characteristic binding of ~ 20 meV and take the sum to get the approximate binding energy of the molecule. With more data, predicting binding in other molecules may be possible, using similar methods.

5.14 Concluding remarks

Although there is presently no quantitative model that can describe Z_{eff} in large molecules, one can make a number of empirical observations. To start, it appears that resonant Z_{eff} depend only weakly on binding via a scale factor $g = \sqrt{\epsilon_b/\epsilon}$. After this dependence is removed, most molecules follow a universal scaling, $Z_{\mathit{eff}}/g \propto N^{4.1}$, where N is the number of atoms. This indicates that enhanced Z_{eff} resonances are likely caused by IVR and that inelastic escape channels in most molecules are weak or inactive. Furthermore, the role of thermal inelastic escape channels appears to be limited based upon the observed weak dependence of resonant Z_{eff} on target gas temperature. The only exceptions to this universal scaling are the partially fluorinated alkanes; in these

molecules, Z_{eff} is suppressed above some threshold energy, likely caused by a strong C-F stretch mode de-excitation escape channel.

After eliminating these effects, there is still a great diversity of behavior seen in large molecules. In a couple molecules, such as 1-chlorohexane and the partially deuterated benzenes, there is enhancement above that dictated by the universal scaling. These effects can possibly be described in terms of changes in the number of dark states and intermediate states in a tiered IVR model. Some molecules, like benzene, have evidence of strong multi-mode VFR, while most do not. The reasons for this are still not clear.

With regard to positron binding, benzene, naphthalene, and 1-chlorohexane all have unusually deep binding for their size. In addition, large alkanes have positronically excited bound states. Positron binding is, at present difficult to calculate in large molecules. The ZRP model is reasonably successful in explaining the growth of binding with size in alkanes. It even indicates the approximate onset of the positronically excited states seen in experiment. However, it is limited in many ways, particularly because it relies on parameters characterizing positron-monomer interactions that must be determined from experiment. As shown in this chapter, positron binding appears to be roughly correlated with factors such as dipole polarizability and number of atoms and weakly correlated with the molecular ionization energy. It is hoped that this information will lead to improved positron binding calculations.

Chapter 6

Conclusions

Positron-molecule annihilation below the threshold for positronium formation is a complex phenomenon, which at present, is best understood in the limiting cases. Some small molecules, such as the substituted methanes, can be described more or less exactly by the Gribakin-Lee theory. In large molecules, annihilation rates increase rapidly and follow a universal scaling with number of vibrational degrees of freedom. While there is no quantitative model which explains this, the trend strongly suggests some kind of vibrational relaxation mechanism, like IVR.

The Gribakin-Lee theory provides an excellent framework for predicting Z_{eff} in small molecules, particularly the halomethanes. It indicates that, as long as the dipole coupling is strong, the relative magnitudes of the VFR are determined entirely by the factor $g = \sqrt{\epsilon_b/\epsilon}$. While the theory originally included only fundamental vibrations, it can be extended to include multi-mode and other vibrations that do not exhibit strong dipole coupling. This leads to good quantitative predictions in methanol and qualitative predictions in molecules such as ethylene.

Outside this relatively narrow range of molecules, the Gribakin-Lee theory fails. Smaller molecules, like water, may not be bound but have significant features that look nothing like VFR. Larger molecules, such as ethane, have clearly enhanced VFR, particularly at the C-H stretch peak. In both cases, there is evidence of considerable chemical

and mode sensitivity. For instance, ethanol, which is larger than ethane, acts like a perfect Gribakin-Lee molecule.

The C-H stretch resonance in large hydrocarbons generally conforms to a scaling, $Z_{\mathit{eff}}/g \propto N^{4.1}$ where N is the number of atoms in the molecule. Likely this dependence on N reflects a dependence on the number of vibrational degrees of freedom, $3N-6$. This provides evidence of an IVR enhancement process in which inelastic escape channels are predominantly either weak or inactive. However, the fluoroalkanes are a notable exception to this trend: they have unusually low values of Z_{eff} at the C-H stretch peak but no suppression below a certain threshold energy. Recent studies of these molecules indicate that this suppression is due to the inelastic de-excitation of a C-F stretch mode. This effect is expected to disappear as the positron binding energy increases.

There are some interesting phenomena which hint at further complexity in the Z_{eff} enhancement process. Some molecules, such as benzene, have strong multi-mode resonances. Other molecules, such as 1-chlorohexane, have extra enhancement beyond the universal scaling. These effects are probably linked to changes in the number of, and coupling to the dark states in IVR.

Positron-molecule binding plays an important role in all of these resonances. Without it, the VFR could not exist. Beyond this, however, its effect on Z_{eff} spectra is surprisingly small. The dependence on binding in large molecules seems to be the same as that for small molecules. The relative heights of first and second bound state peaks in large alkanes are described exactly by the scaling $g = \sqrt{\epsilon_b/\epsilon}$, which comes from Gribakin's model [23, 40, 44].

6.1 Open questions

This research, while illuminating many aspects of positron-molecule annihilation, has also left some dark corners filled with opportunity. Many open questions remain. Below is a summary of such questions, many of which suggest new possibilities for research.

6.1.1 The IVR process

The Z_{eff} enhancement process in larger molecules is still quite mysterious. Evidence suggests that IVR is responsible, but the details are largely unknown. In particular, it is unclear how to achieve the observed scaling with the number of vibrational modes. It appears that only a subset of all possible multi-mode states participate in this process. However, the identities of these modes and their couplings are unknown. Inelastic escape channels are rare, but as discussed in section 5.6, they provide a window into these complex internal processes. Specifically, the C-F stretch escape channel in the fluoroalkanes seems to require an *intermediate* state.

There is the additional question as to what governs the relative heights of the resonances in large molecules. The C-H stretch peak in alkanes is much larger than the low energy bend and the C-C mode peaks. To some degree, this can be attributed to the fact that the density of vibrational states increases with energy. However, the ratio of the high-energy C-H stretch and the low energy Z_{eff} peak heights is nearly constant throughout the alkanes. This is strange as the density of vibrational states at each energy grows at a different rate with molecular size. This suggests that either the density of dark states grows at the same rate at all energies, or low energy modes have better access to dark states than high energy modes.

6.1.2 The capture rate

The Gribakin-Lee model for small molecules is remarkably successful in the halomethanes, because it requires little precision in the calculation of the capture rate. As long as the capture rate is much larger than the annihilation rate, the VFR peak height is essentially independent of the capture rate. This assumption breaks down as soon as marginal resonances like multi-mode and infrared-inactive VFR are introduced. As a result, quantitative predictions of Z_{eff} in molecules like ethylene and acetylene are remarkably difficult within the Born-dipole approximation. More theoretical sophistication is needed for these molecules. This will be aided by additional experimental data

for small molecules.

6.1.3 Positron binding energy

Predicting binding energies in molecules continues to be difficult. To the author's knowledge, no rigorous theory has been able to quantitatively reproduce any of the binding energies observed in experiment. Some models require seemingly unrealistic changes in molecular geometry in order for binding to occur [82, 83]. Arguably, the best qualitative theory is the ZRP model by Gribakin [38, 65, 72]. This model can explain the increasing binding in the alkanes and the appearance of a second bound state, but it is not easily generalized to other molecules. Various trends with polarizability, number of atoms, and ionization energy suggest some other sort of toy model might be possible. The fact that the threshold conditions for binding to alkali atoms (also based on a toy model [48]) are similar to those for polyatomic species is promising.

6.1.4 Other phenomena

In the smallest molecules, such as water and CO_2, there is evidence of additional structure in Z_{eff}. The theory of annihilation seems to have plenty of room for additional, non-VFR features due to interference and direct annihilation resonances. It would be interesting to see which, if any, manifest themselves in experiment.

Another theoretically possible feature, which has yet to be observed, is that of an electronically-excited Feshbach resonance. This occurs when a sufficiently energetic positron drives a molecule into an electronic and vibrationally-excited state while dropping into a bound state. This phenomenon should manifest itself as a comb of resonances near the electronic transition energy corresponding to the various vibrational final states. One reason this has yet to be observed is that the transition frequently occurs above the threshold energy for positronium formation, so the resonance is drowned out by positronium annihilation. Thus, for this experiment to be possible, the threshold for the first electronic excitation must be more than 6.8 eV below the ionization threshold.

6.2 Future experiments

There are a number of ways to gain insights into the above topics. Some involve using present experimental techniques, while others involve complimentary or improved techniques. Continued study of Z_{eff} in a wide variety of molecules would further clarify the observed trends in Z_{eff} and binding. It might also reveal additional phenomena. This is especially important for small molecules, where theoretical progress is likely to be the greatest.

6.2.1 Changes in molecular structure

Within the framework of the current experiments, a very useful technique is to make small changes in the structure of a molecule and observe the effects on Z_{eff} and positron binding. For instance, to probe the internal dynamics, one could make various isotopic substitutions in a molecule. In the context of the IVR model, these changes can alter the density of final "dark" states, the "intermediate" states (i.e., those which stand between the initial excitation and the "dark" states), and the inelastic thresholds. As was shown in chapter 5, partial deuteration should result in an increase in the density of states but may also alter the intermediate states. Separating the competing internal effects requires looking at the C-H and C-D stretch peaks in a number of similar hydrocarbons. Based on hints in thermal Z_{eff} [1,37,101], energy-resolved spectra for substituted benzenes may be particularly insightful.

As the understanding of inelastic channels improves, one can imagine such a channel as a probe of intermediate states. After examining the effects of deuteration on a molecule, for example, one could look at the same molecule with an added C-F mode. Changes in suppression with deuteration could indicate changes in the number and type of intermediate modes. Presently, this analysis may say as much about the inelastic processes as it does about the molecule being probed.

6.2.2 Particularly interesting molecules

There are some molecules that stand out as interesting candidates for future energy-resolved annihilation studies. Studies of partially deuterated fluoroalkanes could provide an important confirmation of the inelastic suppression mechanism. Experiments with hexadecane-derivatives and other large molecules, potentially capable of supporting second bound states, could also provide interesting information. One might expect differential effects of partial fluorination and deuteration on the first and second bound states.

The alcohols may also provide interesting information. Ethanol has little or no IVR at its C-H stretch peak. Will the same hold for propanol or isopropanol? It would be interesting to see if the -OH group has the same suppression effect as a fluorine. It would also be interesting to see if chlorine substitution on a molecule smaller than hexane results in suppression. The going hypothesis is that 1-chlorohexane is too deeply bound for the positron to escape via a C-Cl inelastic de-excitation channel.

On a different note, it is worth looking at the energy-resolved spectra of perfluorinated alkanes. The current view is that they have little or no binding. Thus, they should have little or no VFR peaks. This may change for very large perfluoroalkanes. Furthermore, more experiments are needed in small molecules such as water to clarify the origin of their unusual Z_{eff} features.

6.2.3 A hot cell

Previous experiments in our lab have been limited to molecules with high vapor pressures at room temperature. A new effort is underway to build a "hot" gas cell, which will allow absolute measurements of scattering and annihilation processes for molecules with much lower vapor pressures. For instance, it would allow *absolute* measurements of Z_{eff} in polycyclic aromatic molecules (PAHs) and very large alkanes such as hexadecane.

One particular focus is to measure annihilation and scattering cross sections in atomic clusters such as C_{60}. According to one theory, C_{60} should have distinct shape resonances

from centrifugal barrier states and also cage-state resonances inside the molecule [94]. Also, the hot cell would allow measurements of certain metals. Of particular interest is magnesium, which has been predicted recently to have a large p-wave shape resonance at ∼130 meV with a Z_{eff} of 1500 [95].

6.2.4 Gamma-ray spectra

Positron-molecule binding is ultimately determined by the positron bound-state wave function. Thus, a better understanding of this wave function could lead to a better understanding of binding. While it is impossible to observe this function directly, it is possible to determine how strongly it overlaps with various electron orbitals based on the Doppler broadening measurements of the annihilation gammas. Experiments with thermal positrons determined that the positron wave function is approximately evenly distributed between the valence orbitals and has little overlap with the core electrons in alkanes and fluoroalkanes [1,12,105]. High resolution gamma-ray spectroscopy at specific VFR peaks might provide further insights. For instance, one might compare the gamma-ray spectra of the first and second bound states. Presumably, the former would have a broader width due to greater positron overlap with the core electrons. This experiment is more or less possible with current experimental capabilities.

6.2.5 Scattering processes

Scattering processes provide additional information about the annihilation process. For instance, there should be a resonance in the elastic scattering cross section, σ_ν^e, corresponding to each VFR. Breit-Wigner theory indicates that this cross section has the following magnitude in atomic units,

$$\sigma_\nu^e = \frac{\pi^2}{\epsilon}\frac{(\Gamma_\nu^e)^2}{\Gamma_\nu}(\Delta\epsilon)^{-1} \sim \frac{\pi^2\Gamma_\nu^e}{\epsilon}(\Delta\epsilon)^{-1} \tag{6.1}$$

where ϵ is the positron impact energy, Γ_ν^e is the resonant elastic capture width, and $\Delta\epsilon \sim$ 50 meV is the energy spread of the positron beam. Since $\sigma_\nu^e \propto \Gamma_\nu^e$, a measurement of this cross section could provide a more stringent test of the Gribakin-Lee model. Presently,

there are no experimental scattering data of this type for VFR-active molecules. The resonant elastic cross section is probably quite small, on the order of 0.1 a_0^2 according to the Born-Dipole prediction, which may be an overestimate [44].[1] Since this effect is a few orders of magnitude smaller than the non-resonant cross section [106], it will require a scattering experiment with considerably better signal-to-noise than has been achieved to date.

In addition, the postulated resonant inelastic channel that is responsible for suppressing Z_{eff} in the fluoroalkanes should be directly observable in inelastic scattering. At the energy of the C-H stretch peak, there should be a distinct enhancement of the C-F stretch de-excitation channel. This channel is distinguishable from others, because the positron loses the *difference* in energy between the C-H stretch mode, ω_{CH}, and the C-F stretch mode, ω_{CF}. In other words, if one looks at the flux of scattered positrons with total energy $\omega_{CF} - \epsilon_b$, as a function of incident positron energy, one should observe resonances at the energies of the VFR in the annihilation spectrum. If the inelastic channel is much larger than the elastic channel, this cross section should be identical to the resonant elastic cross section described above (i.e., proportional to Γ_ν^e). The signal-to-noise may be much better than the elastic case.

It is also possible to estimate the binding energy using measurements of the total elastic scattering cross section. As discussed earlier, the binding energy is $\epsilon_b = \kappa^2/2$, where κ is the inverse s-wave scattering length. Assuming s-wave scattering, the total elastic cross section asymptotically approaches $4\pi/\kappa^2$ near zero energy [23]. Thus, the energy dependence of this cross section at small incident positron energies could provide a confirmation of the binding energies determined by the Z_{eff} peak shifts. It would also be more sensitive to small binding energies. However, this requires measurements at low incident positron energies $\epsilon < \epsilon_b$ that have not been possible up to now. A colder positron beam and electrodes with highly uniform electrostatic potentials could enable such measurements.

[1] This cross section will increase if the energy spread of the positron beam is reduced

6.2.6 A cold positron beam

One way to gain insight into the annihilation process is with higher energy resolution. This can be achieved by cooling the positrons down by an order of magnitude in a next-generation trap. The technology for producing cold, intense beams is actively being developed in our lab [107, 108]; and in the future, could provide a positron beam with meV energy resolution. This high resolution beam could better distinguish the different VFR contributing to the Z_{eff} peaks. For instance, one could resolve the individual modes contributing to the low energy plateau in alkanes such as propane. This would provide a much better understanding of the underlying selection rules. One might also be able to study roto-vibrational structure.

A particularly important characteristic to investigate is the natural line width of some of the VFR. Gribakin's calculations suggest that they should be less than 100 μeV in small molecules [44]. However, IVR spreading should result in much broader resonances. In this case, the width could potentially provide important information about the strength of the IVR coupling.

6.2.7 Fragmentation analysis

One last avenue of exploration that has not received as much attention recently is analysis of the annihilation fragments. The last time this was studied in much detail was over a decade ago [109–116]. The final state of the positron-molecule complex before annihilation should be encoded in the resulting gamma-rays and ions following annihilation. As mentioned earlier, the annihilation gamma-rays provide information about the positron wave function. However, the ions left behind may reveal additional information. Immediately after resonant annihilation, the molecule is still vibrationally excited, but missing one of its electrons (there is no additional excitation because the effect of gamma scattering is negligible). According to Ref. [112], there is excess energy in this ion due to the difference in energy between the highest lying molecular orbital and the hole left by the annihilated electron. This energy can lead to the decomposition

of the molecular ion into smaller fragments.

In theory, if one knew the total energy and type of all the exit fragments, one could reconstruct the total energy of the positron-molecule complex prior to annihilation and determine which valence electron was eliminated. In fact, one needs considerably less information. There are different known energy thresholds required to produce each type of molecular fragment. The prevalence of a given fragment places a lower bound on the excess energy in the post-annihilation state. This in turn could be used to discern the likely origin of the annihilated electrons [112].

While previous experiments were limited to a broad energy distribution, new experiments could use the energy-resolved beam to hone in on specific resonances and examine the resulting fragments. One could also compare the fragmentation patterns on and off resonance or between first and second bound state resonances. With recent improvements in our understanding of positron-molecule complexes, much deeper analyses may be possible than in the past.

Appendix A

Table of positron-molecule annihilation data

This appendix contains a table with physical parameters and annihilation data for all molecules studied to date using our energy-resolved measurement techniques. The values presented are the number of atoms N; number of electrons Z; static dipole moment μ; dipole polarizability α; ionization energy E_i; positron binding energy ϵ_b; average energy of the C-H (or C-D) stretch modes, ω_{CH}; annihilation rate at the C-H stretch VFR $Z_{eff}^{(CH)}$; annihilation rate at room temperature $Z_{eff}^{(th)}$; and the normalized annihilation rate $Z_{eff}^{(CH)}/g$, where $g = \sqrt{(\omega_{CH} - \epsilon_b)/\epsilon_b}$. The values for $Z_{eff}^{(th)}$ are from Ref. [1]. The values for ϵ_b and $Z_{eff}^{(CH)}$ were determined experimentally from the energy-resolved Z_{eff} data discussed in Chapters 4 and 5 and presented in Refs. [24, 43, 45, 70]. The binding energy is assigned the value "$\gtrsim 0$" if the molecule is VFR-active but ϵ_b is ambiguous or too small to determine with the present data. Dipole moments are taken from Ref. [1], polarizabilities from Refs. [1, 96], and ionization energies from Refs. [1, 66]. Some values of α have been calculated using the method described in Ref. [96].

Table A.1: Table of positron-molecule annihilation data

Species	N	Z	μ [D]	α [Å^3]	E_i [eV]	ϵ_b [meV]	ω_{CH} [meV]	$Z_{eff}^{(CH)}$	$Z_{eff}^{(th)}$	$Z_{eff}^{(CH)}/g$
SMALL MOLECULES										
H_20	3	10	1.85	1.47	12.61	n/a	n/a	n/a	319	n/a
CO_2	3	22	0	2.66	13.77	n/a	n/a	n/a	55	n/a
NH_3	4	10	1.47	2.26	10.19	$\gtrsim 0$	n/a	n/a	1,600	n/a
CF_4	5	42	0	2.86	16.25	n/a	n/a	n/a	54	n/a
HALOMETHANES										
CH_3F	5	18	1.85	2.39	12.85	$\gtrsim 0$	366	35	1,390	n/a
CH_3Cl	5	26	1.87	4.43	11.22	25	366	585	15,000	2,160
CH_3Br	5	44	n/a	5.55	10.54	40	366	820	n/a	2,300
CH_2F_2	5	26	1.97	2.48	12.6	$\gtrsim 0$	366	600	799	n/a
CHF_3[a]	5	34	1.65	2.65	14.8	$\gtrsim 0$[a]	366	n/a	247	n/a
ALKENES & ALKYNES										
acetylene	4	14	0	3.33	11.4	$\gtrsim 0$	366	n/a	3,160	n/a
ethylene	6	16	0	4.23	10.51	20	366	720	1,200	3,000
ALCOHOLS										
Methanol	6	18	1.7	3.28	10.85	5	366	500	1,510	4,200
Ethanol	9	26	n/a	5.11	10.48	45	366	1,840	n/a	4,900

[a]Strong inelastic scattering may have caused some spurious features in the Z_{eff} spectrum of this molecule, making it difficult to identify the C-H stretch VFR.

Table A.1: (*Continued*).

Species	N	Z	μ [D]	α [Å^3]	E_i [eV]	ϵ_b [meV]	ω_{CH} [meV]	$Z_{eff}^{(CH)}$	$Z_{eff}^{(th)}$	$Z_{eff}^{(CH)}/g$
ALKANES										
methane	5	10	0	2.6	12.7	n/a	366	n/a	142	n/a
ethane	8	18	0	4.44	11.52	$\gtrsim 0$	366	900	660	n/a
propane	11	26	0.08	6.29	11.14	10	366	10,500	3,500	63,000
butane	14	34	0	8.14	10.63	35	366	21,000	11,300	65,000
pentane	17	42	0	9.98	10.35	60	366	80,000	37,800	180,000
hexane	20	50	0	11.83	10.18	80	366	184,000	120,000	350,000
heptane	23	58	0	13.68	9.9	105	366	590,000	242,000	930,000
octane	26	66	0	15.52	10.03	115	366	1,090,000	585,000	1,610,000
nonane	29	74	0	17.37	10.02	145	366	2,900,000	643,000	3,600,000
dodecane	38	98	0	22.91	9.93	220	366	9,800,000	1,780,000	8,000,000
2^{nd} B.S.	38	98	0	22.91	9.93	$\gtrsim 0$	366	1,200,000	n/a	n/a
tetradecane	44	114	n/a	26.61	n/a	260	366	$11x$[b]	n/a	$6.8x$[b]
2^{nd} B.S.	44	114	n/a	26.61	n/a	50	366	$2.8x$[b]	n/a	$7.0x$[b]
hexadecane	50	130	0	30.31	9.91	310	366	$15y$[b]	2,230,000	$6.4y$[b]
2^{nd} B.S.	50	130	0	30.31	9.91	100	366	$4.0y$[b]	n/a	$6.5y$[b]
ALKANE ISOMERS										
isopentane	17	42	0.13	9.98	10.32	60	366	80,000	50,500	180,000

[b] Absolute Z_{eff} could not be determined for these molecules so their values are multiplied by arbitrary common factors 'x' and 'y.'

Table A.1: (*Continued*).

Species	N	Z	μ [D]	α [Å^3]	E_i [eV]	ϵ_b [meV]	ω_{CH} [meV]	$Z_{eff}^{(CH)}$	$Z_{eff}^{(th)}$	$Z_{eff}^{(CH)}/g$
RINGS										
cyclopropane	9	24	n/a	n/a	n/a	10	366	3,600	n/a	21,500
cyclohexane	18	48	0	9.88	9.88	80	366	94,000	20,000	180,000
benzene	12	42	0	10.4	9.25	150	379	47,000	15,000	58,000
naphthalene	18	68	0	16.59	8.15	300	379	1,240,000	494,000	640,000
HALOALKANES			n/a							
1-fluoropropane	11	34	n/a	5.97	n/a	35	366	1,520	n/a	4,700
2,2-difluoropropane	11	42	n/a	5.88	11.42	25	366	900	8,130	3,300
1-fluorobutane	14	42	n/a	7.8	n/a	70	366	5,600	n/a	11,500
1-fluorohexane	20	58	n/a	11.46	n/a	80	366	$60,000 \pm 30,000$	269,000	$110,000 \pm 60,000$
1-chlorohexane	20	66	n/a	13.59	10.3	175	366	520,000	n/a	540,000
1-fluorononane	29	82	n/a	16.98	n/a	145	366	930,000	n/a	1,150,000
DEUTERATED										
CD_3Cl	5	18	n/a	n/a	n/a	25	278	660	n/a	2,100
CD_3Br	5	26	n/a	n/a	n/a	40	278	810	n/a	1,980
d-benzene	12	68	0	10.4	9.25	150	283	61,000	36,900	57,500
d-butane	14	34	n/a	n/a	n/a	35	278	28,500	n/a	75,000
d-nonane[c]	29	74	0	17.37	n/a	145	278	3,500,000[c]	641,000	3,300,000
d-naphthalene	18	68	n/a	n/a	n/a	~ 300	283	n/a	n/a	n/a

[c] Z_{eff} for d-nonane has been rescaled to preserve its magnitude relative to an older measurement of nonane performed under the same experimental conditions.

References

[1] K. Iwata. *Positron Annihilation on Atoms and Molecules*. Ph.D. thesis, University of California, San Diego (1997).

[2] P. A. M. Dirac. On the annihilation of electrons and protons. *Proceedings of the Cambridge Philosophical Society* **26**, 361–375 (1930).

[3] P. A. M. Dirac. A theory of electrons and protons. *Proceedings of the Royal Society of London* **126**, 360–365 (1930).

[4] C. D. Anderson. The apparent existence of easily deflectable positives. *Science* **76**, 238–239 (1932).

[5] C. D. Anderson. The positive electron. *Physical Review* **43**, 491–494 (1933).

[6] R. L. Wahl. *Principles and Practice of Positron Emission Tomography* (Lippincott, Williams and Wilkins, Philadelphia, PA, 2002).

[7] M. H. Holzscheiter, N. Bassler, N. Agazaryan, G. Beyer, E. Blackmore, J. J. DeMarco, M. Doser, R. E. Durand, O. Hartley, K. S. Iwamoto, H. V. Knudsen, R. Landua, C. Maggiore, W. H. McBride, S. P. Moller, J. Petersen, L. D. Skarsgard, J. B. Smathers, T. D. Solberg, U. I. Uggerhoj, S. Vranjes, H. R. Withers, M. Wong and B. G. Wouters. The biological effectiveness of antiproton irradiation. *Radiotherapy and Oncology* **81**, 233–242 (2006).

[8] P. J. Schultz and K. G. Lynn. Interaction of positron beams with surfaces, thin films, and interfaces. *Rev. Mod. Phys.* **60**, 701–779 (1988).

[9] A. Dupasquier and A. P. Mills Jr. (editors) *Positron Spectroscopy of Solids* (IOS Press, Amsterdam, 1995).

[10] A. David, G. Kögel, P. Sperr and W. Triftshäuser. Lifetime measurements with a scanning positron microscope. *Physical Review Letters* **87**, 067402 (2001).

[11] S. Tang, M. D. Tinkle, R. G. Greaves and C. M. Surko. Annihilation gamma-ray spectra from positron-molecule interactions. *Physical Review Letters* **68**, 3793–6 (1992).

[12] K. Iwata, R. G. Greaves and C. M. Surko. γ-ray annihilation spectra from positron-molecule interactions. *Physical Review A* **55**, 3586–3604 (1997).

[13] P. A. Milne. Distribution of positron annihilation radiation. *New Astronomy Reviews, Astronomy with Radioactivities. V* **50**, 548–552 (2006).

[14] N. Prantzos. Positron production and annihilation in the milky way. *New Astronomy Reviews; Astronomy with Radioactivities. V* **50**, 553–556 (2006).

[15] M. Amoretti, C. Amsler, G. Bonomi, A. Bouchta, P. Bowe, C. Carraro, C. L. Cesar, M. Charlton, M. J. T. Collier, M. Doser, V. Filippini, K. S. Fine, A. Fontana, M. C. Fujiwara, R. Funakoshi, P. Genova, J. S. Hangst, R. S. Hayano, M. H. Holzscheiter, L. V. Jrgensen, V. Lagomarsino, R. Landua, D. Lindelf, E. L. Rizzini, M. Macr, N. Madsen, G. Manuzio, M. Marchesotti, P. Montagna, H. Pruys, C. Regenfus, P. Riedler, J. Rochet, A. Rotondi, G. Rouleau, G. Testera, A. Variola, T. L. Watson and D. P. van der Werf. Production and detection of cold antihydrogen atoms. *Nature* **419**, 456–459 (2002).

[16] G. Gabrielse, N. S. Bowden, P. Oxley, A. Speck, C. H. Storry, J. N. Tan, M. Wessels, D. Grzonka, W. Oelert, G. Schepers, T. Sefzick, J. Walz, H. Pittner, T. W. Hänsch and E. A. Hessels. Background-free observation of cold antihydrogen with field-ionization analysis of its states. *Physical Review Letters* **89**, 213401 (2002).

[17] G. Andresen, W. Bertsche, A. Boston, P. D. Bowe, C. L. Cesar, S. Chapman, M. Charlton, M. Chartier, A. Deutsch, J. Fajans, M. C. Fujiwara, R. Funakoshi, D. R. Gill, K. Gomberoff, J. S. Hangst, R. S. Hayano, R. Hydomako, M. J. Jenkins, L. Jrgensen, L. Kurchaninov, N. Madsen, P. Nolan, K. Olchanski, A. Olin, A. Povilus, F. Robicheaux, E. Sarid, D. M. Silveira, J. Storey, H. H. Telle, R. I. Thompson, D. P. van der Werf, J. S. Wurtele and Y. Yamazaki. Antimatter plasmas in a multipole trap for antihydrogen. *Physical Review Letters* **98**, 023402 (2007).

[18] D. Grzonka, D. Comeau, G. Gabrielse, F. Goldenbaum, T. W. Hänsch, E. A. Hessels, P. Larochelle, D. Lesage, B. Levitt, W. Oelert, H. Pittner, T. Sefzick, A. Speck, C. H. Storry, J. Walz and Z. Zhang. ATRAP - Progress Towards Trapped Antihydrogen. In D. Grzonka, R. Czyzykiewicz, W. Oelert, T. Rozek and P. Winter (editors) *Low Energy Antiproton Physics*, vol. 796 of *American Institute of Physics Conference Series*, 296–300 (2005).

[19] T. J. Phillips. Measuring the gravitational acceleration of antimatter with an antihydrogen interferometer. *Hyperfine Interactions* **100**, 163–172 (1996).

[20] A. P. Mills, Jr. Chemistry and physics with many positrons. *Radiation Physics and Chemistry* **76**, 76–83 (2007).

[21] A. P. Mills, Jr., D. B. Cassidy and R. G. Greaves. Prospects for making a bose-einstein-condensed positronium annihilation gamma ray laser. *Material Science Forum* **445-446**, 424429 (2004).

[22] G. R. Schmidt, H. P. Gerrish, J. J. Martin, G. A. Smith and K. J. Meyer. Antimatter requirements and energy costs for near-term propulsion applications. *Journal of Propulsion and Power* **16**, 923–928 (2000).

[23] G. F. Gribakin. Mechanisms of positron annihilation on molecules. *Physical Review A* **A61**, 022720 (2000).

[24] S. J. Gilbert, L. D. Barnes, J. P. Sullivan and C. M. Surko. Vibrational-resonance enhancement of positron annihilation in molecules. *Physical Review Letters* **88**, 043201 (2002).

[25] J. P. Marler and C. M. Surko. Positron-impact ionization, positronium formation, and electronic excitation cross sections for diatomic molecules. *Physical Review A* **72**, 062713 (2005).

[26] J. P. Marler and C. M. Surko. Systematic comparison of positron- and electron-impact excitation of the ν_3 vibrational mode of CF_4. *Physical Review A* **72**, 062702 (2005).

[27] F. Jacobsen, M. Strongin, M. Ruckman, A. Wiess and W. C. Turner. The development of a positron ionization gauge. *NASA STI/Recon Technical Report N* **95**, 24623–+ (1994).

[28] C. M. Surko, G. F. Gribakin and S. J. Buckman. Low-energy positron interactions with atoms and molecules. *Journal of Physics B* **38**, R57–R126 (2005).

[29] J. P. Marler, G. F. Gribakin and C. M. Surko. Comparison of positron-impact vibrational excitation cross sections with the born-dipole model. *Nuclear Instruments and Methods in Physics Research B* **247**, 87–91 (2006).

[30] J. P. Marler. *New Results for Positron Scattering from Noble Gas Atoms and Diatomic Molecules*. Ph.D. thesis, University of California, San Diego (2005).

[31] D. W. Gidley, A. Rich, E. Sweetman and D. West. New precision measurements of the decay rates of singlet and triplet positronium. *Physical Review Letters* **49**, 525–528 (1982).

[32] P. A. Fraser. Positrons and positronium in gases. *Advancements in Atomic and Molecular Physics* **4**, 63 (1968).

[33] D. A. L. Paul and L. Saint-Pierre. Rapid annihilation of positrons in polyatomic gases. *Physical Review Letters* **11**, 493 (1963).

[34] V. I. Goldanskii and Y. S. Sayasov. On the resonance annihilation of positrons in collision with neutral atoms or molecules. *Physics Letters* **13**, 300–301 (1964).

[35] C. M. Surko, A. Passner, M. Leventhal and F. J. Wysocki. Bound states of positrons and large molecules. *Physical Review Letters* **61**, 1831–4 (1988).

[36] T. J. Murphy and C. M. Surko. Annihilation of positrons on organic molecules. *Physical Review Letters* **67**, 2954–7 (1991).

[37] K. Iwata, R. G. Greaves, T. J. Murphy, M. D. Tinkle and C. M. Surko. Measurements of positron-annihilation rates on molecules. *Physical Review A* **51**, 473–87 (1995).

[38] K. Iwata, G. F. Gribakin, R. G. Greaves, C. Kurz and C. M. Surko. Positron annihilation on large molecules. *Physical Review A* **A61**, 022719 (2000).

[39] P. M. Smith and D. A. L. Paul. Positron annihilation in methane gas. *Canadian Journal of Physics* **48**, 2984–2990 (1970).

[40] G. Gribakin. Theory of positron annihilation on molecules. In C. M. Surko and F. A. Gianturco (editors) *New Directions in Antimatter Physics and Chemistry*, 413–435 (Kluwer Academic Publishers, 2001).

[41] S. J. Gilbert, C. Kurz, R. G. Greaves and C. M. Surko. Creation of a monoenergetic pulsed positron beam. *Applied Physics Letters* **70**, 1944–1946 (1997).

[42] S. J. Gilbert. *A New Ultra-Cold Positron Beam and Applications To Low-Energy Positron Scattering and Electron-Positron Plasmas.* Ph.D. thesis, University of California, San Diego (2000).

[43] L. D. Barnes, S. J. Gilbert and C. M. Surko. Energy-resolved positron annihilation for molecules. *Physical Review A* **67**, 032706 (2003).

[44] G. F. Gribakin and C. M. R. Lee. Positron annihilation in molecules by capture into vibrational Feshbach resonances of infrared-active modes. *Physical Review Letters* **97**, 193201 (2006).

[45] L. D. Barnes, J. A. Young and C. M. Surko. Energy-resolved positron annihilation rates for molecules. *Physical Review A* **74**, 012706 (2006).

[46] V. A. Dzuba, V. V. Flambaum, G. F. Gribakin and W. A. King. Many-body calculations of positron scattering and annihilation from noble gas atoms. *Journal of Physics B* **29**, 3151–3175 (1996).

[47] J. J. Sakurai. *Modern Quantum Mechanics* (Addison-Wesley Publishing Company, Reading, MA, 1994), Revised edn.

[48] J. Mitroy, M. W. J. Bromley and G. Ryzhikh. Positron binding to a model alkali atom. *Journal of Physics B* **32**, 2203 (1999).

[49] G. F. Gribakin and P. M. W. Gill. The role of vibrational doorway states in positron annihilation with large molecules. *Nuclear Instruments and Methods in Physics Research B* **221**, 30–35 (2004).

[50] G. Laricchia and C. Wilkin. Semiempirical approach to positron annihilation in molecules. *Physical Review Letters* **79**, 2241–2244 (1997).

[51] G. Laricchia and C. Wilkin. On the annihilation of positrons in binary encounters with molecules. *Nuclear Instruments and Methods in Physics Research B* **143**, 135–139 (1998).

[52] G. F. Gribakin and J. Ludlow. Enhancement of positron-atom annihilation near the positronium threshold. *Physical Review Letters* **88**, 163202/1–4 (2002).

[53] J. Mitroy, M. W. J. Bromley and G. G. Ryzhikh. Positron and positronium binding to atoms. *Journal of Physics B* **35**, R81 (2002).

[54] R. G. Greaves, M. D. Tinkle and C. M. Surko. Creation and uses of positron plasmas. *Physics of Plasmas* **1**, 1439–1446 (1994).

[55] M. Hirose, M. Washio and K. Takahashi. Production of an intense slow positron beam using a compact cyclotron. *Applied Surface Science* **85**, 111–17 (1995).

[56] T. Omori, M. Fukuda, T. Hirose, Y. Kurihara, R. Kuroda, M. Nomura, A. Ohashi, T. Okugi, K. Sakaue, T. Saito, J. Urakawa, M. Washio and I. Yamazaki. Efficient propagation of polarization from laser photons to positrons through compton scattering and electron-positron pair creation. *Physical Review Letters* **96**, 114801 (2006).

[57] R. Krause-Rehberg, N. van der Walt, L. Büttnera and F. Börner. A 22na positron source for use in uhv. *Nuclear Instruments and Methods in Physics Research B* **221**, 165–167 (2004). Proceedings of the XII International Workshop on Positron and Positronium Physics.

[58] R. Xie, M. Petkov, D. Becker, K. Canter, F. M. Jacobsen, K. G. Lynn, R. Mills and L. O. Roellig. Production of a low energy positron beam using the ^{12}C(d,n)^{13}N reaction. *Nuclear Instruments and Methods in Physics Research B* **93**, 98–102 (1994).

[59] D. B. Cassidy, K. F. Canter, R. E. Shefer, R. E. Klinkowstein and B. J. Hughey. Positron beam production with a deuteron accelerator. *Nuclear Instruments and Methods in Physics Research B* **195**, 442–448 (2002).

[60] A. P. Mills, Jr. and E. M. Gullikson. Solid neon moderator for producing slow positrons. *Applied Physics Letters* **49**, 1121–3 (1986).

[61] R. Khatri, M. Charlton, P. Sferlazzo, K. G. Lynn, A. P. Mills, Jr. and L. O. Roellig. Improvement of rare-gas solid moderators by using conical geometry. *Applied Physics Letters* **57**, 2374–6 (1990).

[62] L. D. Barnes. *Positron Annihilation on Atoms and Molecules*. Ph.D. thesis, University of California, San Diego (2005).

[63] J. P. Sullivan, S. J. Gilbert, J. P. Marler, R. G. Greaves, S. J. Buckman and C. M. Surko. Positron scattering from atoms and molecules using a magnetized beam. *Physical Review A* **66**, 042708 (2002).

[64] J. A. Young and C. M. Surko. Dependence of resonant positron-molecule annihilation on molecular temperature. *Nuclear Instruments and Methods in Physics Research B* submitted for publication (2007).

[65] G. F. Gribakin and C. M. R. Lee. Application of the zero-range potential model to positron annihilation on molecules. *Nuclear Instruments and Methods in Physics Research B* **247**, 31–37 (2006).

[66] NIST Chemistry WebBook (2005). URL `http://webbook.nist.gov/chemistry/`.

[67] Y. N. Demkov and V. N. Ostrovskii. *Zero-range potentials and their applications in atomic physics* (Plenum Press, New York, 1988).

[68] M. W. Schmidt, K. K. Baldridge, J. A. Boatz, S. T. Elbert, M. S. Gordon, J. H. Jensen, S. Koseki, N. Matsunaga, K. A. Nguyen, S. J. Su, T. L. Windus, M. Dupuis

and J. A. Montgomery, Jr. General atomic and molecular electronic structure system. *Journal of Computational Chemistry* **14**, 1347–1363 (1993).

[69] J. Mitroy and I. A. Ivanov. Semiempirical model of positron scattering and annihilation. *Physical Review A* **65**, 042705 (2002).

[70] J. A. Young and C. M. Surko. Role of binding energy in Feshbach-resonant positron-molecule annihilation. *Physical Review Letters* **99**, 133201 (2007).

[71] G. F. Gribakin and C. M. R. Lee. private communication (2006).

[72] G. F. Gribakin. Enhancement of positron annihilation on molecules due to vibrational feshbach resonances. *Nuclear Instruments and Methods in Physics Research B* **192**, 26–39 (2002).

[73] K. Strasburger. Adiabatic positron affinity of LiH. *Journal of Chemical Physics* **114**, 615–616 (2001).

[74] J. R. Mohallem, F. Rolim and C. P. Gonalves. A molecular model for positron complexes: long-range effects on 2γ pair-annihilation rates. *Journal of Physics B: Atomic Molecular and Optical Physics* **37**, 1045–1053 (2004).

[75] M. Tachikawa, R. J. Buenker and M. Kimura. Geometry relaxation effects for molecules as a result of binding with a positron. *Journal of Chemical Physics* **121**, 9191–9192 (2004).

[76] R. J. Buenker, H. P. Liebermann, V. Melnikov, M. Tachikawa, L. Pichland and M. Kimura. Positron binding energies for alkali hydrides. *Journal of Physical Chemistry A* **109**, 5956–5964 (2005).

[77] F. A. Gianturco, J. Franz, R. J. Buenker, H.-P. Liebermann, L. Pichl, J.-M. Rost, M. Tachikawa and M. Kimura. Positron binding to alkali-metal hydrides: The role of molecular vibrations. *Physical Review A* **73**, 022705 (2006).

[78] R. J. Buenker, H. P. Liebermann, L. Pichl, M. Tachikawa and M. Kimura. Role of the electric dipole moment in positron binding to the ground and excited states of the BeO molecule. *Journal of Chemical Physics* **126**, 104305 (2007).

[79] M. Tachikawa, I. Shimamura, R. J. Buenker and M. Kimura. Positron binding by molecules. *Nuclear Instruments and Methods in Physics Research B* **192**, 40–41 (2002).

[80] M. Tachikawa, R. J. Buenker and M. Kimura. Bound states of positron with urea and acetone molecules using configuration interaction *ab initio* molecular orbital approach. *Journal of Chemical Physics* **119**, 5005–5009 (2003).

[81] O. H. Crawford. Bound states of a charged particle in a dipole field. *Proceedings of the Physical Society* **91**, 279–84 (1967).

[82] T. Nishimura and F. A. Gianturco. Low-energy positron scattering: Modelling the formation of bound [M-e^+] states in deformed polyatomic molecules. *Europhysics Letters* **68 (3)**, 377–383 (2004).

[83] T. Nishimura and F. A. Gianturco. Enhanced positron annihilation in small hydrocarbons: Threshold effects from symmetric c-h bond deformations. *Physical Review A* **72**, 022706 (2005).

[84] J. E. Bertie and S. L. Zhang. Infrared intensities of liquids .2. integrated absorption intensities of CH_3OH, CH_3OD, CD_3OH and CD_3OD and dipole moment derivatives of methanol. *Journal of Molecular Structure* **333**, 413–414 (1997).

[85] J. Florian, J. Leszczynski, B. G. Johnson and L. Goodman. Coupled-cluster and density functional calculations of the molecular structure, infrared spectra, raman spectra, and harmonic force constants for methanol. *Molecular Physics* **91**, 439 – 448 (1997).

[86] G. F. Gribakin. Private communication (2007).

[87] C. R. C. de Carvalho, M. T. d. N. Varella, M. A. P. Lima and E. P. da Silva. Elastic positron scattering by C_2H_2: Differential cross sections and virtual state formation. *Physical Review A* **68**, 062706 (2003).

[88] G. F. Gribakin. Private communication.

[89] F. A. Gianturco and T. Mukherjee. Positron annihilation in CO_2 molecules: The role of vibration excitation. *Europhysics Letters* **48**, 519–525 (1999).

[90] T. Nishimura and F. A. Gianturco. The dominant "heating" mode: bending excitation of water molecules by low energy positron impact. *European Physical Journal D* **33**, 221–228 (2005).

[91] T. Nishimura and F. A. Gianturco. Virtual-state formation in positron scattering from vibrating molecules: A gateway to annihilation enhancement. *Physical Review Letters* **90**, 183201 (2003).

[92] D. Dill, J. Welch, J. L. Dehmer and J. Siegel. Shape-resonance-enhanced excitation at intermediate energies (10-40 eV) in electron-molecule scattering. *Physical Review Letters* **43**, 1236 (1979).

[93] J. P. Sullivan, S. J. Gilbert, S. J. Buckman and C. M. Surko. Search for resonances in the scattering of low-energy positrons from atoms and molecules. *Journal of Physics B: Atomic Molecular and Optical Physics* **34**, L467–L474 (2001).

[94] F. A. Gianturco and R. R. Lucchese. Computational investigation of positron scattering from C_{60}. *Physical Review A* **60**, 4567 – 4576 (1999).

[95] J. Mitroy and M. W. J. Bromley. Generating phase shifts from pseudostate energy shifts. *Physical Review Letters* **98**, 173001 (2007).

[96] K. J. Miller and J. A. Savchick. A new empirical method to calculate average molecular polarizabilities. *Journal of the American Chemical Society* **101:24**, 7206–7213 (1979).

[97] R. Z. Lei, A. J. Gellman and B. E. Koel. Desorption energies of linear and cyclic alkanes on surfaces: anomalous scaling with length. *Surface Science* **554**, 125–140 (2004).

[98] S. M. Wetterer, D. J. Lavrich, T. Cummings, S. L. Bernasek and G. Scoles. Energetics and kinetics of the physisorption of hydrocarbons on Au(111). *Journal of Physical Chemistry B* **102**, 9266 (1998).

[99] S. M. Wetterer. *Helium Atom Reflectivity Study of Physisorption and Chemisorption on Single Crystal Metal Surfaces.* Ph.D. thesis, Princeton University (1998).

[100] G. A. Guirgis, X. Zhu and J. R. Durig. Conformational and structural studies of 1-fluoropropane from temperature dependant FT-IR spectra of rare gas solutions and ab initio calculations. *Structural Chemistry* **10**, 445–461 (1999).

[101] K. Iwata, R. G. Greaves and C. M. Surko. Annihilation rates of positrons on aromatic molecules. *Hyperfine Interactions* **89**, 271–8 (1994).

[102] V. May and O. Kühn. *Charge and Energy Transfer Dynamics in Molecular Systems* (Wiley_VCH, 2000).

[103] Y. Yamata, N. Mikami and T. Ebata. Real-time detection of doorway states in the intramolecular vibrational energy redistribution of the OH/OD stretch vibration of phenol. *Journal of Chemical Physics* **121**, 11530 (2004).

[104] M. W. J. Bromley and J. Mitroy. Excited states of positronic atoms. *Physical Review A* **75**, 042506 (2007).

[105] K. Iwata, G. F. Gribakin, R. G. Greaves and C. M. Surko. Positron annihilation with inner-shell electrons in noble gas atoms. *Physical Review Letters* **79**, 39–42 (1997).

[106] A. Zecca, N. Moser, C. Perazzolli, A. Salemi and M. J. Brunger. Total cross sections for positron scattering from benzene, cyclohexane, and aniline. *Physical Review A* **76**, 022708 (2007).

[107] J. R. Danielson, P. Schmidt, J. P. Sullivan and C. M. Surko. A cryogenic, high-field trap for large positron plasmas and cold beams. In M. Schauer, T. Mitchell and R. Nebel (editors) *Non-Neutral Plasma Physics V*, 692, 149–161 (AIP, New York, NY, USA, 2003).

[108] C. M. Surko and R. G. Greaves. Emerging science and technology of antimatter plasmas and trap-based beams. *Physics of Plasmas* **11**, 2333–2348 (2004).

[109] L. D. Hulett, Jr., D. L. Donohue, G. L. Glish, S. A. McLuckey and T. A. Lewis. Mass spectrometry studies of the ionization on large organic molecules by slow positrons. *Materials Science Forum* **105-110**, 273–80 (1992).

[110] L. D. Hulett, Jr., D. L. Donohue, J. Xu, T. A. Lewis, S. A. McLuckey and G. L. Glish. Mass spectrometry studies of the ionization of organic molecules by low-energy positrons. *Chemical Physics Letters* **216**, 236–40 (1993).

[111] J. Xu, L. D. Hulett, Jr., T. A. Lewis, D. L. Donohue, S. A. McLuckey and G. L. Glish. Positron-induced dissociation of organic molecules. *Physical Review A* **47**, 1023–30 (1993).

[112] O. H. Crawford. Mechanism for fragmentation of molecules by positron annihilation. *Physical Review A* **49**, R3147–50 (1994).

[113] G. L. Glish, R. G. Greaves, S. A. McLuckey, L. D. Hulett, C. M. Surko, J. Xu and D. L. Donohue. Ion production by positron-molecule resonances. *Physical Review A* **49**, 2389–93 (1994).

[114] J. Xu, L. D. Hulett, Jr., T. A. Lewis, D. L. Donohue, S. A. McLuckey and O. H. Crawford. Internal energy deposition into molecules upon positron-electron annihilation. *Physical Review A* **49**, R3151–4 (1994).

[115] J. Xu, L. D. Hulett, Jr., T. A. Lewis and S. A. McLuckey. Chemical selectivity in the dissociative ionization of organic molecules by low-energy positrons. *Physical Review A* **52**, 2088–94 (1995).

[116] L. D. Hulett, Jr., J. Xu, T. A. Lewis, O. H. Crawford and S. A. McLuckey. Mass spectrometry studies of the ionization of organic molecules by slow positrons. *Materials Science Forum* **175-178**, 687–90 (1995).